A STUDY OF HIGH PRESSURE RIDGES TO THE EAST OF THE APPALACHIAN MOUNTAINS

by

DENNIS GRAHAM BAKER

B.A., Harvard University
(1964)

M.S., Massachusetts
Institute of Technology
(1967)

SUBMITTED IN PARTIAL FULFILLMENT

OF THE REQUIREMENTS FOR THE

DEGREE OF DOCTOR OF

PHILOSOPHY

at the

MASSACHUSETTS INSTITUTE OF

TECHNOLOGY

August, 1970 (i.e. Feb. 1971)

Signature of Author.....
Department of Meteorology, August 31, 1970

Certified by.....
Thesis Supervisor

Accepted by.....
Chairman, Departmental Committee
on Graduate Students

A STUDY OF HIGH PRESSURE RIDGES TO THE EAST OF THE APPALACHIAN MOUNTAINS

by

DENNIS GRAHAM BAKER

Submitted to the Department of Meteorology on 31 August 1970 in partial fulfillment of the requirements for the degree of Doctor of Philosophy

ABSTRACT

This thesis considers the orographically induced high pressure ridge that appears in the sea-level pressure field on the windward side of mountain ranges. The outstanding characteristic of these synoptic-scale ridges is their persistence. Many appear to be in a steady-state, even though the broad-scale flow in which they are embedded is changing.

Two distinctly different types of pressure ridges form to the east of the Appalachian Mountains. This investigation is limited to the type of ridge associated with a shallow, cold airflow topped by a strong low-level inversion. Previously proposed theories of the pressure ridge assume there is no inversion present. Hence, they are not applicable to this type of ridge.

A detailed synoptic study is made of one pressure ridge case. It is found that there are two kinds of pressure ridges with low-level inversions. It is shown that these two ridges have fundamentally different airflows. In the first, called the corner ridge, the cold air flows over the mountains. In the second, called the wedge ridge, the cold air is blocked by an adverse pressure gradient and forced to flow parallel to the mountains.

The available radiosonde data is insufficient to resolve variations in the inversion height. Therefore, a method, which assumes the existence of an inversion discontinuity, is used in order to obtain the inversion heights from the synoptic surface stations. In addition, frictionless dynamic trajectories are used to estimate the cold airflow trajectories. From these two techniques the variation of the inversion along the cold airflow is found. It is concluded that the pressure ridge is only a reflection in the sea-level pressure field of changes in the inversion height.

In order to explain the observed features of this cold airflow, it is concluded that, in addition to the inversion height, the pressure gradient above the inversion, the coriolis force, surface friction, and mixing of warm and cold air are all important physical factors in the cold airflow.

Thesis Supervisor: Frederick Sanders
Title: Professor

ACKNOWLEDGMENTS

I would like to thank the many people who made this thesis possible: Professor Frederick Sanders and Professor James Austin for their comments and constructive criticism; Mr. Stephen Ricci for drafting the illustrations; Miss Brenda Baker for typing the final manuscript; Miss Anna Corrigan and Mr. Edward Nelson for plotting the original data; and, especially, my wife for editing and general encouragement.

TABLE OF CONTENTS

Section 1. Introduction

The lee-side pressure trough is a well-known orographically induced phenomenon. A similar, but less familiar, orographic phenomenon, however, is the windward-side pressure ridge. The goal of this thesis is to increase the understanding of this phenomenon.

The pressure ridge is a phenomenon worthy of attention for the following reasons. First, it is a common and widespread phenomenon (see Section 2).

Second, the pressure ridge is often accompanied by unpredictable bad weather, at least along the east coast of the United States. The results of a case study presented in Section 6 suggest that even the present six-layer primitive equation model does not predict this bad weather 24 hours in advance. Hence, from a weather forecasting viewpoint, further knowledge of the pressure ridge is desirable.

Third, this ridge is associated with several little understood atmospheric phenomena: the foehn, "back-door" cold fronts, and one type of east-coast cyclogenesis. A better understanding of the ridge should also help explain these phenomena.

To the author's knowledge, no observational study of the upper-air conditions associated with the pressure ridge has even been made. This research provides such a synoptic study by analyzing in detail pressure ridges that form to the east of the Appalachian Mountains.

Section 2. Description and climatology of the pressure ridge

2.1 Examples of ridges

In this paper the pressure ridge is defined as a stationary, anticyclonic curvature of the sea-level isobars such that along a line perpendicular to the mountains there is a pressure maximum on the windward slopes. Possibly, for a very weak case, instead of a pressure maximum only a change of gradient would occur. Such cases have not been considered in this investigation.

An example of an orographic pressure ridge is given in Figure 1a (taken from Malberg, 1967). In this figure, a pressure ridge in the sea-level pressure field extends along the windward (south) side of the Alps. In fact, there is even a pressure ridge east of the Apennine Mountains in Italy. The most remarkable feature of this example is the very strong pressure difference across the Alps to the north of the orographic ridge. This difference corresponds at its strongest place to a geostrophic wind of 100 m/sec. The formation of a ridge is almost always associated with such an increased pressure difference across a mountain range.

Figure 1b gives the ground elevation and sea-level pressure as a function of distance along a line perpendicular to the Alps—line AA' in Figure 1a. The pressure ridge appears as a maximum in the sea-level pressure on the windward slopes.

Figure 1b discloses that the rapid pressure drop mentioned above is limited mainly to the region where the terrain is highest. Even if the 1000-meter pressure field is the same as the sea-level field, the pressure drop still occurs within the mountain and, hence, is physically

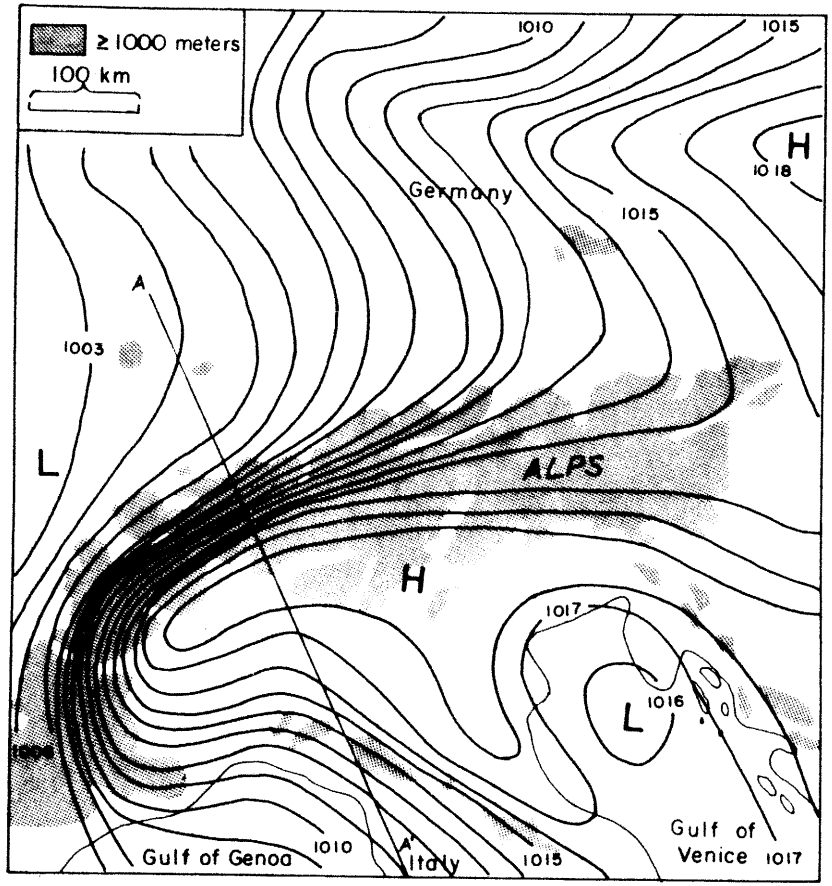

SURFACE ANALYSIS 25 FEB. 1964 0600 GMT
RIDGE OF HIGH PRESSURE SOUTH OF THE ALPS
(after Malberg (1967)).

1a

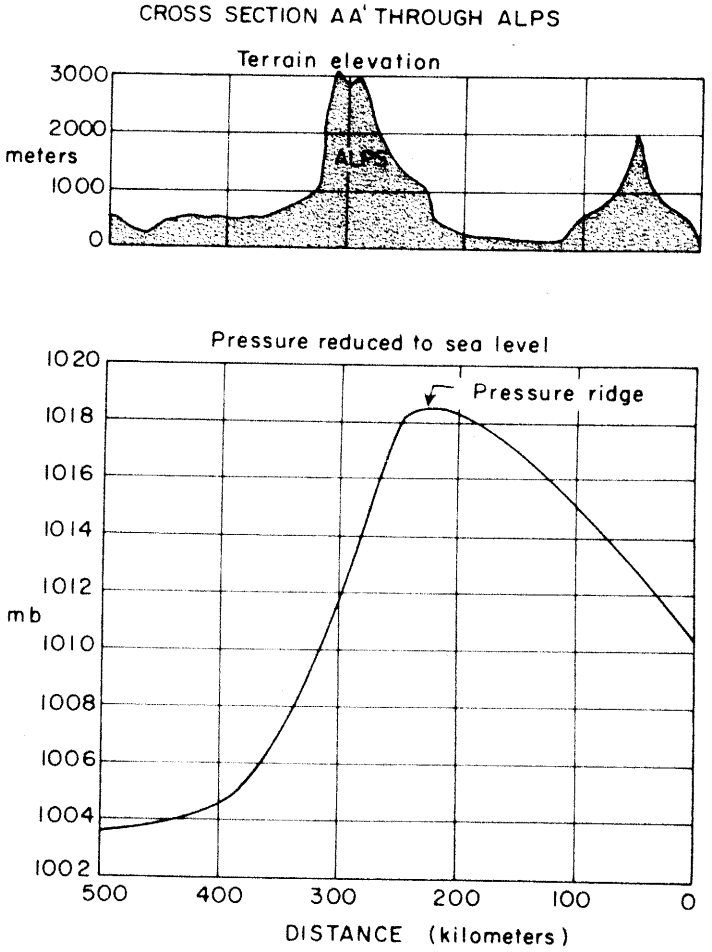

1b

Figure 1. Example of an orographic pressure ridge

meaningless at this level. This drop is meteorologically significant only if it is still present above the top of the mountain range. In this thesis it is shown that for one type of ridge, the gradient does extend above the top.

Figure 2a illustrates an orographic pressure ridge to the east of the Appalachian Mountains. This pressure ridge extends from Virginia to Connecticut. In general, the ridge line lies parallel to the crest of the Appalachians between the coast and the mountain crest.

The pressure ridge in this case has two distinct shapes. In the northern part of the analysis area, the isobars forming the ridge make a sharp "corner." In the southern part, the isobars are shaped like a "wedge." It is shown in Section 4 that this difference in shape in the sea-level pressure field reflects fundamentally different airflow patterns aloft. Henceforth, in this paper these ridges are called the corner ridge and the wedge ridge.

The terrain elevation and sea-level pressure along two lines perpendicular to the Appalachians is given in Figure 2b. The actual path of these lines is given in Figure 2a. (Station call letters, as given in Figure 2b, are used throughout this paper. Appendix B gives the station locations corresponding to these call letters.) Along both lines the sea-level pressure has a maximum on the windward slope with a sharp drop in pressure across the mountains.

2.2 Climatology of the pressure ridge

The importance of a phenomenon depends, in part, on its frequency of occurrence and its global extent. To the author's knowledge, no such climatological study of the pressure ridge has ever been made. Some

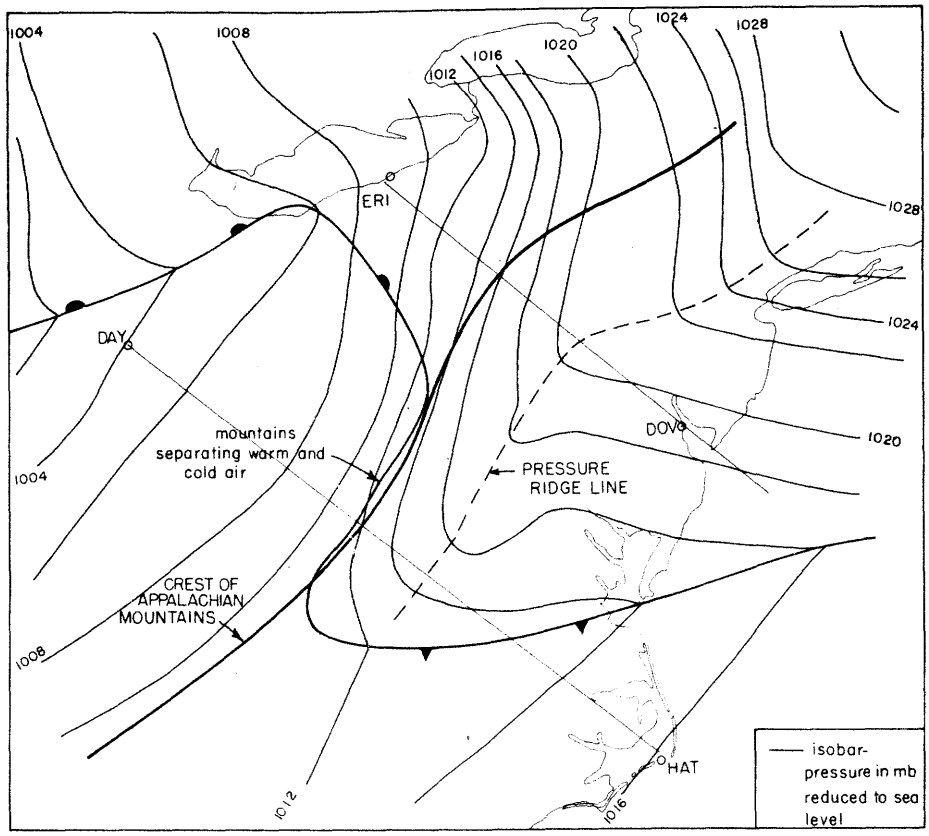

2a

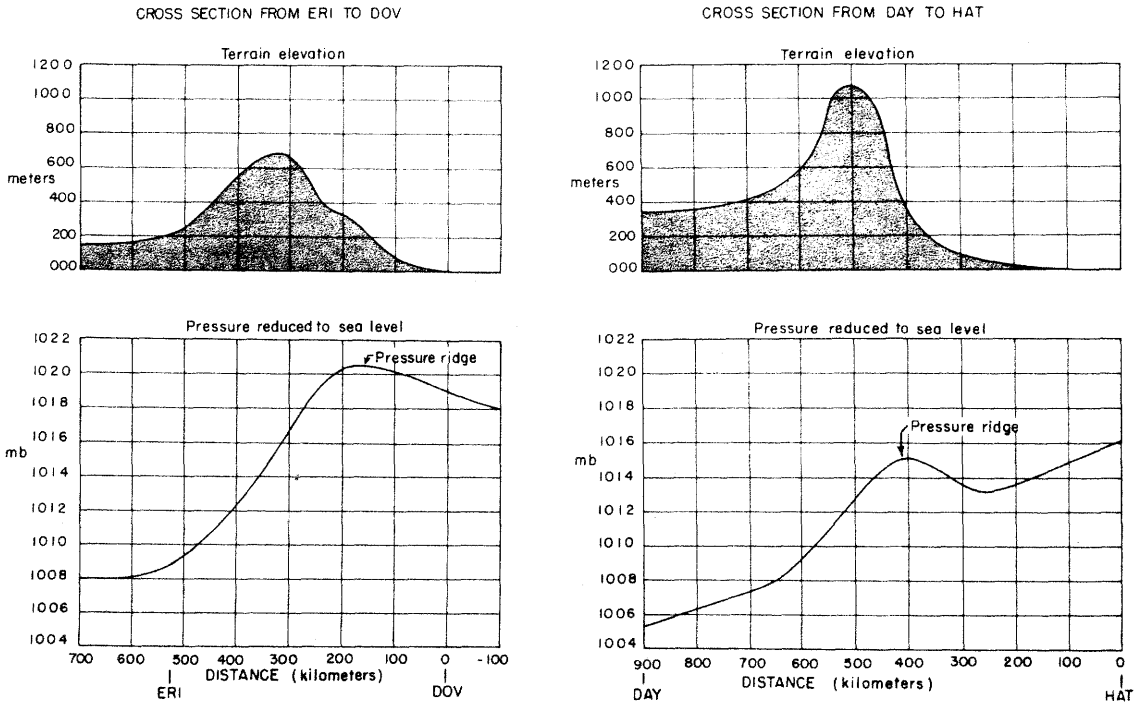

2b

Figure 2. Example of an orographic pressure ridge at 0500 GMT 24 January 1965

pertinent data is, however, found in the literature.

The presence of pressure ridges around the Alps has been well documented at least since Erk (1886) described the formation of a ridge in his account of a strong foehn. This association between the ridge and the foehn is now well-established. In fact, in the Alps the ridge is known as the "foehn's knee" (Streiff-Becker, 1942). The ridge can form on either side of the Alps, depending upon the direction of the large-scale flow (see, for instance, Defant, 1951). Ridges form on the north side of the Alps about once a week with no seasonal variation (Exner, 1905b). On the south side ridges develop less frequently with a maximum in late winter or spring. Because of this asymmetry of frequency, Bullrich (1941) found a ridge north of the Alps in a mean eleven-year sea-level pressure field.

Information on pressure ridges associated with mountains other than the Alps is very limited. In fact, Malberg (1967) is the only investigator, to the author's knowledge, to describe explicitly the formation of pressure ridges around other mountain ranges. He illustrates orographic ridges associated with the Greenland Icecap, the Rocky Mountains, the Andes, the Coast Range in western Canada, and the central Asiatic mountains.

The author has found in the literature examples of ridges around still other mountain ranges. However, in all of these examples the pressure ridge was just an incidental feature of the phenomena being considered. In fact, several of the investigators did not even point out the presence of the pressure ridge in their illustrations.

In the pressure analyses of Little (1931), ridges appear on the windward side of the Sierra Nevadas in California. Watts (1945) and Garnier (1958) show pressure ridges associated with the New Zealand Alps (see Figure 8). Arakawa (1968) describes a windward ridge associated with strong orographic winds in Japan. Spinnangr and Johansen (1954) point out ridges on the north side of the Scandinavian Mountains. Defant (1951) gives an example for the south side of these mountains. In Scorer (1952) a pressure ridge can also be seen to the east of mountains in Spain.

The only references to ridges east of the Appalachian Mountains are in connection with secondary cyclogenesis. Austin (1941) suggested that there are two types of east-coast cyclogenesis. Miller (1946) verified the existence of these two types from detailed surface analyses. One type (Type A) develops in a stationary front situated approximately along the Gulf Stream. The other type (Type B) forms to the east of the Appalachian pressure ridge.

Since the orographic ridge precedes Type B cyclogenesis, the ridge is probably conducive to cyclogenesis. In spite of the global extent of the pressure ridge, it is surprising how little evidence there is in the literature that Type B cyclogenesis occurs in other parts of the world. The only cyclone that appears to have features similar to Type B is the "Skagerak" cyclone that forms at the southwestern end of the Scandinavian Mountains (J. Bjerknes and H. Solberg, 1922). Clearly, the global distribution of Type B cyclogenesis should be investigated further.

The discussion in Sections 2.1 and 2.2 contains all the synoptic and statistical information about the pressure ridge that the author has

uncovered in the literature. Several conclusions can be drawn from this discussion. (1) The orographic ridge occurs frequently in many parts of the world. (2) The pressure ridge always forms on the windward side of mountains and is accompanied by an intensification of the pressure gradient across the mountains. (3) Pressure ridges can occur no matter what the orientation of the mountain range and, in fact, are able to form on either side of the same mountain range.

2.3 Statistics of Appalachian pressure ridges

Statistics of ridges appearing along the East Coast of the United States from 1965 through 1967 were compiled using Daily Weather Maps (United States Environmental Data Service) as the data source. The ridges were subjectively identified in accordance with the definition in Section 2.1. The results are given in Table 1. (Table 2 contains a list of the strongest cases from October, 1964 to April, 1968.) Ridges occurred on the average about three times per month. They were most frequent in January, February, and March (five per month) and least frequent in April through September (two per month). There was a large variation in size, duration and intensity. In general, the ridges were much stronger in winter than in summer. Many were accompanied by low ceilings, fog, drizzle and rain. The average duration for the cases listed in Table 2 was 30 hours. Ridges also appeared west of the Appalachians. However, these ridges were not included in the statistics in Table 1.

2.4 Synoptic patterns producing Appalachian pressure ridges

Two types of synoptic patterns accounted for most of the ridges in the above survey. The first pattern, consisting initially of a cold high in eastern Canada and an intensifying midwestern cyclone, is illustrated in Figure 3. Figure 3a shows a cyclone moving east-northeastward across the Midwest. East of the center a warm front separates cold Canadian air from warm tropical air. According to the classical model of cyclone development (Bjerkness and Solberg, 1922), the warm front should move northward. However, twelve hours later (Figure 3b) the warm front east of the Appalachians has actually pushed southward. Coincident with this push was the formation of a pressure ridge to the north of the front.

Such southward frontal movements, contrary to the motion expected from the classical cyclone model, occur frequently along the East Coast and are called "back-door" cold fronts. They are always associated with ridge formation (Wexler, 1951). In Figure 3d one can see that the primary cyclone has occluded over the Great Lakes. A secondary low is forming off the coast. Twelve hours after Figure 3d, this secondary low has completely taken over the circulation from the primary cyclone. This secondary development is a typical example of Type B cyclogenesis.

The second type of pattern producing a ridge is illustrated in Figure 4. As the large high pressure area covering the eastern half of the United States in Figure 4a moved eastward, a ridge developed on the eastern side of the Appalachians and a trough on the western side (Figure 4b).

In Figure 4c cyclogenesis has occurred east of the ridge off the

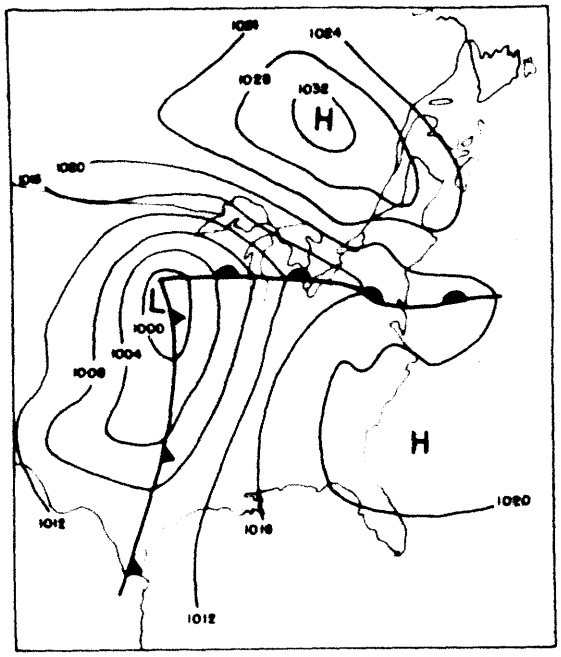

3a

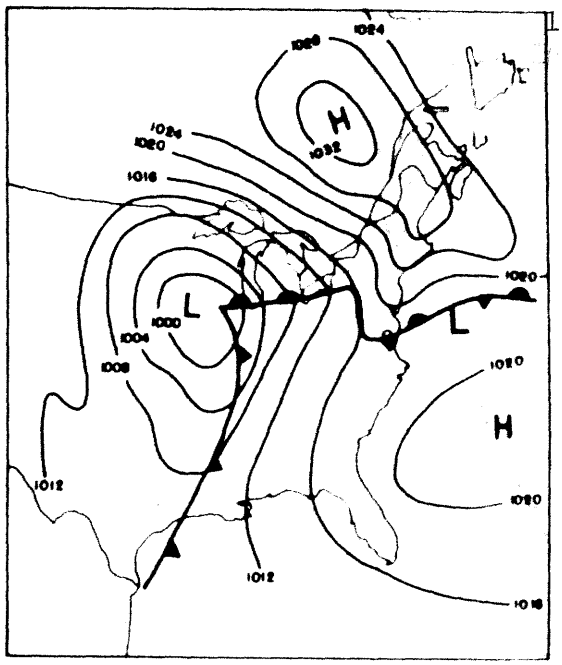

3b

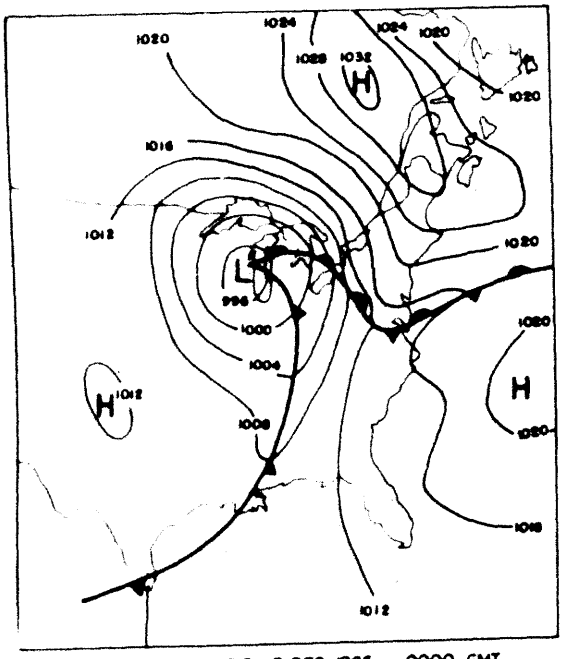

3c

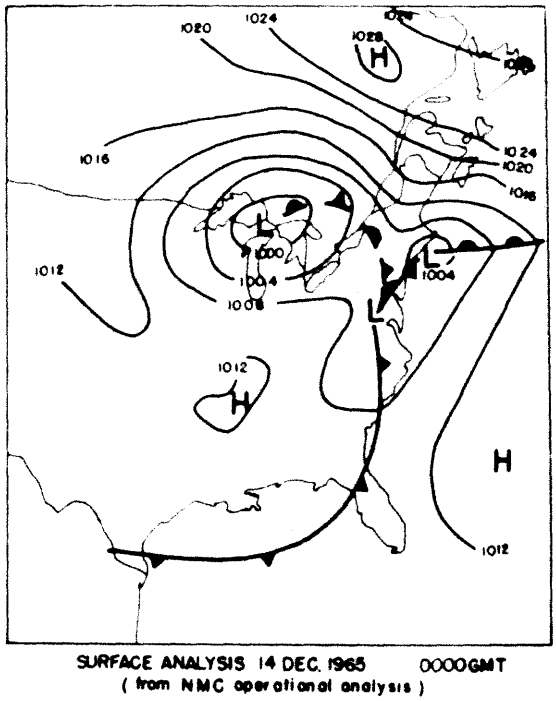

3d

Figure 3. Example of a synoptic pattern producing a pressure ridge

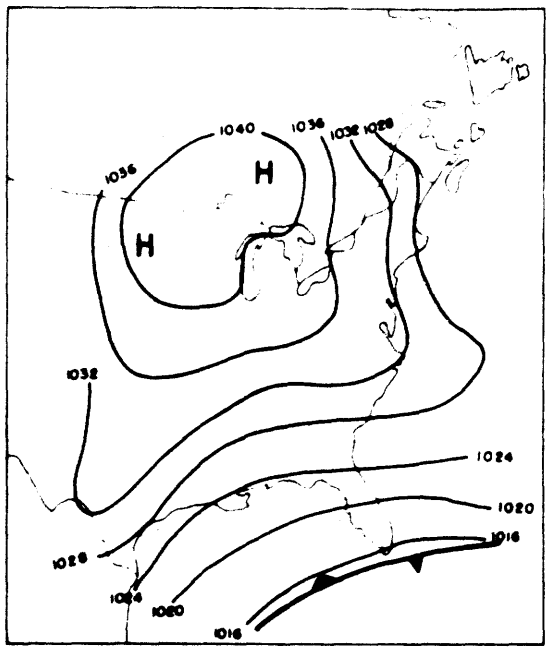

SURFACE ANALYSIS 23 FEB. 1966 0000 GMT
(from NMC operational analysis)

4a

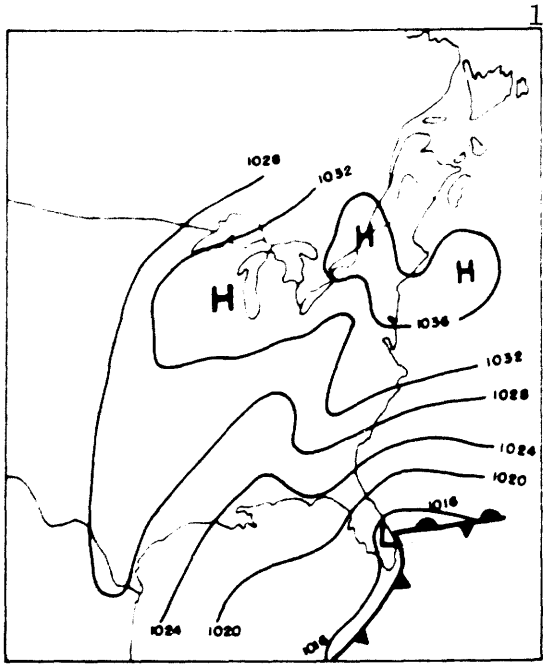

SURFACE ANALYSIS 24 FEB. 1966 0000 GMT
(from NMC operational analysis)

4b

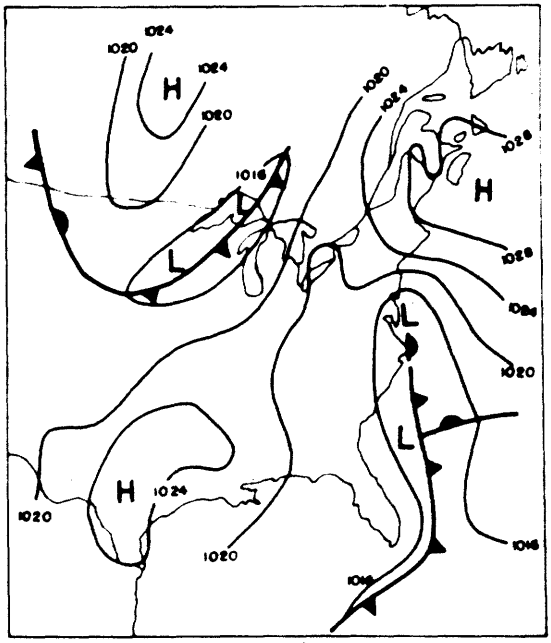

SURFACE ANALYSIS 25 FEB. 1966 0000 GMT
(from NMC operational analysis)

4c

Figure 4. Example of a synoptic pattern producing a pressure ridge

Virginia coast. This second type of pattern can often be found north of cyclones developing in the Gulf of Mexico.

The troughs that form in this type of pattern are very similar to troughs associated with the foehn. Studies of several cases showed that temperatures were indeed warmer in the trough than elsewhere, although the difference was not usually more than 10°F. However, unlike the foehn, no strong winds were reported.

The pressure ridges associated with these two types of synoptic patterns behave similarly on the windward side. Differences occur only on the lee side. For this reason, it is assumed in what follows that the dynamic explanation for the formation of the ridge does not depend on which synoptic pattern produced it.

The subsequent histories of ridges differ markedly from case to case. In some cases, the ridges dissipate as secondary cyclogenesis takes place. For the second type of pattern, often the ridge dissipates as the Gulf of Mexico cyclone intensifies and moves inland. More rarely, a low center forms in the trough and becomes the primary cyclone. Sometimes in the first type of pattern the pressure falls of the primary cyclone penetrate across the mountains, destroying the ridge.

A common type of development is the enlargement of a ridge until it extends along the entire East Coast. An example of such an extensive ridge is given in Figure 5.

2.5 Restriction of investigation to pressure ridges with low-level inversions

A brief study of a number of ridges revealed that the more

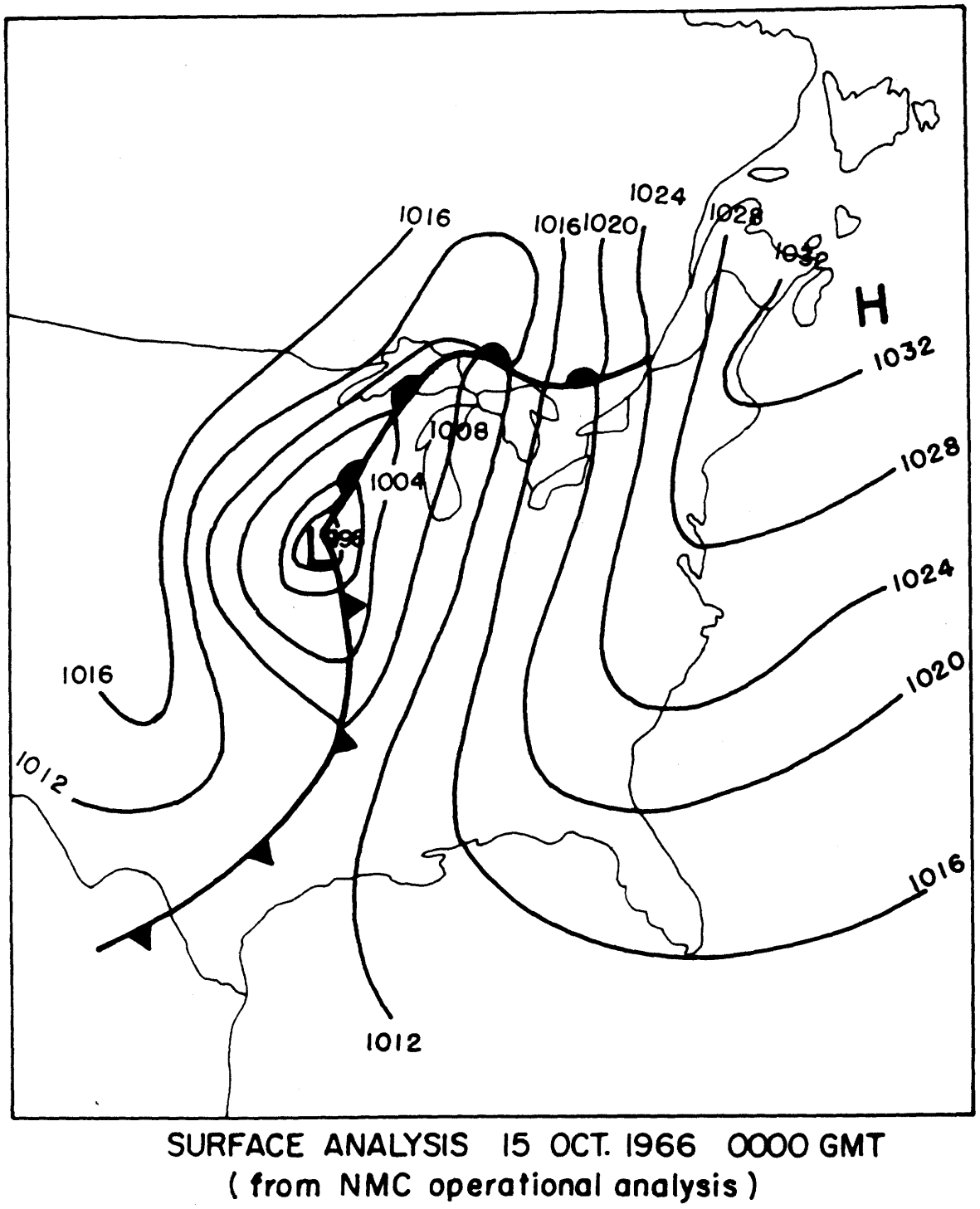

Figure 5. Example of a type of pressure ridge not considered in this thesis

extensive ridge does not have the same structure as the ridge shown in Figures 1 through 4. First of all, the smaller ridge has a strong low-level inversion, while this ridge does not. Second, this larger ridge is accompanied by fair weather. The smaller ridge usually is characterized by low ceilings and precipitation. Third, there is usually a pronounced stationary ridge at 500 mb over the larger ridge at the surface. Such a ridge does not occur with the smaller ridge. Fourth, the smaller ridge is completely stationary while the larger ridge sometimes moves eastward away from the mountains which produced it.

Of the two sizes of ridges, the smaller ridge is the more important since it is associated with unpredictable weather and phenomena like the foehn. Only the smaller ridge is considered in this thesis in order to reduce the scope of this investigation.

Section 3. Previously proposed theories of the pressure ridge

3.1 Introduction

In the previous section, the observational and climatological aspects of the pressure ridge were considered. In this section, four theories attempting to explain the pressure ridge are given. these four theories are the only previously proposed explanations known to the author.

3.2 Exner's theory

Exner (1905a) attributed the pressure ridge to an increase in dynamic pressure produced by low-level airflow encountering a mountain range. To support this contention, Exner visualized placing a mountain suddenly in a uniform airflow. He then calculated the pressure difference that developed across the mountain immediately afterwards. His results showed a dynamic pressure increase that could account for the ridge. However, Schmidt (1910) argued justifiably that the pressure ridge is a steady-state phenomenon. Using a steady-state assumption, Schmidt calculated that the dynamic pressure increase should be two orders of magnitude smaller than the pressure increase actually observed. This finding indicates that the pressure ridge cannot be attributed to the dynamic pressure.

In the synoptic investigation presented in Section 4, a hydrostatically consistent airflow pattern associated with the pressure ridge is proposed. Since this airflow configuration is supported by

radiosonde data, the results of this synoptic investigation support the conclusion that dynamic pressure effects cannot account for the ridge.

3.3 The non-adiabatic theory of v. Ficker and Trabert

Since observations of the free atmosphere were not available, v. Ficker (1908) and Trabert (1908a) assumed that at some level not too far above the mountain top, the atmosphere is no longer perturbed. Hence, at this level the pressure and temperature remain constant along a line perpendicular to the mountain range. Beneath the undisturbed level they visualized the two-dimensional flow given in Figure 6. In this flow pattern, they assumed that air parcels ascend the windward slope moist-adiabatically and descend the lee slope dry-adiabatically as a foehn. Such a flow produces in a column beneath the undisturbed level a higher mean temperature on the lee slopes than on the windward slopes. This mean temperature difference is reflected in the sea-level pressure field as a drop in pressure from the windward to the lee side.

The above proposal can explain the sharp pressure drop across the mountains, but cannot explain the increase in pressure as the air approaches the mountains. Trabert (1908b) proposed that this increase resulted from a cooling of the mean temperature of the air column as a consequence of reduced incoming radiation and evaporation of precipitation. This latter explanation appears to be physically unrealistic since a net cooling would be difficult to achieve in a column where large amounts of latent are being released into the upper portion from condensation.

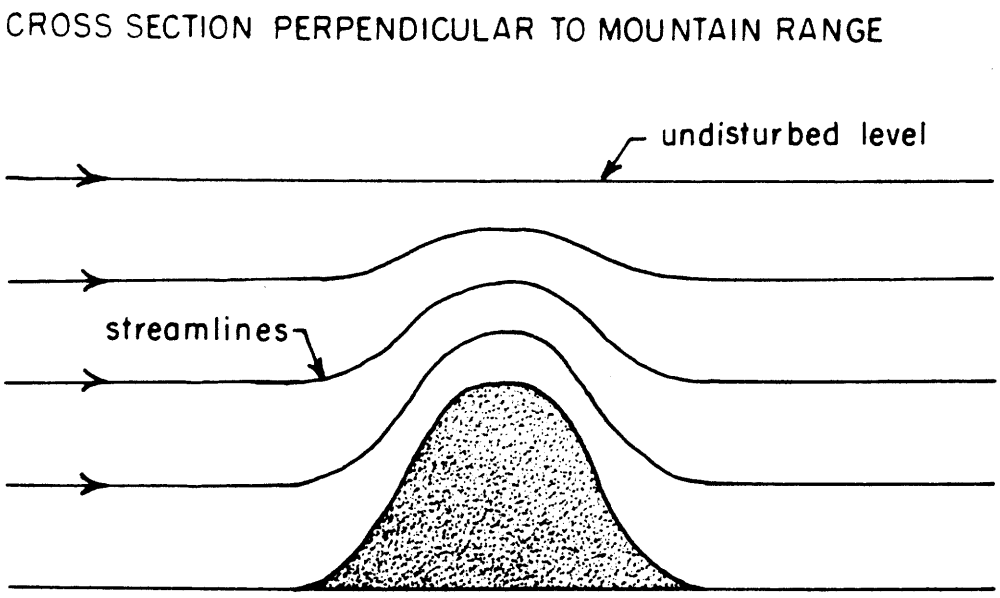

Figure 6. Idealized airflow over a mountain

3.4 Ekman's vorticity theory

Ekman (1932) proposed that the pressure ridge is a consequence of changes in the vertical vorticity of an airstream. Bjerknes and Solberg (1933), Holmboe, Forsyth, and Gustin (1945) and others have elaborated upon this idea. This theory postulates the two-dimensional flow pattern given in Figure 6. A column of air from the surface to the undisturbed level shrinks as it goes over the mountain and then returns to its original depth on the lee side. This change in the column is accompanied by horizontal divergence on the windward slope and convergence on the lee slope. The vorticity equation states that divergence contributes to a decrease in the vorticity and vice versa for convergence. In natural coordinates, the vorticity is equal to a term involving the curvature of the streamline plus a term involving the lateral shear. Since the flow is two-dimensional the velocity component perpendicular to the mountains must have zero shear in the direction along the mountain. Therefore, except in the special case of flow parallel to the mountain, the lateral shear term of the vorticity must be zero. Consequently, any vorticity change is reflected only in a change in the curvature of the airstream. It follows that for the airflow in Figure 6, there is anticyclonic curvature on the windward side of the mountain and cyclonic on the lee side.

Next, Ekman proposed that the flow could be treated as geostrophic. Accordingly, the isobars would have the same curvature as the streamlines; i.e., the pattern of a corner ridge. This theory appears to provide a reasonable explanation of a pressure ridge.

3.5 Queney's theory

Queney (1948) calculates the airflow over mountains of widely differing dimensions. In each case the atmosphere upstream of the mountain is assumed to have a velocity and lapse rate which are constant with height. In addition, a stably stratified lapse rate of temperature is chosen. Queney's Figure 3 gives the results for the obstacle closest in dimension to the Appalachian Mountains. These results show a distinct windward ridge in the sea-level pressure field.

Queney's treatment is almost wholly mathematical. Unfortunately, he does not give a clear physical interpretation of his results. Moreover, the author is unable to deduce any simple explanation from his results. Still, since Queney's results are derived from the basic meteorological equations, the fact that a pressure ridge is predicted is significant. Hence, Queney's theory has been included as a possible explanation.

3.6 Need for observational verification of assumed airflows

Except for Exner's explanation, which has been eliminated, each of the above-mentioned theories depends upon a prescribed airflow pattern. However, all of these theories were advanced before upper-air data became routinely available. For this reason investigators had to postulate the conditions aloft without corroborating observational evidence. To the author's knowledge, no observational studies have determined the actual upper-air conditions associated with the pressure ridge. Section 4 attempts to reveal, through a synoptic study of the

Appalachian pressure ridge, these unknown conditions. The applicability of the previously assumed airflows are then evaluated from the results of this study.

Section 4. Case Study

4.1 Choice of case

The ridges in Table 2 were examined and the strongest case with good surface and upper-air data coverage along with type B cyclogenesis was chosen. Although cases of this intensity occur only about twice a year, it was assumed that an extreme case would bring out most clearly the significant features of the pressure ridge.

4.2 Measurement of pressure

The pressure ridge represents an increase of pressure on the order of 3 mb from the coast to the ridge line along an axis perpendicular to the mountains. Because of the small pressure differences between stations, the reliability of the pressure measurements should be considered.

In general, pressures were reported to an accuracy of 0.1 mb. However, the accuracy of pressure measurements is affected by instrumental errors (such as drift and sticking), micrometeorological pressure changes, observation errors, and the effects of the wind pressure on the building housing the barometer (Baldit, 1929). Hence, overall accuracy is probably more nearly ± 0.5 mb. Since this is an order of magnitude smaller than the accuracy needed to establish the ridge, observational accuracy is sufficient. A few stations reported pressures that consistently disagreed with nearby stations. These pressures were checked against analyses during periods before the ridge developed and after it dissipated. If the differences still

existed, corrections were applied. These corrections are listed in Appendix A.

Because of the relative inaccuracy of pressures reported from ships, special efforts were made to improve these measurements. Ships which could be followed for several days were singled out and given more weight in the analyses than other ships. Each of these ships was given a single pressure correction based upon differences found in regions where the pressure field is known more reliably.

Improvements in the analysis resulting from these ship corrections were, unfortunately, not great. This fact, coupled with the sparcity of ship observations in time and space, made the analyses over the oceans considerably less reliable than those over land.

4.3 Data sources

The land surface data source was Service A teletype (the hourly airways surface observations). The land stations used in this study are presented in Appendix A. Ship observations were obtained from Service C teletype and Northern Hemisphere Data Tabulations. Radiosonde observations were taken from the latter source. Available special soundings were obtained from the original WBAN-31 forms. Pibal data was taken from Service C teletype. However, the amount of pibal data was limited because of low ceilings in the regions of greatest interest. Precipitation data came from Hourly Precipitation Totals (United States Environmental Data Service).

In Figures 9 through 16 and Figure 24, analyses of the surface and 850-mb level are given. The 850-mb level was chosen because the

ridge is mostly confined below this level. Hence, 850 mb represents the "undisturbed" state of the atmosphere above the ridge. Inserts on the 850-mb maps give regions where the ceiling is less than 5000 feet (hatched) and where measurable precipitation occurred within two hours of the observation time (shaded).

Although in this paper analyses are presented mostly at twelve-hour intervals, analyses were actually made every six hours (every three hours on the 28th). Time cross sections of the hourly weather conditions at selected stations were used to locate the fronts accurately.

4.4 Reduction of pressure to sea level

Errors in the reduction of pressure to sea level are greatest in mountainous terrain. Since the pressure ridge is an orographic phenomenon, the ridge can possibly be explained by systematic errors in the reduction of pressure to sea level. Wild (1901) investigated this possibility in his study of the strong transalpine pressure gradient associated with the foehn. He reduced station pressures to several other levels besides sea level in order to study the reduction errors. He obtained approximately the same pressure gradient at each level.

A similar test was made in my study of the 26-28 April 1966 case. Where the reduction was upward, the atmospheric lapse rate was assumed to be dry-adiabatic to the cloud base, and moist-adiabatic above. Where the reduction was beneath the ground, a moist-adiabatic lapse rate was assumed. (Appendix A gives station elevations;

Appendix C gives contours of terrain elevation.) Figure 7 presents the pressure field reduced to 500 meters by the above method. The basic features of the pressure ridge still exist at this level. In particular, the sharp gradient across the Appalachians appears as well as the flow from the east along the coast (although reduced in strength). According to the results of this technique, the sharp gradient across the mountains extends above the 1500-meter level. This level is above the height of all the reporting surface stations.

Several locations in the world have mountain ranges surrounded by oceans. In these places pressure observations made along the coast require only minor reduction to sea level. In Figure 8 (taken from Garnier, 1958, Figure 3) a ridge-trough system across the New Zealand Alps is clearly present. This system cannot be explained by reduction errors.

All of the above results indicate that the pressure ridge is a real atmospheric phenomenon.

4.5 Formation of the ridge

27 April, 1966 0000 GMT (Figures 9 and 10)

Cold air from a high in Canada is moving rapidly southward, particularly at 850 mb. A cold front at the edge of this cold air extends from New York through Illinois. Just to the north of the front in New York, the first hint of a ridge development can be seen. South of the front, a broad current of warm air is flowing northward, except just north of a weak frontal system extending across the southern states. A very weak orographic ridge is present in western

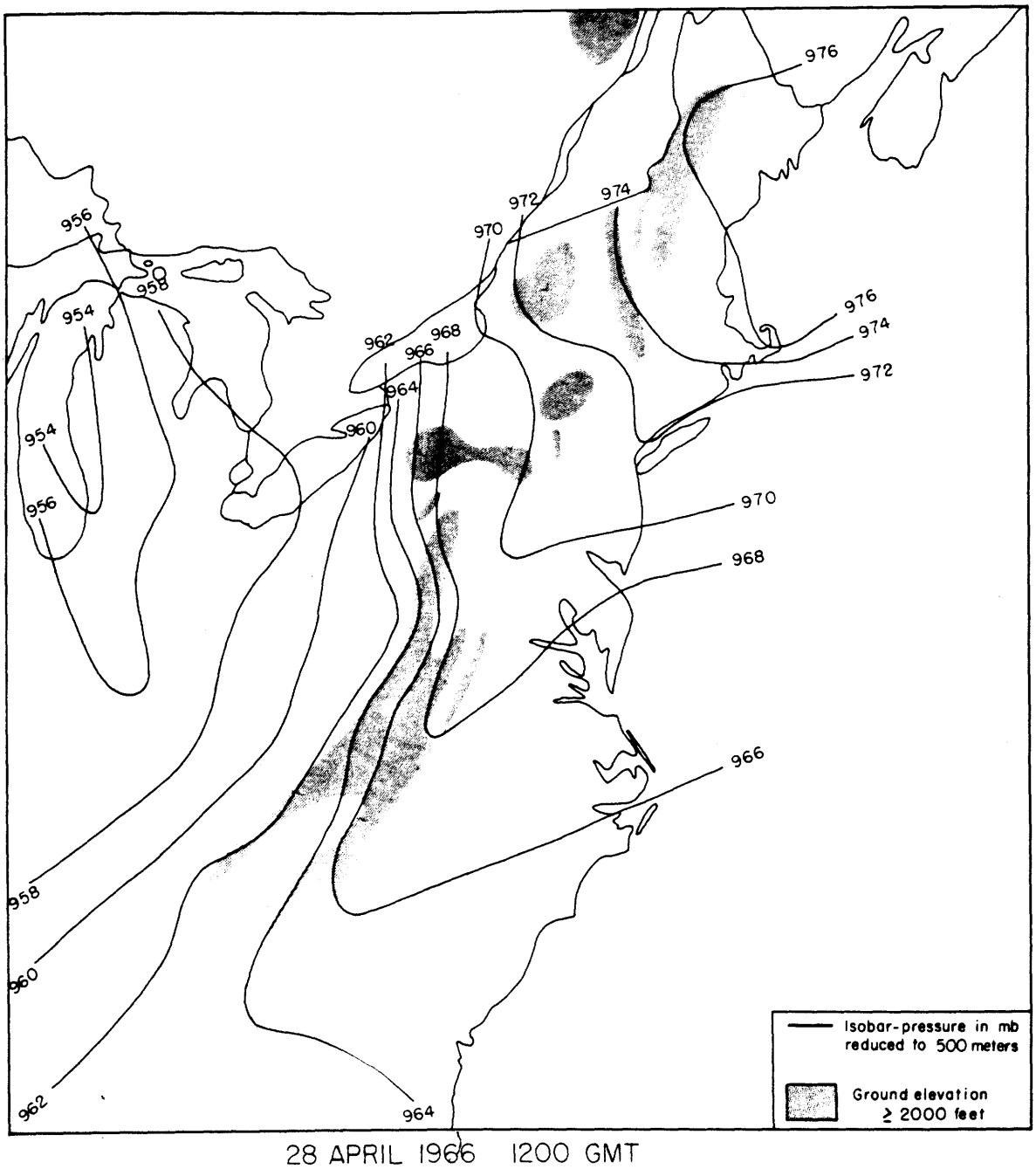

Figure 7. Analysis of pressure reduced to the 500-meter level

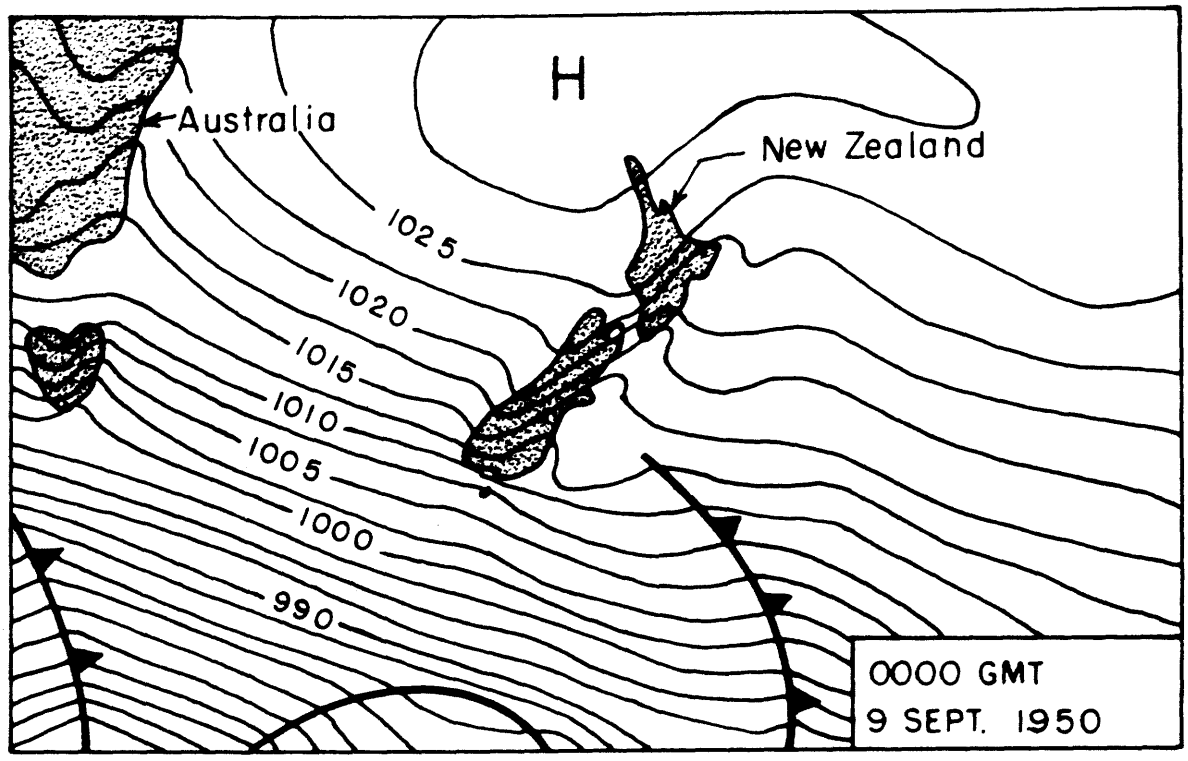

Figure 8. Example of an orographic pressure ridge associated with the New Zealand Alps

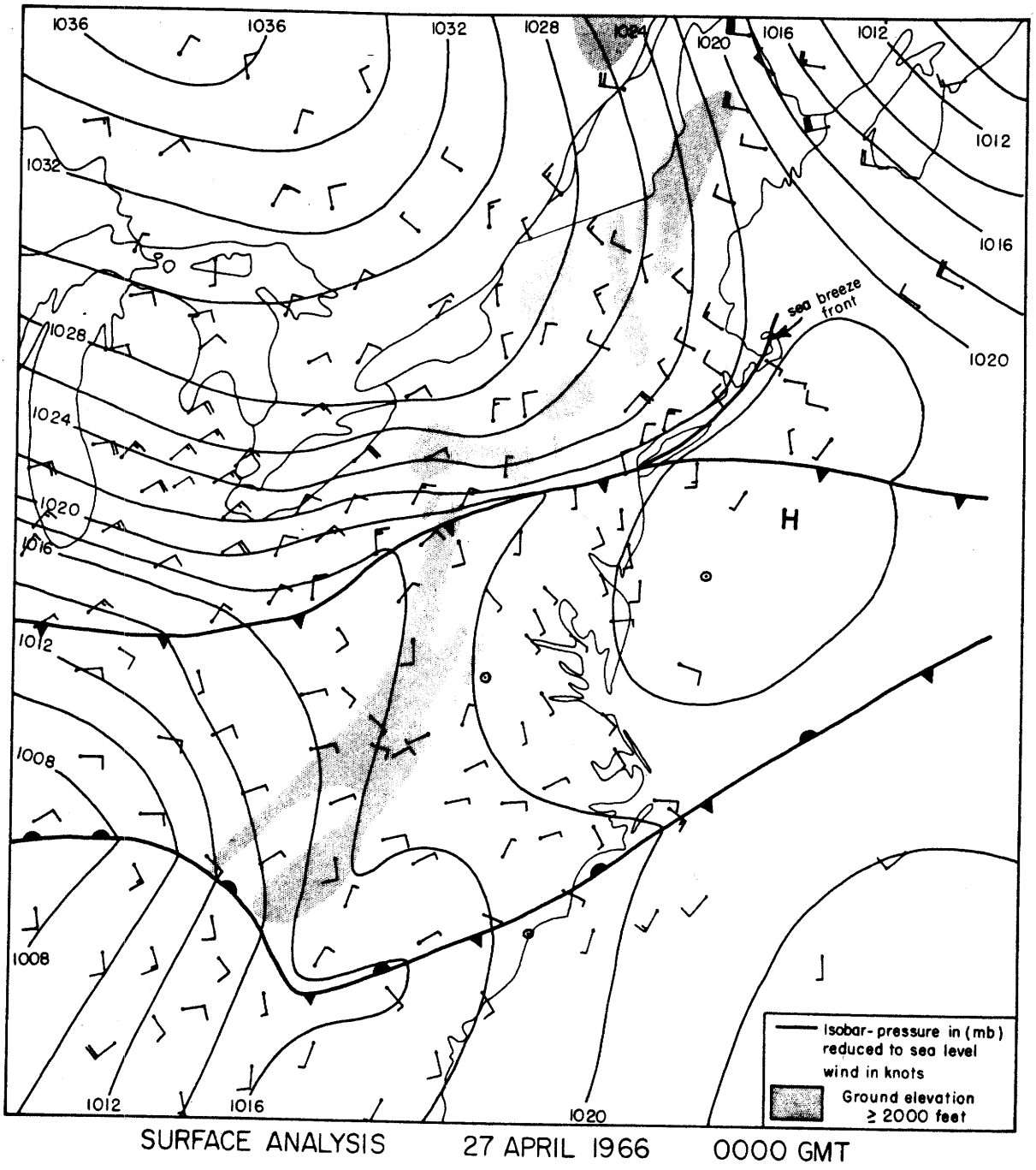

Figure 9. Case study

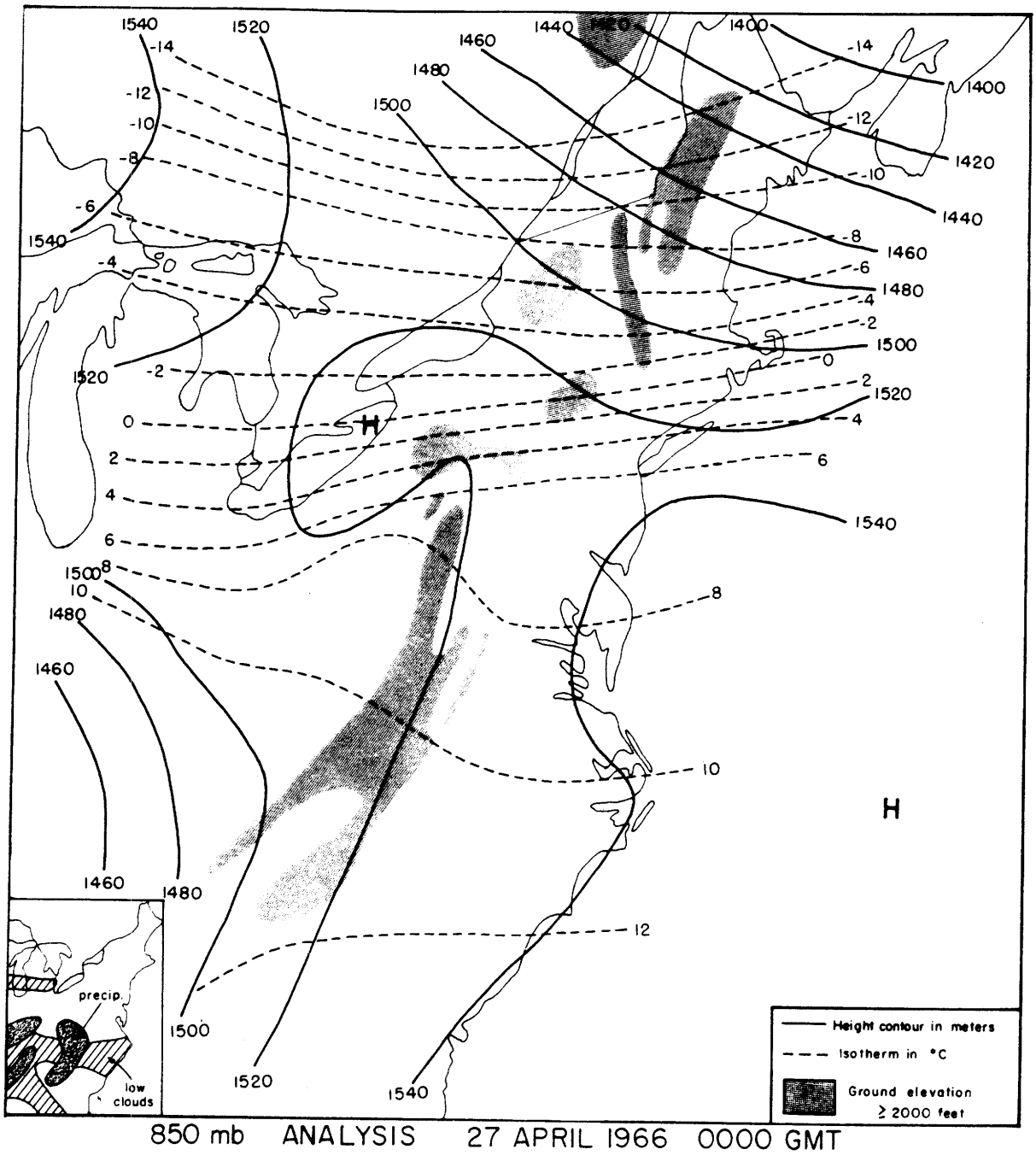

Figure 10. Case study

North Carolina. By 0600 GMT this ridge had disappeared. Low clouds and precipitation are associated with the southern frontal system, while the cold front has very little cloudiness.

27 April 1966 1200 GMT (Figures 11 and 12)

The cold front has pushed southward faster to the east of the mountains than to the west. This difference in speed has resulted in an S shape to the front— a characteristic of fronts associated with ridges. Indeed, to the north of the front, a corner ridge has formed on the windward side of the mountains, and a trough on the lee side. In addition, the pressure gradient across the Appalachians has increased. A strong current of cold air is flowing westward. Because of its long fetch over water, the cold air temperature is equal to the water temperature. (Appendix C gives the water temperature distribution for this case.) The only exception to the east wind is a narrow zone along the Appalachian slopes in Virginia. The wind in this region is blowing from the northeast, parallel to the mountain range and perpendicular to the isobars. This narrow zone is a characteristic of the pressure ridge in this area.

The frontal system to the south has moved northward and is merging with the cold front. Low clouds and precipitation are widespread west of the Appalachians but are confined to the two frontal zones to the east.

At the surface the cold air has continued moving southward, especially from New York to Virginia. However, the 850 mb pattern has directed the cold air at 850 mb toward the east, rather than

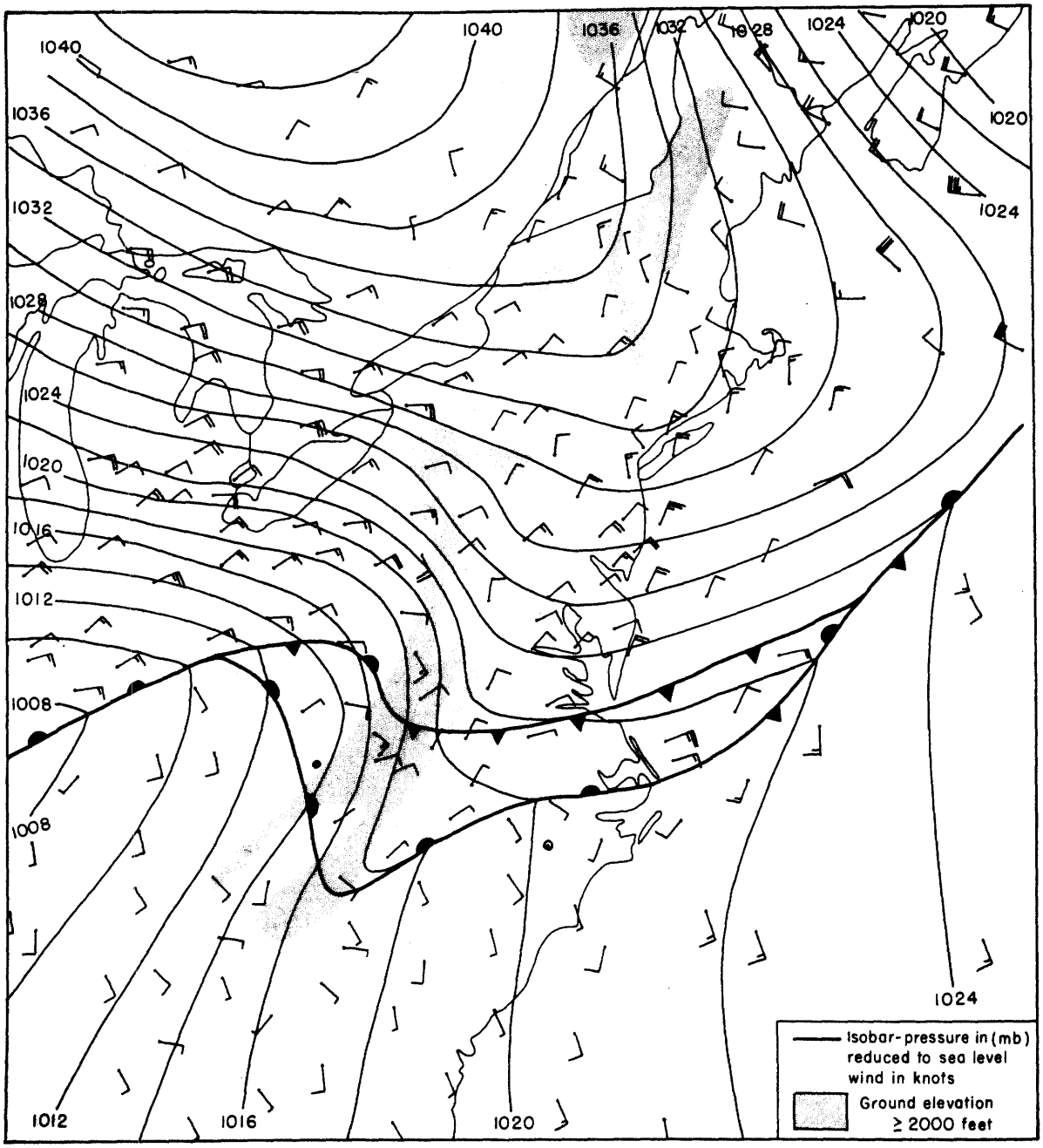

Figure 11. Case study

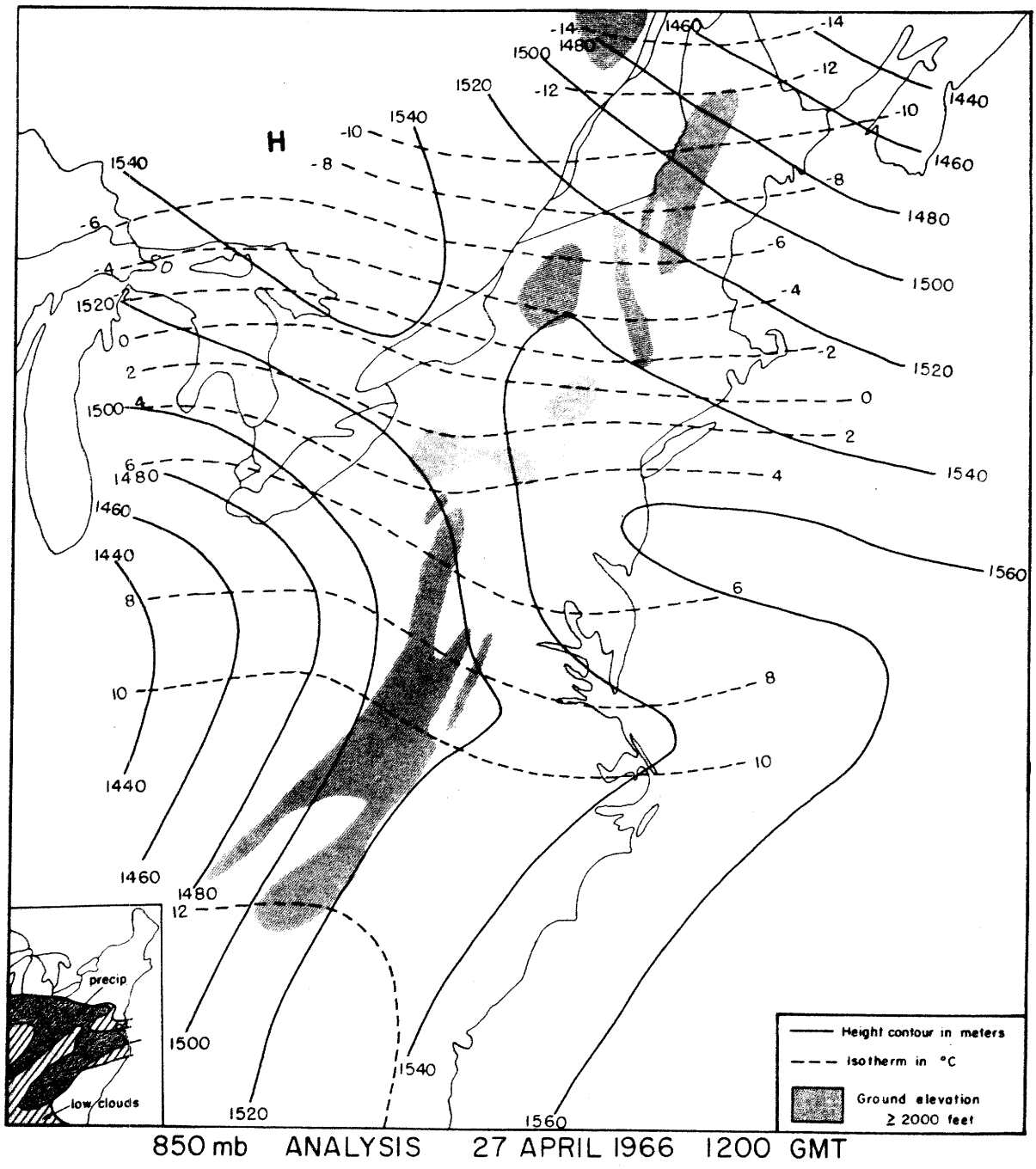

Figure 12. Case study

toward the south. This differential movement of cold air produced a low-level inversion from New York to Virginia.

28 April 1966 0000 GMT (Figures 13 and 14)

The two fronts have completely merged. Between the Appalachians and the coast the front is moving southward, while to the west it is moving northward. This differential movement has made the S shape more pronounced. The S shape of the front can even be seen at the southern edge of the low cloud distribution. Over the ocean the front is stationary. Ship data indicates that it has stalled along the northern edge of the Gulf Stream.

Diurnal temperature changes in the cold air have been reduced by low clouds and precipitation mostly confined to north of the front. Hence, a temperature contrast of around 30°F has developed between the cold and warm air. Precipitation is associated with a region where warm advection at 850 mb is coincident with positive vorticity advection at 500 mb. A band of precipitation is located along the mountains, also.

The corner ridge north of the front has intensified considerably. The pressure gradient across the mountains is also stronger. In eastern Pennsylvania the pressure gradient is very flat. This feature appeared in several other cases and may be the result of the change in orientation of the mountain range across this region. Surface winds in eastern Pennsylvania show no deviation toward the south, although from Washington, D.C. southward, the zone of winds blowing parallel to the mountains has expanded. Because the air of this zone originated further north (where the water temperature is lower) it

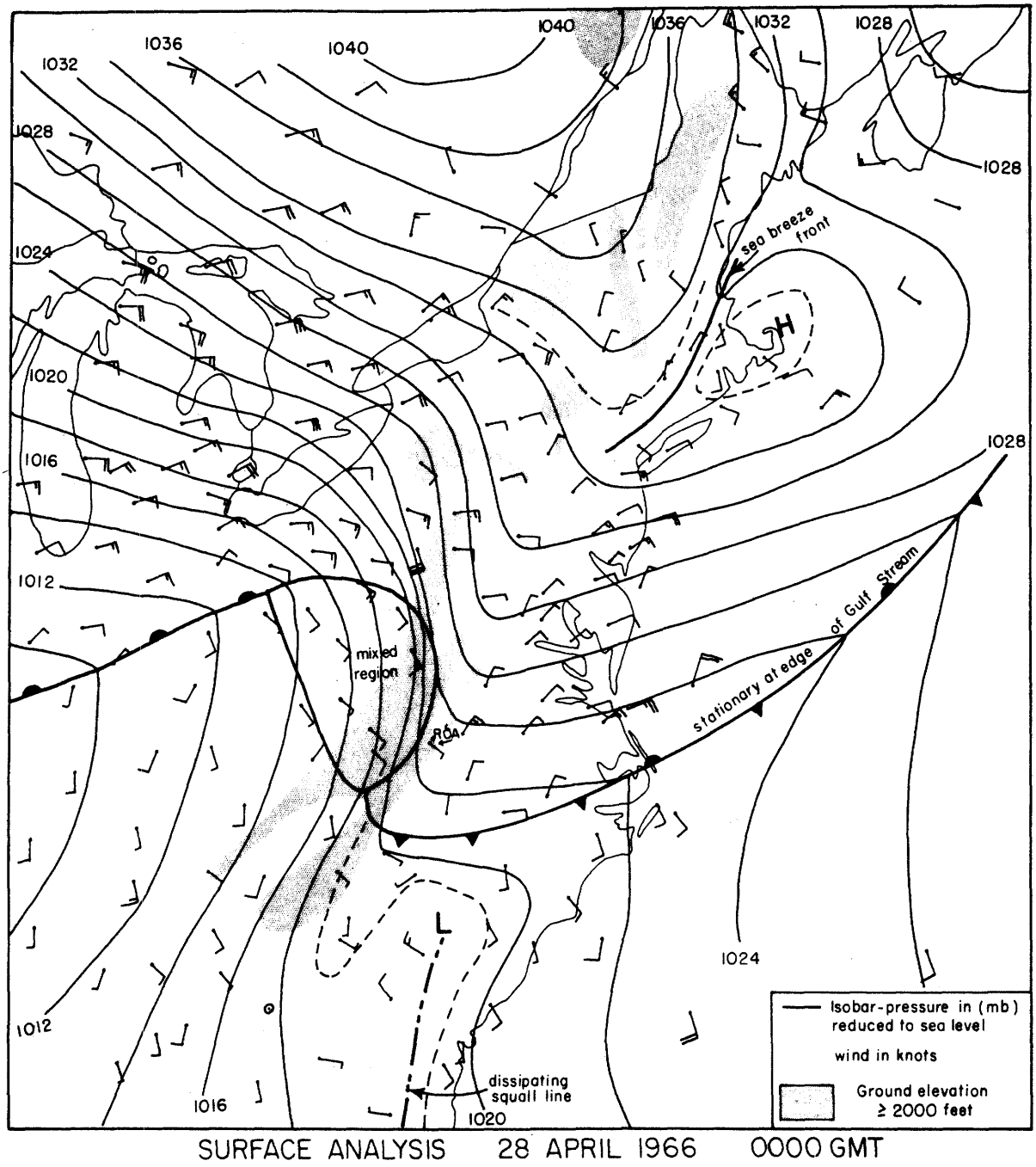

Figure 13. Case study

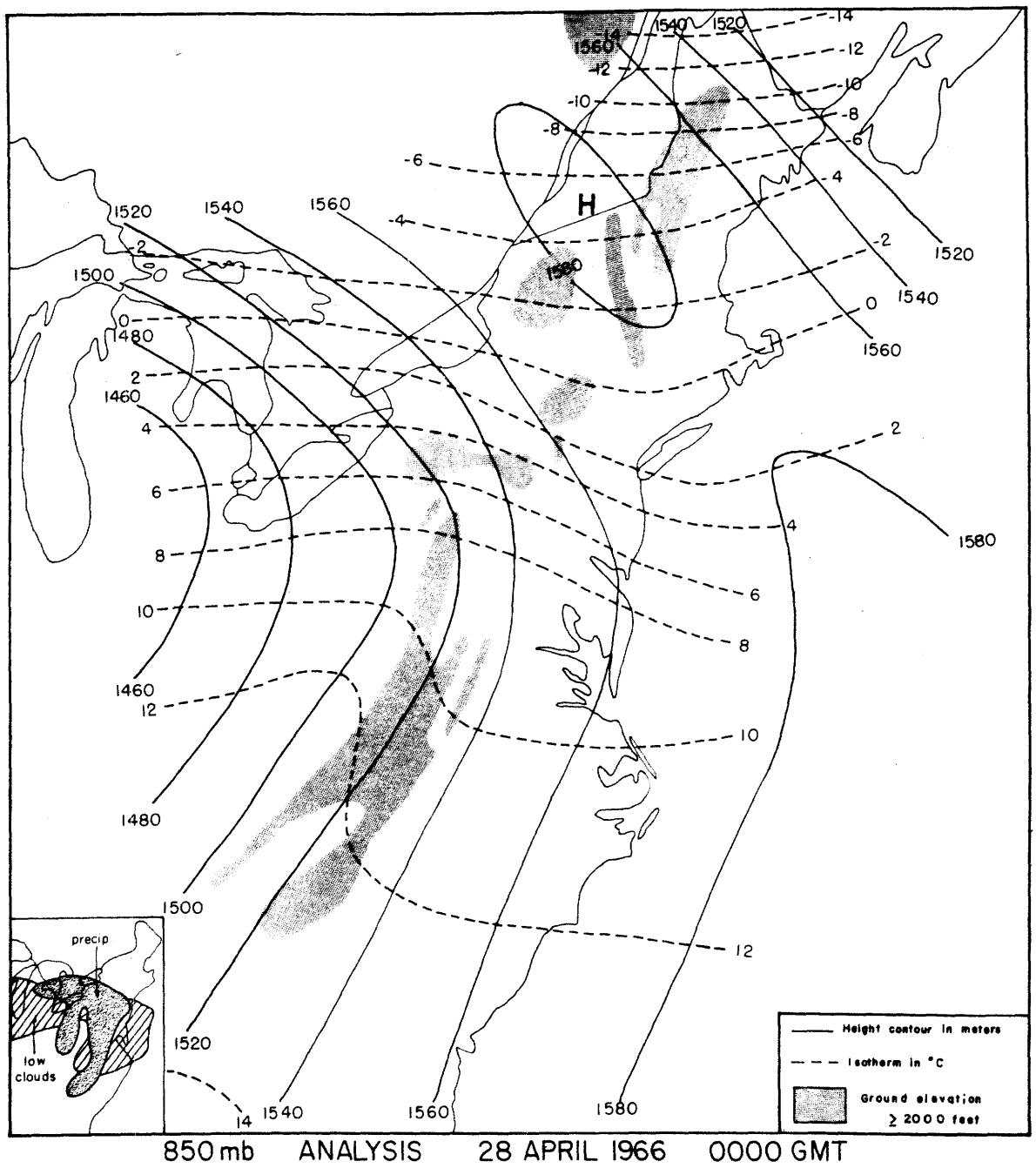

Figure 14. Case study

has a slightly colder temperature.

The only station in this zone not reporting north-northeast winds is ROA which reported southeast winds for the whole period. Possibly, this wind direction can be explained by a channeling effect of the local valley which runs in the same direction as the reported winds.

Of special interest is the region in West Virginia which has been labeled "mixed region." Surface winds in this mixed region are southeast, indicating an air trajectory over the mountains. In addition, the high ceilings can be explained by a current flowing down a slope. Temperatures and dew points are about halfway between those of the warm and cold air. Although the release of latent heat into air coming over the mountain might explain the higher temperatures, such a process cannot explain the higher dew point. Hence, the weather in the mixed region appears to be a mixture of the cold air to the east and the warm air to the west.

This mixed region could be explained at this particular time by local meteorological phenomena unassociated with the pressure ridge. However, its persistence in this case, and its appearance in other regions in several of the pressure ridge cases studied suggest that it is a recurrent phenomenon associated with the pressure ridge.

Two explanations of the mixed region seem plausible: (1) The cold air coming over the mountains is considerably mixed with the warm air above. (2) The warmer air along the coast flows over the colder air next to the mountains and then over the mountains themselves.

Hence, it is this warmer air that is observed in the mixed region. No conclusive evidence backing only one of these possibilities has been found.

28 April 1966 1200 GMT (Figures 15 and 16)

The high to the north has continued to move eastward, while the low that was over the northern plains has moved northeastward. The movement of this low has caused the trough west of the mountains to disappear. However, the strong pressure gradient across the mountains, as well as the ridge to the east, still remains.

East of the Appalachians, the cold air has continued to move southward over the land. To the west, the warm front has advanced northward. The mixed region in West Virginia is still present but diminished in size. A cold front with a pre-frontal squall-line is moving into the analysis area from the west.

At 850 mb a broad flow of warm air is flowing northward. As the primary cyclone moves northeastward, the 850-mb winds are shifting from the south-southwest to southwest. In the isotherm pattern there is a cool region between the Appalachians and the coast. However, even if this cooling is extrapolated linearly to sea level, it cannot account for the pressure ridge.

There is a suggestion of a weak Type B cyclogenesis off the coast. However, this cyclone only intensifies slowly in the next 18 hours.

The ridge has changed its character considerably since 0000 GMT. North of Washington, there is still a corner ridge present. In this region surface winds are mostly from the east. South of Washington

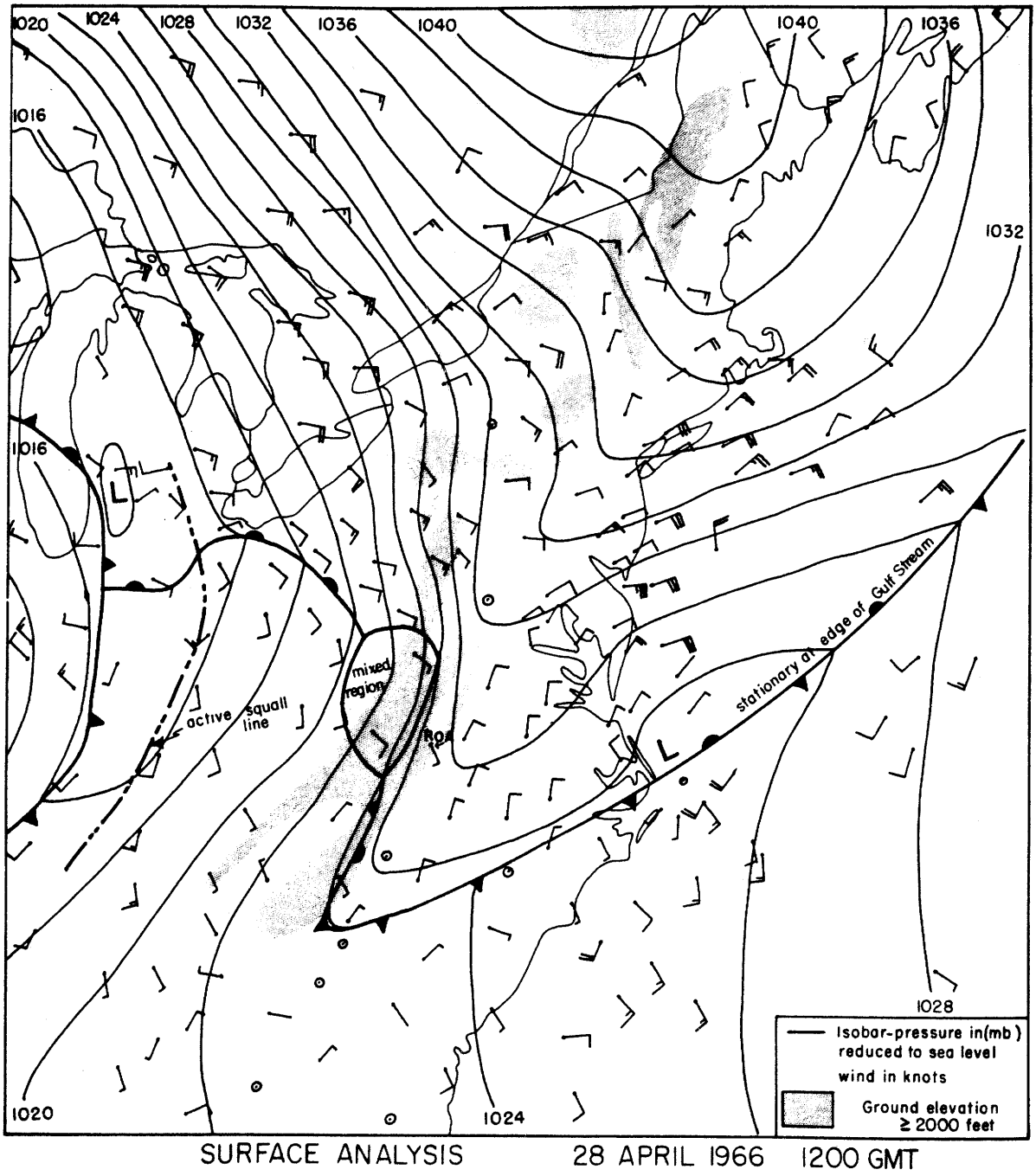

Figure 15. Case study

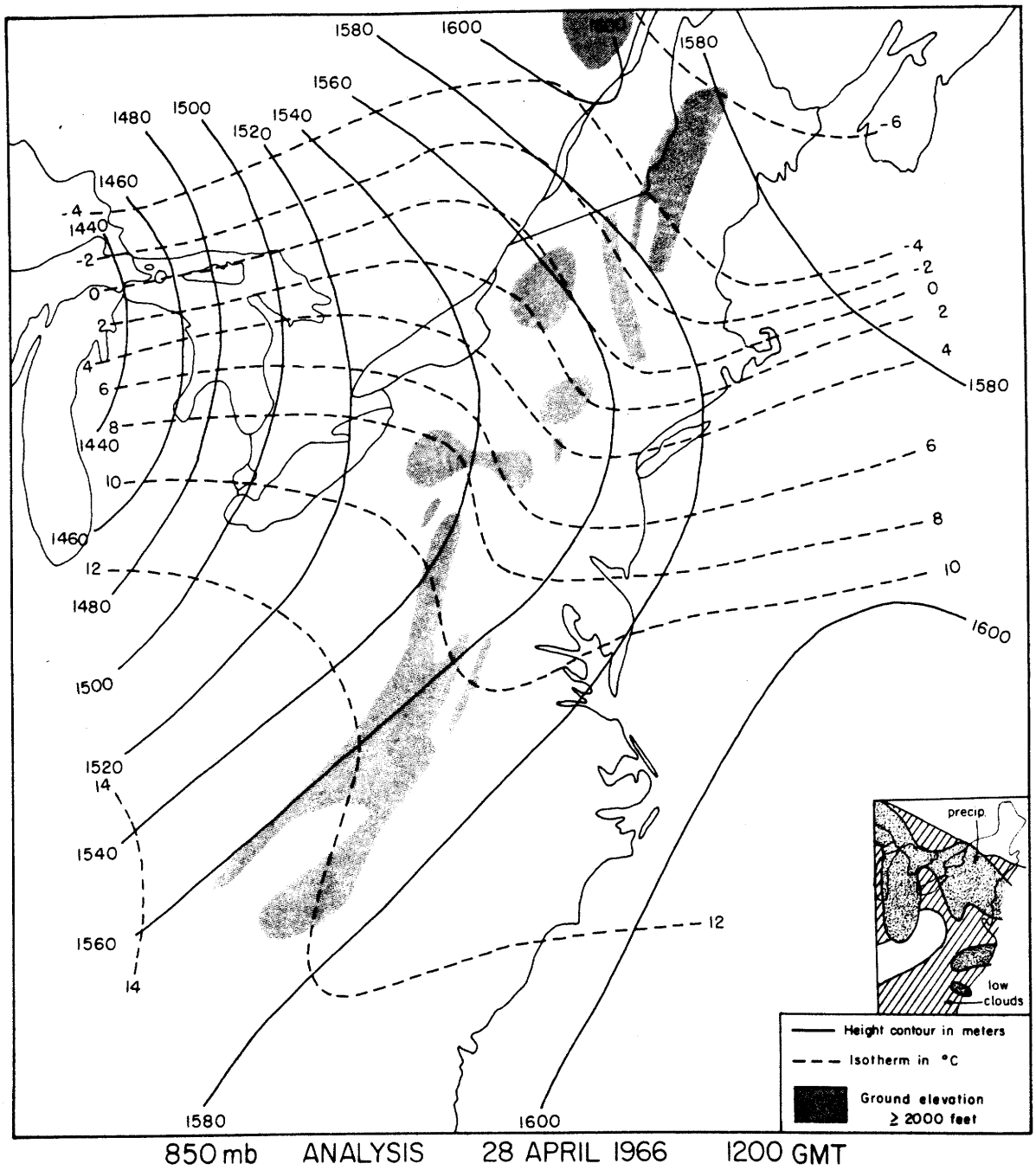

Figure 16. Case study

a wedge ridge has developed. Here north-northeast to northeast surface winds extend all the way to the coast.

The major precipitation region is now over Pennsylvania and Ohio, where warm advection is occurring. West of the Appalachians, the precipitation seems to be associated with the warm and cold fronts. To the east of the mountains, precipitation is completely separated from the front,possibly because the location of the front at the surface is considerably further south than the region of strong thermal contrast at 850 mb and above.

4.6 Inversion Height

Figures 17 and 18 show the potential temperature as a function of height at 0000 GMT and 1200 GMT 28 April 1966 for each radiosonde station. The pressure-height coordinate extends from the surface to 800 mb. A marked inversion can be seen at almost all of the stations in the cold air, while no sharp inversion exists for stations in the warm air. In the north-south direction, the base of the inversion slopes upward from the front. In the east-west direction the height of the inversion has a remarkable variation. Stations along the coast have inversion bases which are much closer to the ground than stations between the coast and the Appalachians (for instance, compare WAL and IAD). Moreover, on the west side of the Appalachians the inversion base is lower again (for instance, compare PIT and IAD, especially in Figure 18). This same pattern was found not only at other times in this case, but in other cases as well.

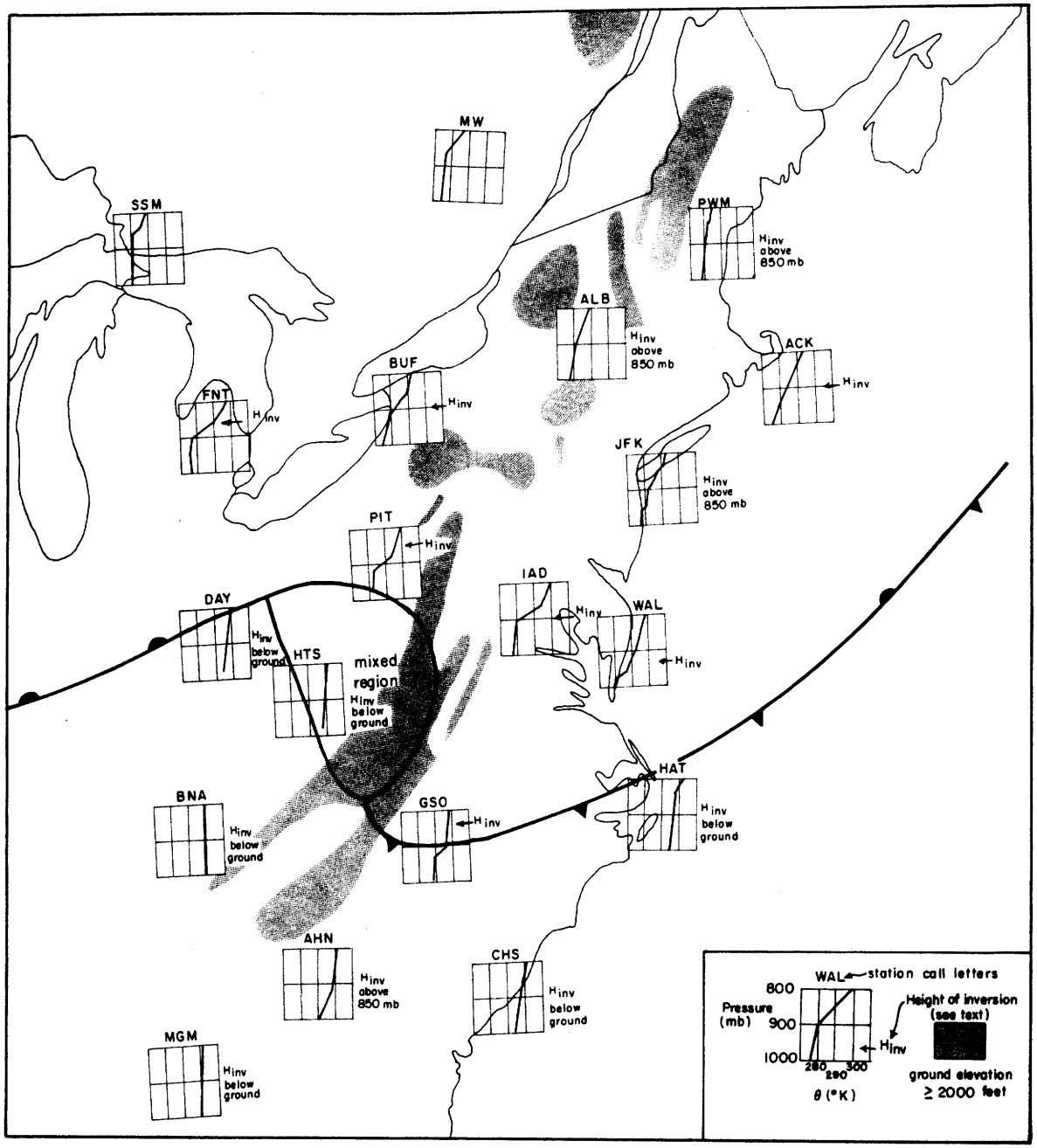

VARIATION OF POTENTIAL TEMPERATURE WITH HEIGHT 28 APRIL 1966 0000 GMT

Figure 17. Case study

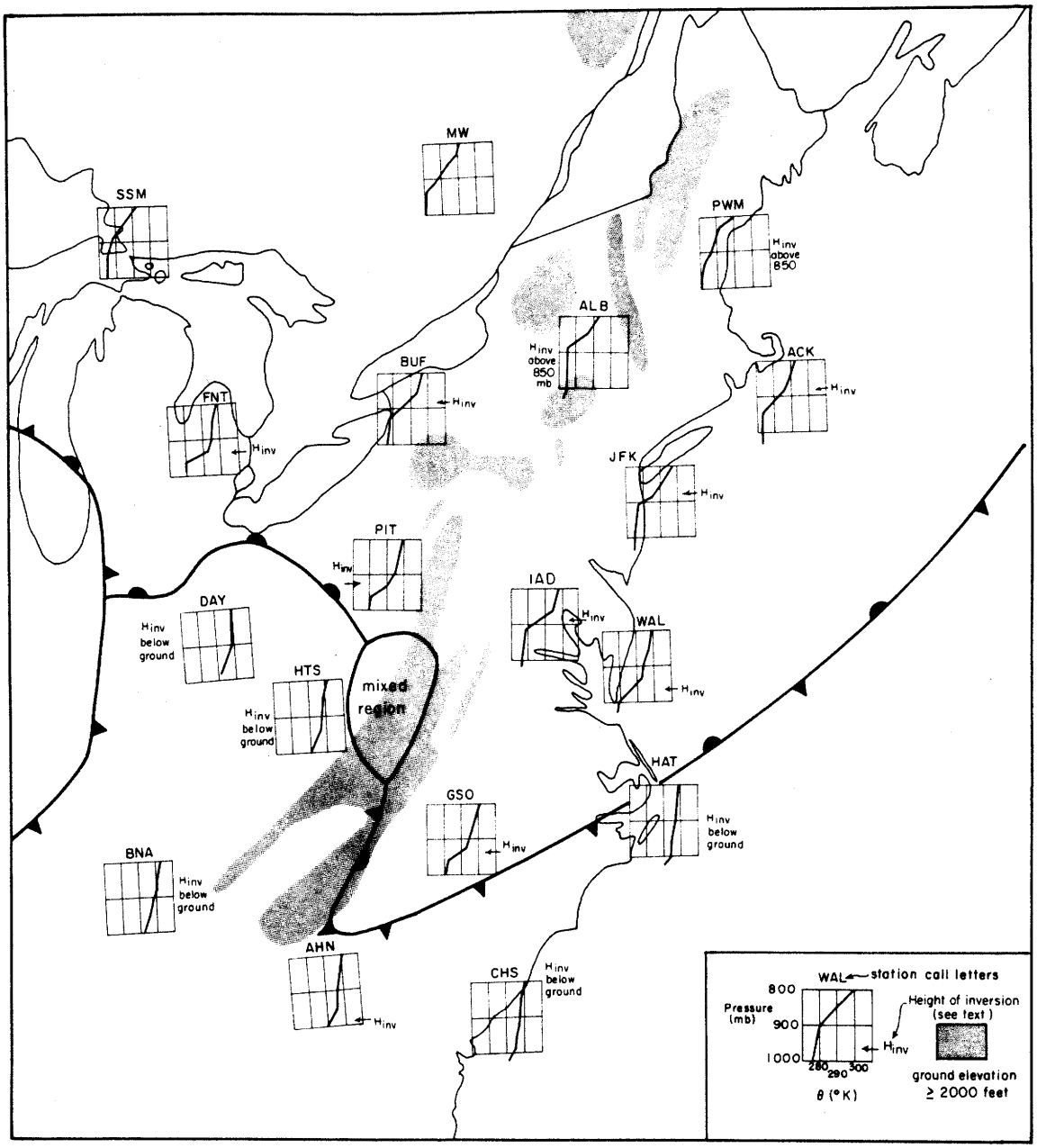

Figure 18. Case study

In order to determine the effects of these changes in the inversion height on the sea-level pressure field, let us consider the conditions at WAL and IAD at 1200 GMT 28 April 1966. Figure 16 shows that WAL has a higher 850-mb height than IAD. Figure 15 indicates that IAD has the higher 1000-mb height (assuming the 1000-mb height field has approximately the same shape as the surface pressure field). Hence, the 850-1000-mb thickness must be smaller at IAD than at WAL. Consequently, the 1000-850-mb mean temperature is lower at IAD.

Consider now the soundings at IAD and WAL given in Figure 18. Both soundings have approximately the same potential temperature at 1000 mb and 850 mb. Hence, the lower mean temperature (or, equivalently, lower mean potential temperature) at IAD noted above is directly related to the higher inversion over that station. In conclusion, it appears reasonable that the pressure ridge is a necessary consequence of changes in the inversion height aloft.

Unfortunately, the density of radiosonde stations is too low to separate distinctly the north-south variation of the inversion height from the east-west variation by the type of analysis presented in Figures 17 and 18. Therefore, another type of analysis was carried out in order to test the above conclusions concerning the inversion height.

Let us idealize the inversion as a temperature discontinuity, and assume that between the surface and 850 mb the temperature varies linearly with height as shown in Figure 19. On the basis of these

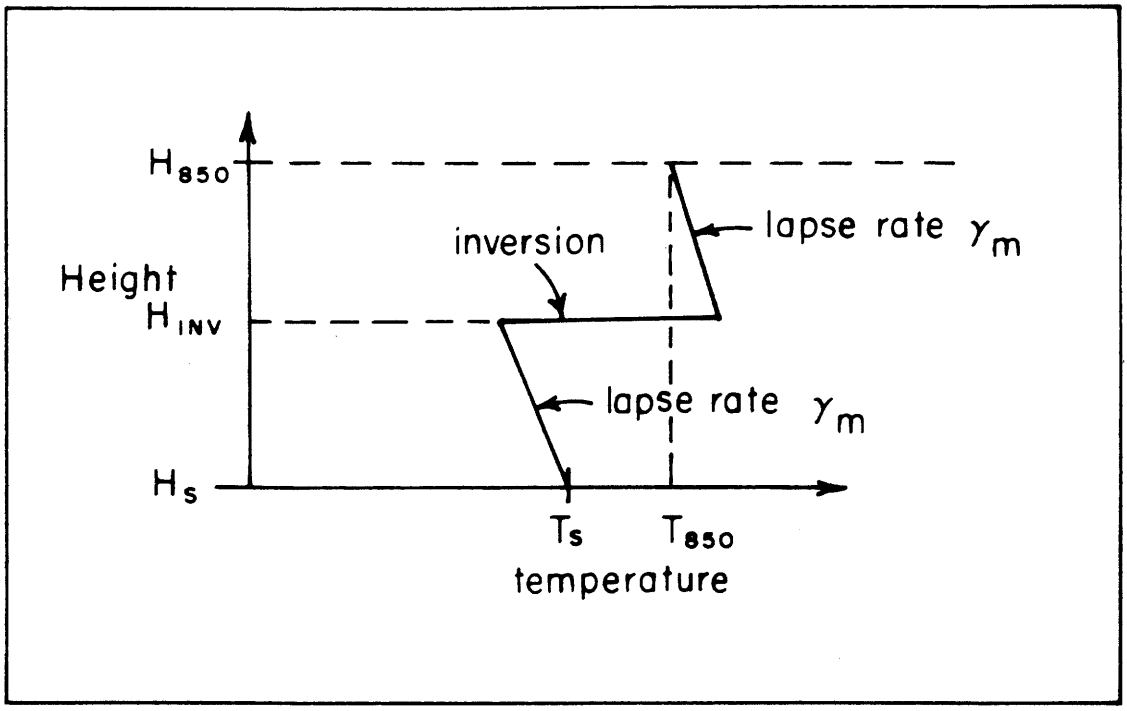

Figure 19. Idealized inversion

assumptions, a theoretical height of the inversion, H_{INV}, can be calculated from observed data, once the lapse rates in the warm and cold air are assigned.

An examination of Figures 17 and 18 shows that in the region of the pressure ridge the lapse rate in the cold air is approximately moist-adiabatic. It is more difficult to choose a single lapse rate for the warm air, but again moist-adiabatic seems to be the best approximation. The calculations were based on station pressures to avoid reduction problems. Station pressures, P_S, were found by subtracting the altimeter correction from the altimeter setting for each station (Bellamy, 1944). The observed surface temperature, T_S, and dew point, T_{DP}, were used as reported. 850 mb temperatures, T_{850}, and heights, H_{850}, were obtained by interpolation from the analyses.

First, the mean virtual temperature, $\bar{T}_v$, from the surface to the 850-mb surface was calculated for each station from the hypsometric formula

$$\bar{T}_v\,(^\circ K) = \frac{H_{850} - H_s\,(m)}{29.27 \ln (P_S/850)} \qquad (4.1)$$

where H_S is the station elevation.

In order to find the mean temperature, $\bar{T}$, it was assumed that the surface dew point was an adequate measure of the moisture above a station. Since this correction from $\bar{T}_v$ to $\bar{T}$ is a second-order correction, this assumption is justified. The equations were as follows:

$$\bar{T}\,(^\circ C) = \frac{\bar{T}_v}{1.0 + 0.6r} - 273.16 \qquad (4.2)$$

where

$$r = \frac{3.80}{P_s} \exp\left[\frac{19.7 \times T_{DP}}{T_{DP} + 273.16}\right] . \qquad (4.3)$$

The inversion height can be found by straightforward algebraic manipulations (the derivation is given in Appendix D); the result is

$$H_{INV} = -\frac{C}{B} \qquad (4.4)$$

where

$$C = \frac{\gamma_m (H_{850}^2 - H_s^2)}{2} - T_s H_s + T_{850} H_{850} - (H_{850} - H_s)\overline{T} \qquad (4.5)$$

$$B = T_s - T_{850} + \gamma_m (H_s - H_{850}) .$$

γ_m is the moist adiabatic lapse rate.

The calculated values of H_{INV} for each radiosonde station are given in Figures 17 and 18. In the warm regions where an inversion is not present, H_{INV} is predicted to be below the ground. Similarly, in regions to the north where the inversion was above 850 mb, no inversions are predicted. For stations reporting inversions, H_{INV} is generally predicted to be somewhere in the region of sharpest potential temperature rise with height. There are, however, two

notable exceptions: GSO and PIT, both in Figure 17. An investigation traced these discrepancies to a difference of around 1.5 mb between the reported radiosonde station pressure (which is used in determining the 850-mb height) and the official station pressure (which is used directly as data for H_{INV}).

Since many conclusions in this thesis are based upon analyses of H_{INV} , it is important to establish the probable error of this method. Only errors in measuring surface pressure are considered. If the reported station pressure is off by 0.5 mb, then the corresponding error in the 1000-850-mb thickness is four meters, or equivalently, a mean temperature error of 0.8°C. In Appendix D, it is shown that a 0.5°C error in mean temperature results in around a 60 meter error in H_{INV} . Hence, the probable error is ±100 meters. Since H_{INV} varies in magnitude from zero meters to 1500 meters, the probable error is not significant.

H_{INV} was calculated for each synoptic station in the eastern United States. Analyses of H_{INV} for the same observation times as Figures 17 and 18 are given in Figures 20 and 22.

These analyses confirm the conclusions reached on the basis of the radiosonde data in Figures 17 and 18. H_{INV} intersects the ground near the location of the front, as one would expect. To the north, H_{INV} is inclined upward to the north with a slope of 1:300. Over the water the data suggest that the inversion height contours parallel the front. A very pronounced inversion height maximum extends along the whole length of the Appalachians. The inversion height decreases rapidly on the lee side of the Appalachians.

It is difficult to compare the inversion height with the terrain elevation in Figures 20 and 22. Such a comparison can be made more easily in Figures 21 and 23 where the variation of the terrain elevation, inversion height (H_{INV}), and sea-level pressure along two lines perpendicular to the Appalachians is given. (Figures 20 and 22 show the location of these lines: ERI to DOV and DAY to HAT.)

In Figures 21 and 23, the sea-level pressure has a maximum on the windward slopes; i.e., the characteristic feature defining a pressure ridge. In Figure 21 the inversion height on the ERI to DOV line follows approximately the outline of the ground elevation. The cold air depth increases toward the mountains at the coast. On the windward slope the depth is approximately constant, but decreases at the crest of the mountains. On the lee side there is little change in the depth. On the line from DAY to HAT the inversion intersects the ground on both sides of the mountains because, as can be seen in Figure 20, both DAY and HAT are in the warm air. As noted along the ERI to DOV line, the cold air depth from right to left in Figure 21 at first increases on the windward side, and then decreases as the mountain summit is reached.

In Figure 23 the sea-level pressure and inversion height have some features similar to those noted in Figure 21. The main differences along the ERI to DOV line are (1) the inversion crest is not over the mountain crest but is displaced toward the windward side, and (2) the depth of the cold air decreases significantly on the lee side of the mountains. The main difference along the DAY to HAT line is that the

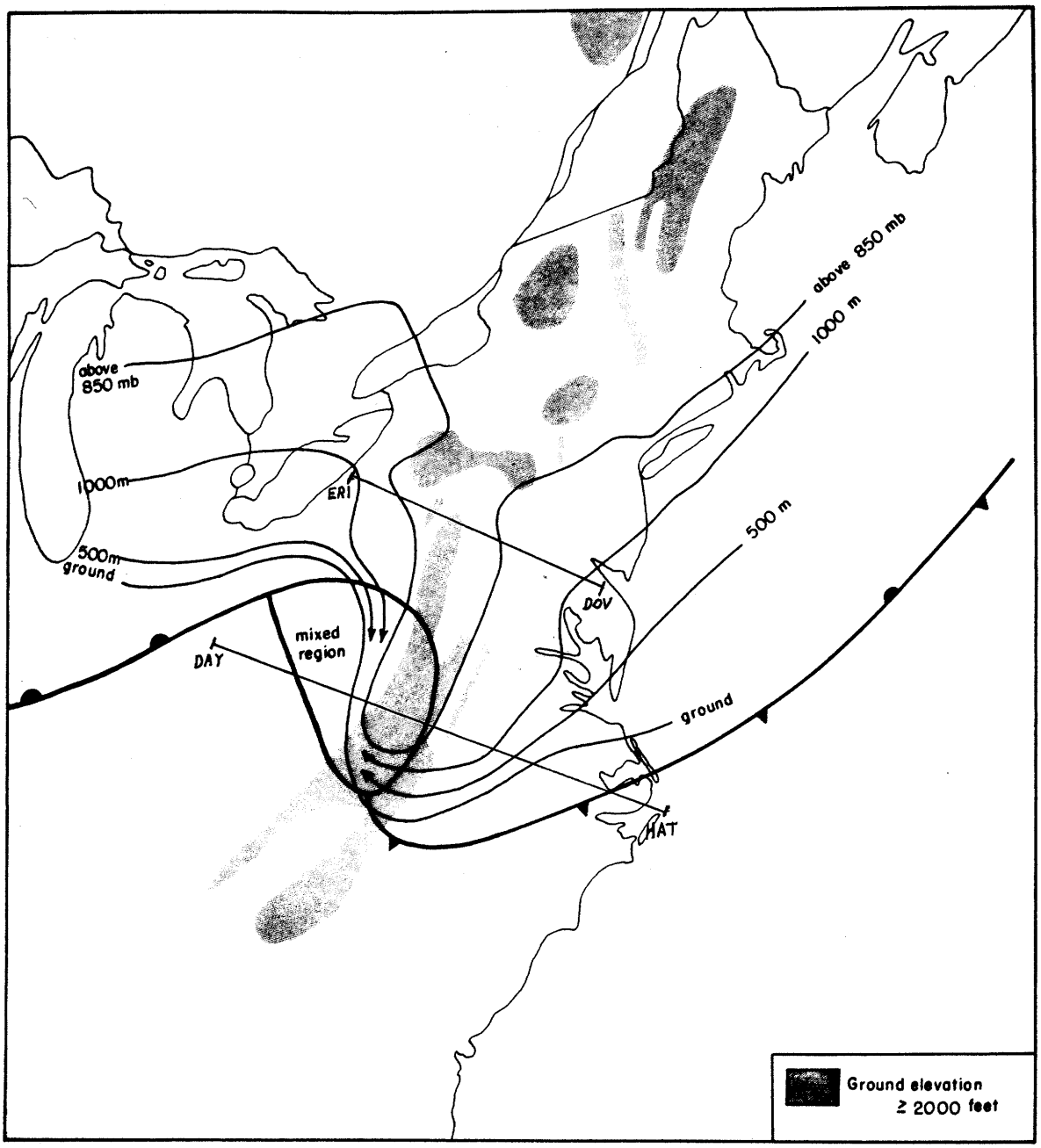

Figure 20. Case study

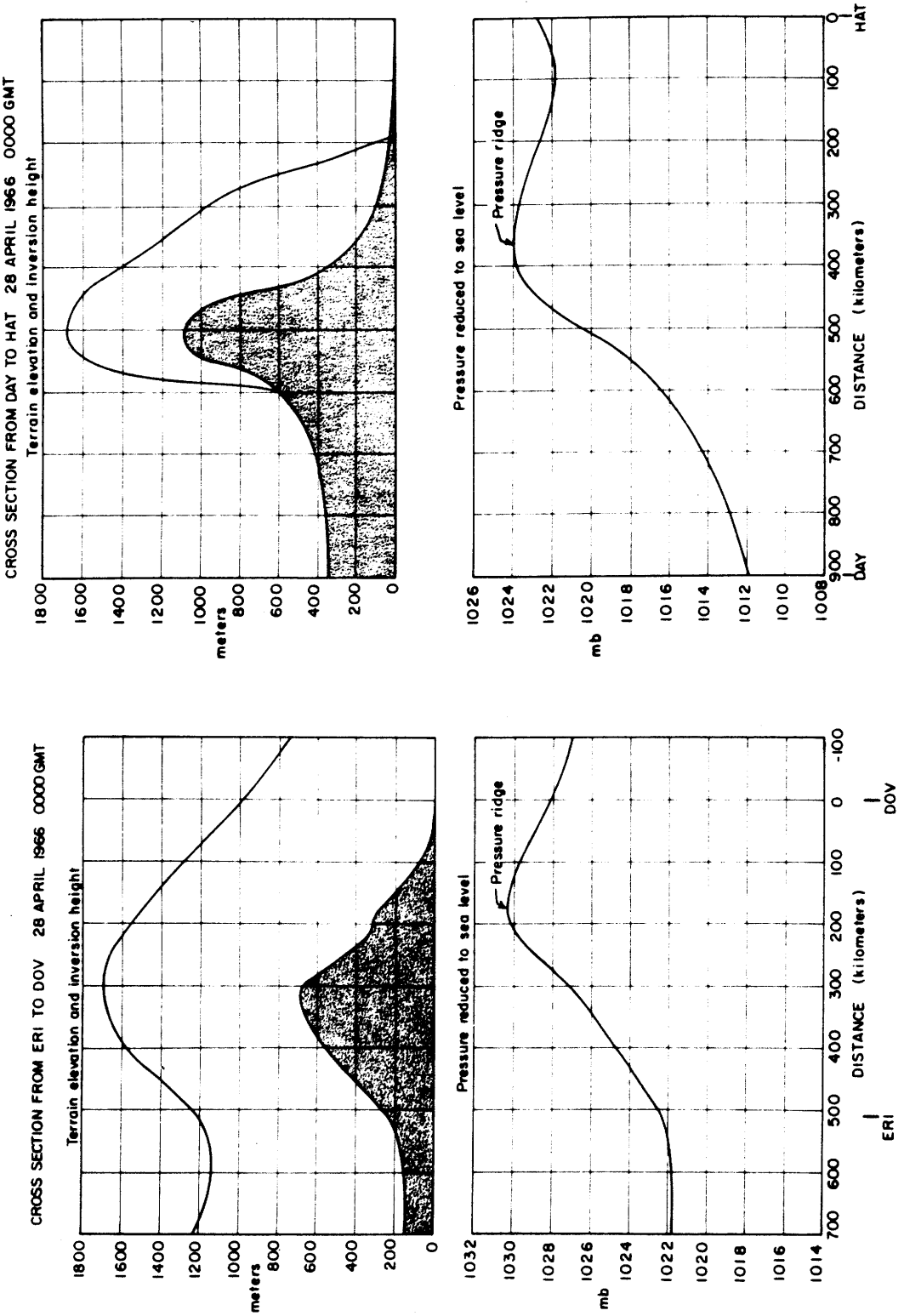

Figure 21. Case study

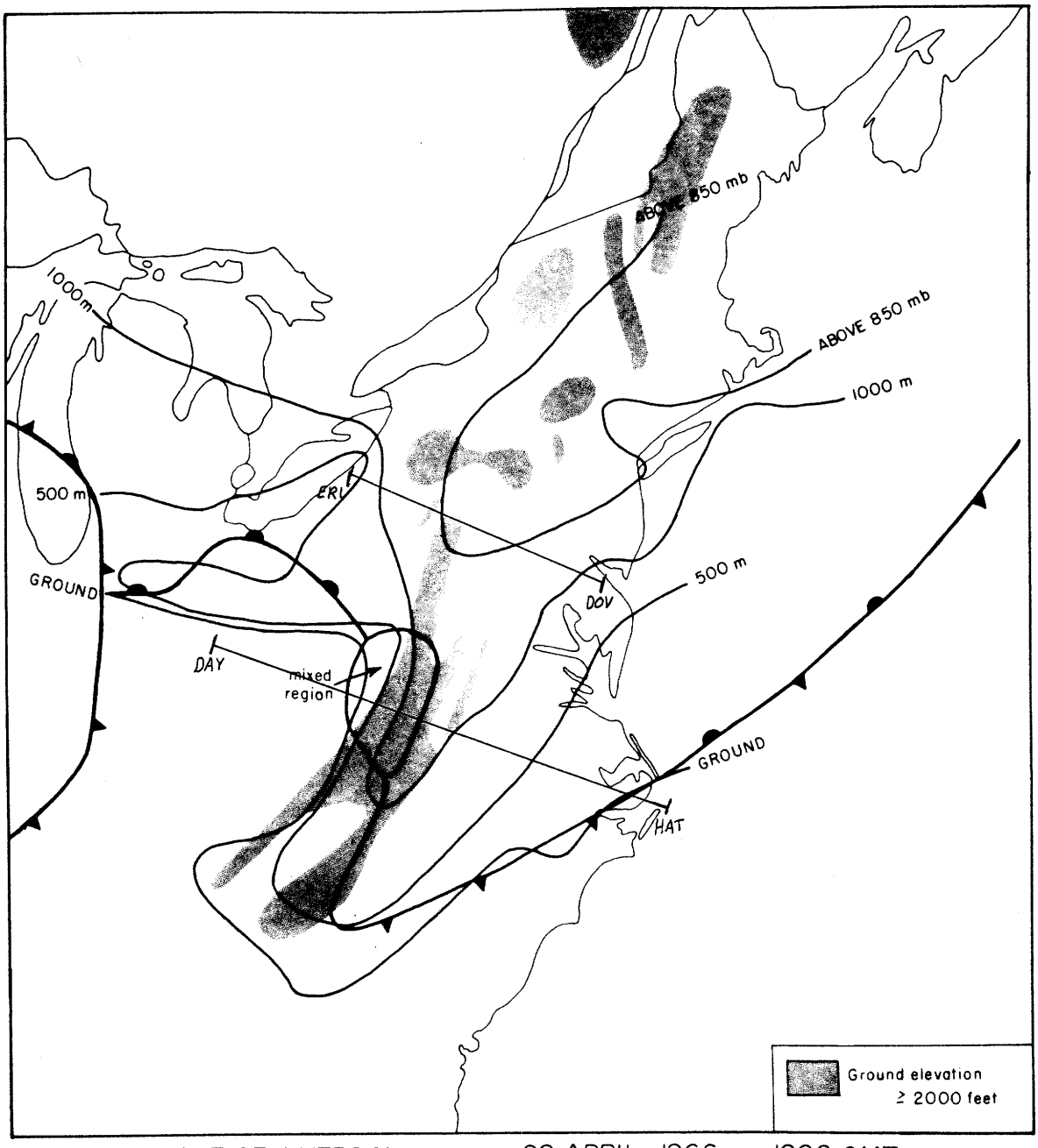

HEIGHT OF INVERSION 28 APRIL 1966 1200 GMT
Calculated from 850 mb and surface data.

Figure 22. Case study

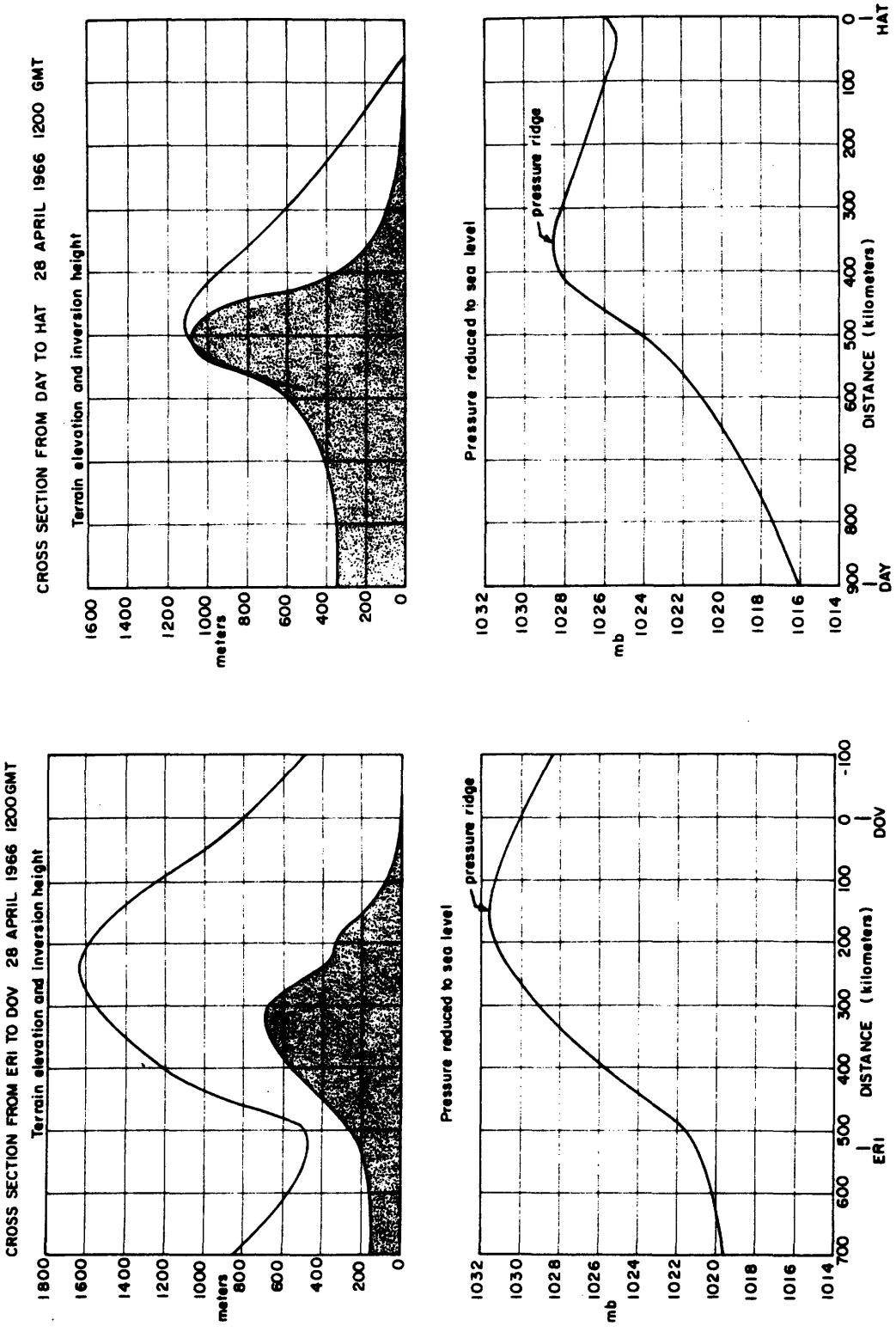

Figure 23. Case study

inversion height is lower than twelve hours earlier. In fact, now it does not extend above the mountain crest at all. Evidently, the cold air has been blocked by the mountains. Surface data supporting the conclusion that blocking is occurring is given in Section 4.7.

In Figure 21 the inversion crest is located right over the mountain crest, while in Figure 23 it is displaced further toward the east. The author feels that the inversion heights given in Figure 22 and 23 are more reliable than those in Figures 20 and 21 because, as noted above, there was better agreement between H_{mw} and the radiosonde data at 1200 GMT (Figure 22) than at 0000 GMT (Figure 20). It is felt, therefore, that the inversion crest in reality is situated to the east of the mountain crest. However, more accurate observations are required to verify this observation.

The above cross sections were perpendicular to the mountains. However, the large-scale flow in a pressure ridge situation makes an oblique angle to the mountain range (see Figure 13, for instance). Hence, the cross sections in Figure 21 and 23 cut across the large-scale flow. For a better understanding of the pressure ridge, a study of the inversion variations along a trajectory would seem to be physically relevant, since, as a first approximation, the cold air mass flux should be conserved and temperature changes should be either adiabatic or moist-adiabatic along a trajectory.

The fundamental problem in using a trajectory technique is how to determine the actual trajectories. The use of surface observation undoubtedly would not be satisfactory since surface winds are affected

too much by surface friction to be representative of the cold airflow as a whole. In addition, upper-air observations are too scarce to be of any assistance. Since the observational data is inadequate, theoretical trajectories have been used in this investigation (see Section 4.9).

4.7 Evidence for blocking of the cold airflow by the mountains

At 1200 GMT the cold air is still flowing over the mountains in West Virginia where there is a mixed region. However, as shown in Figure 24, by 1800 GMT this mixed region has moved out of West Virginia. Warm air is now flowing in from the southwest. Figure 25 presents a detailed examination of the meteorological conditions in the West Virginia region (see the insert in Figure 25 for exact area of the United States covered in this figure). In this figure an analysis of maximum temperatures is given along with 1800 GMT observations (see Appendix E for details of the method used to determine the maximum temperatures).

The sharp contrast in weather across the mountains is brought out clearly in Figure 25. To the west, ceilings are 5000 ft or more, temperatures are in the 70's, and there are scattered thunderstorms. To the east, ceilings are below 1000 ft, temperatures are in the 40's, and a few places report drizzle. Pilot reports indicate the top of the overcast is only 4000 feet. Evidently, the warm air flows from the west up the mountain slope and then out horizontally over the cold air. The observed surface temperature decreases by more than 25°F in less than 60 miles across the mountains east of EKN.

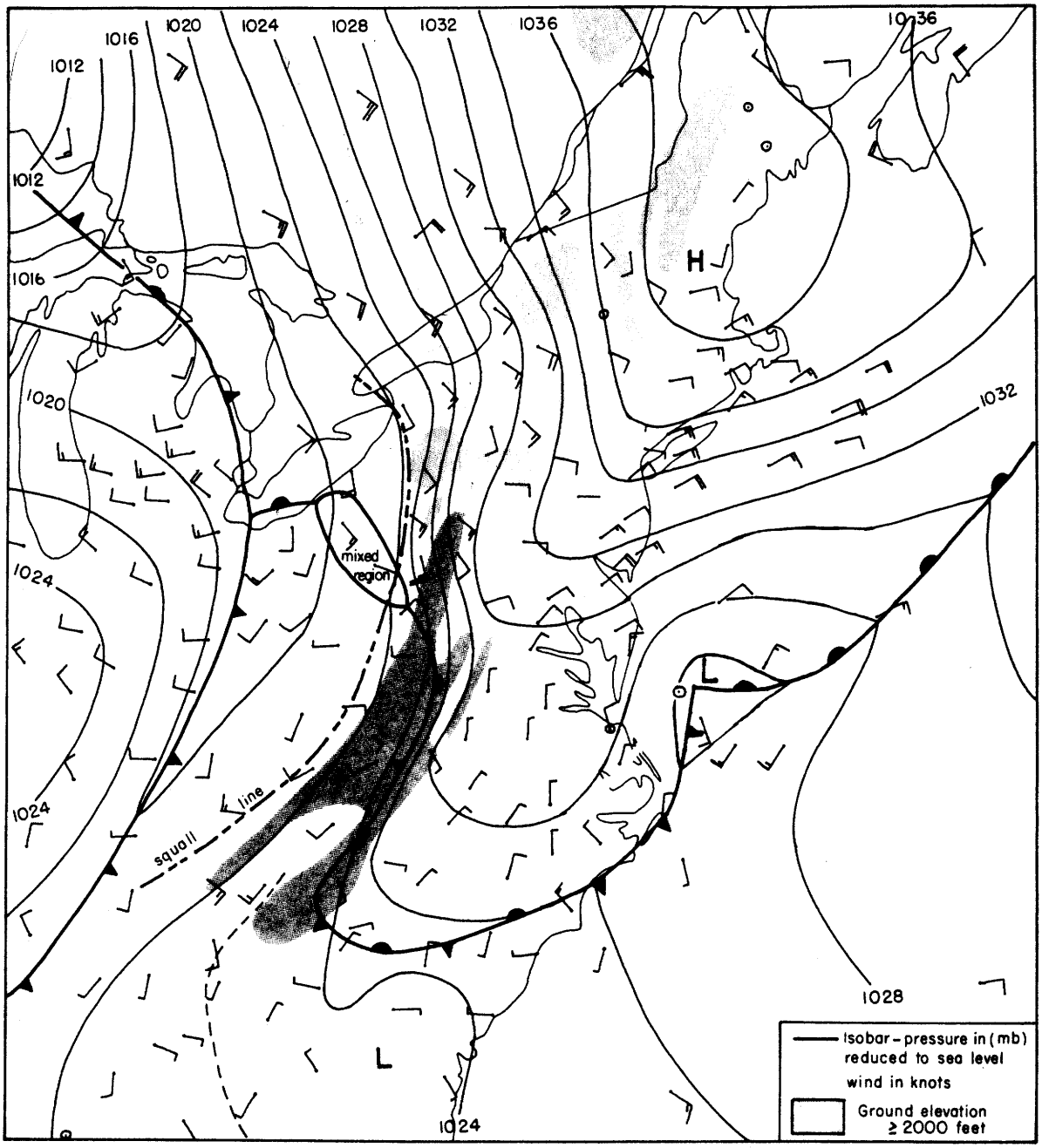

Figure 24. Case study

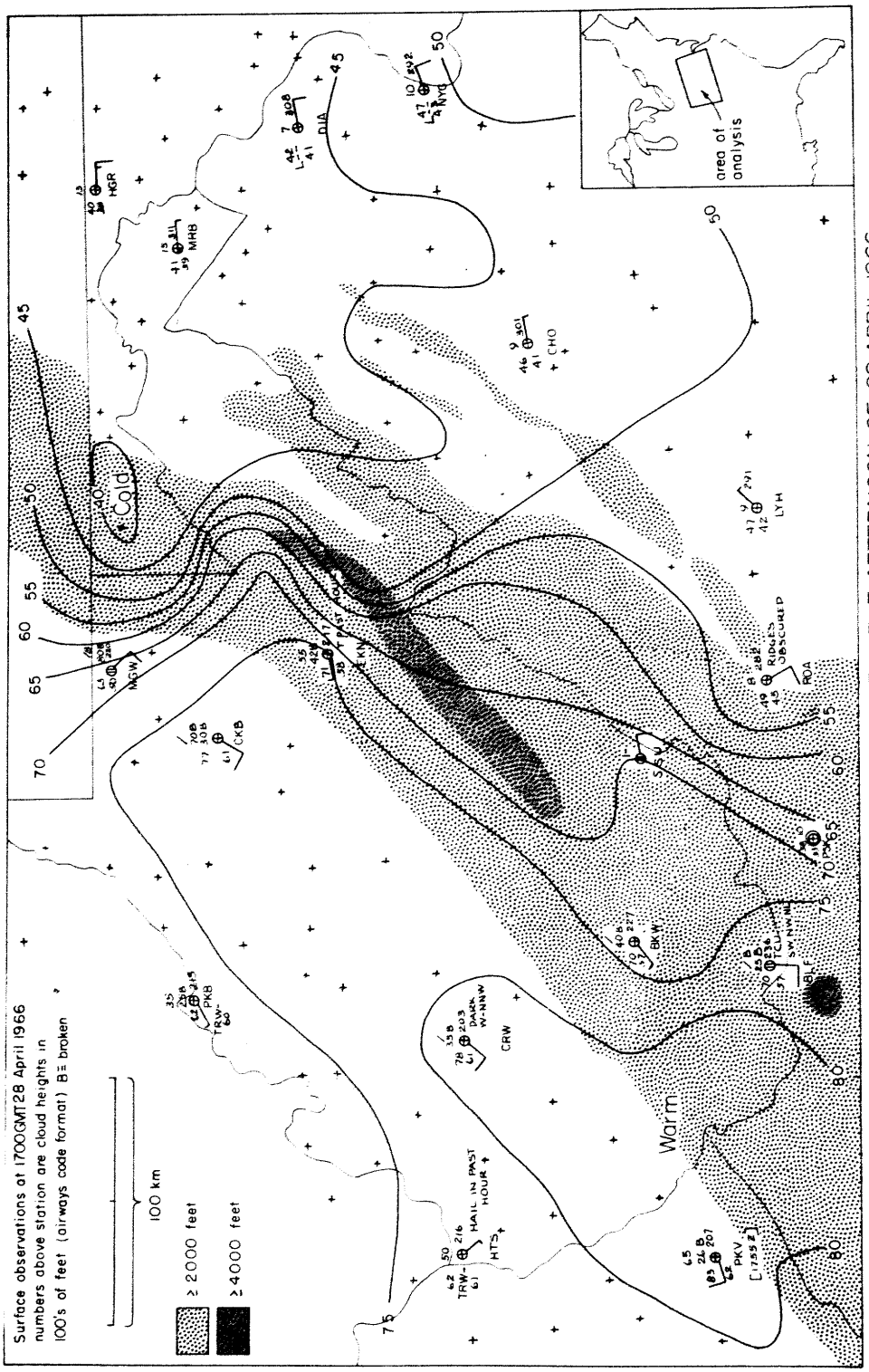

Figure 25. Case study

Even though the cold air is blocked to the south, the maximum temperature analysis indicates that it is still flowing over the mountains to the north of the highest ground elevations. This fact is also evident in the 1800 GMT analysis (Figure 24). Evidently, the height of the mountains is important in determining whether or not blocking occurs.

Since no cold air is flowing across the mountains into West Virginia at 1800 GMT, the zone with north-northeast winds east of the mountains must now extend through the whole depth of the cold air. There are no available wind observations aloft at 1800 GMT to verify this conclusion.

4.8 Further development of the ridge

By 1800 GMT (Figure 24), the low off the coast is somewhat more intense than it was at 1200 GMT. Most of the precipitation along the east coast has ended by 1800 GMT.

Let us consider the events after 1800 GMT. The squall line, which was approaching the mountains at 1800 GMT, very quickly dissipated when it encountered the cold air. However, the thunderstorms did produce a pressure oscillation on the inversion surface which could be tracked eastward. As the cold front moved over the pressure ridge region, it became difficult to follow. Apparently, the cold air behind the front did not penetrate the even colder air associated with the ridge. Such a phenomenon has been described by v. Ficker (1926) in Vienna and Takeuchi (1951) in Japan. Von Ficker called it a

"masked cold air invasion."

The pressure ridge persisted along the coast after 1800 GMT, although it slowly weakened. The low clouds persisted east of the mountains even past 1800 GMT on the 29th.

4.9 Theoretical trajectories of the cold airflow

As noted earlier, it is more physically meaningful to consider the inversion height variations along a trajectory than along a line perpendicular to the mountains. In addition, a trajectory analysis is useful in the investigation of the orographic blocking of the cold airflow. For the above reasons, a computer program was developed which calculates dynamic trajectories.

The change in the position and speed of a parcel are computed at 20-minute increments by means of the spherical equations of motion. Given the location and velocity of a parcel, a rough approximation of the position and velocity of the parcel 20 minutes later is made. The values at this later position are then used to improve the rough approximation so that a more accurate final position and velocity are obtained. (See Appendix F for the details of the technique.) Uncertainties in the given pressure field, in the given initial conditions, and in the assumptions made about friction (discussed below) probably cause much larger departures of the trajectories from reality, than the accumulation of errors in the

method employed here.

The initial velocity and position of a parcel has to be assigned in order to compute the trajectories. Only parcels originating over the ocean are considered. Initial velocities are assumed to be geostrophic since friction is much less over the ocean than over the land. Suuporting this assumption are the observed winds at WAL which are approximately geostrophic.

The observed sea-level pressure field is used to determine the pressure gradient force. For convenience, pressure values are obtained for a latitudinal-longitudinal grid with grid points spaced every 1^{o} of latitude and 1^{o} of longitude. Pressure values, which are linearly interpolated in space and time, are taken from analyses at 3-hour intervals.

Since the pressure field is given rather than predicted, the calculated dynamic trajectories are diagnostic rather than prognostic.

Trajectories for parcels beginning at 0600 GMT are shown in Figure 26. Frictionless flow is assumed. The hatches on the trajectories are the positions of the parcels at 3-hour intervals. Since the pressure field was changing continuously, no one time represents the actual pressure field. However, for reference, some of the 1200 GMT isobars have been included in Figure 26. Those parcels originating near the coast are shown as solid lines (designated A,B,C in Figure 26). Those starting further off-shore are shown as dashed lines (designated D through I).

Parcels A,B, and C pass through the ridge region while a corner ridge is still present. These parcels continue in geostrophic

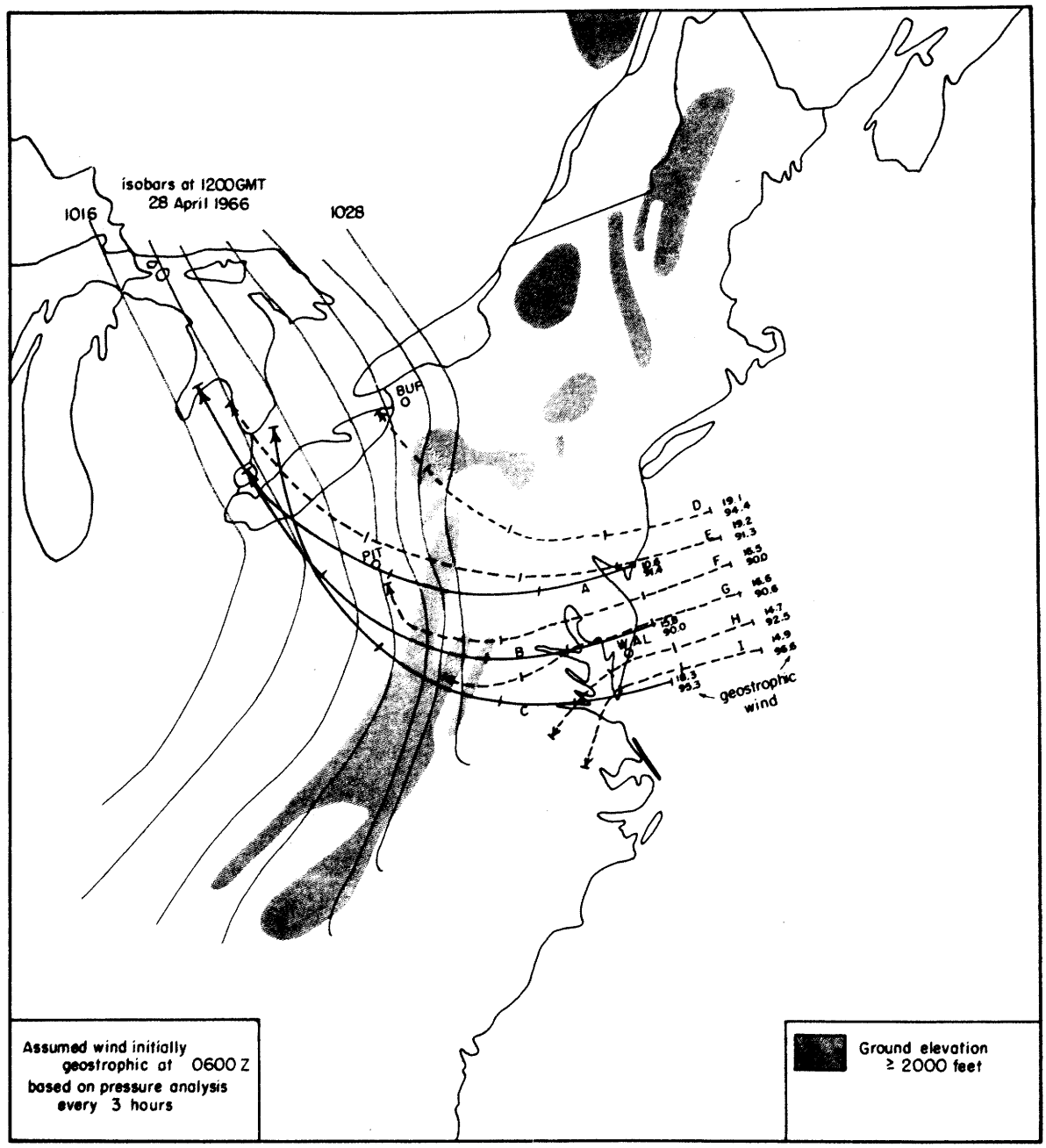

Figure 26. Case study

balance until they pass the "corner" of the corner ridge. At this point they suddenly start traveling perpendicular to the isobars; i.e., very ageostrophically. In the new pressure field the parcels accelerate both westward and northward. The northward acceleration produces an anticyclonic curvature in the trajectories. Later, the parcels approach the direction of the isobars on the lee side. As the northward velocity of the parcels increases,the coriolis force component increases toward the east. Hence, this force component acts in the opposite direction to the pressure gradient force and, thus, reduces the acceleration of the parcels that would occur if only the pressure gradient force were acting.

Parcels D through I are initially flowing toward the Appalachians. These parcels arrive in the wedge ridge region after the wedge ridge has formed. The observed data presented in Section 4.7 suggest that the parcels are blocked. However, in order to be blocked, the velocity component of the parcels perpendicular to the mountains must decelerate to zero. One way to accomplish this deceleration is for the parcels to encounter an adverse pressure gradient. As can be seen in Figure 15, parcels coming off the ocean do encounter an adverse pressure gradient in a wedge ridge situation. However, is the wedge ridge strong enough to cause blocking?

Parcels D and E travel to the north of the wedge ridge and thus still follow the trajectory pattern of A,B, and C. Parcels F and G are diverted somewhat to the south but still pass over the mountains. However, parcels H and I curve so that they travel parallel to the mountain range. Evidently, the wedge ridge is strong enough to block

the prevailing flow.

4.10 Verification of trajectories

It is difficult to verify these trajectories against actual wind observations. Not only are wind observations too limited in space and time, but also the present averaging technique used in reporting winds is inadequate. In this technique, the radiosonde position is recorded every minute (approximately, every 200 meters of ascent). The wind calculated for each minute is a two-minute average centered on that minute. From this average, the wind speed and direction at a desired height is found by linear interpolation. Hence, every reported wind is a three-minute (600-meter) weighted average. The strong wind shear between the cold and warm air is undoubtedly considerably smoothed by this averaging technique. Because of the shallowness of the cold air, usually only the first reported level is based upon data taken solely in the cold air. In fact, for some stations like WAL (see Figure 32), which has the base of the inversion at 300 meters, not even the first level is based solely on cold air data. In future studies of the ridge, unsmoothed one-minute average winds calculated from the original WBAN forms should be used.

Another problem encountered was the frequent loss of wind data at low levels. Probably, the RAWIN equipment lost the balloon when it changed direction too quickly in the low-level shear. Hence, some of the potentially useful soundings failed to report low-level wind data.

One fact is clearly evident, however, from these trajectory calculations: predicated winds on the lee side of mountains are substantially higher than the reported winds. In Figure 28, for instance, the predicated wind near PIT is 43 m/sec at 0720 GMT. The observed wind in the cold air (see diagram in the lower left of Figure 28) is only 10 m/sec. This discrepancy will be considered in detail in Section 5.6.

4.11 Proposed explanation of the zone of parallel flow next to the mountains

As noted earlier, south of Washington, D.C., there is a zone of surface winds parallel to the mountains when a corner ridge is present. Since cold air is observed on the western side of the mountains, it seems reasonable to assume that this parallel flow exists only right at the surface.

One possible explanation of this zone is the change in the trajectory of an air parcel produced by the change in surface friction as the parcel moves from the ocean to the land. To test this theory, a friction term of the form $\vec{F} = -\rho a \vec{u}$ was included in the trajectory program. The value assigned to a was 1.0 sec^{-1} — which is the order of magnitude necessary to balance forces for a wind blowing 30° across the isobars at one-half the geostrophic velocity.

Trajectories computed with friction are given in Figure 27. The solid lines are the flow without friction and the dashed lines with friction. The trajectories were started at 0000 GMT 28 April 1966

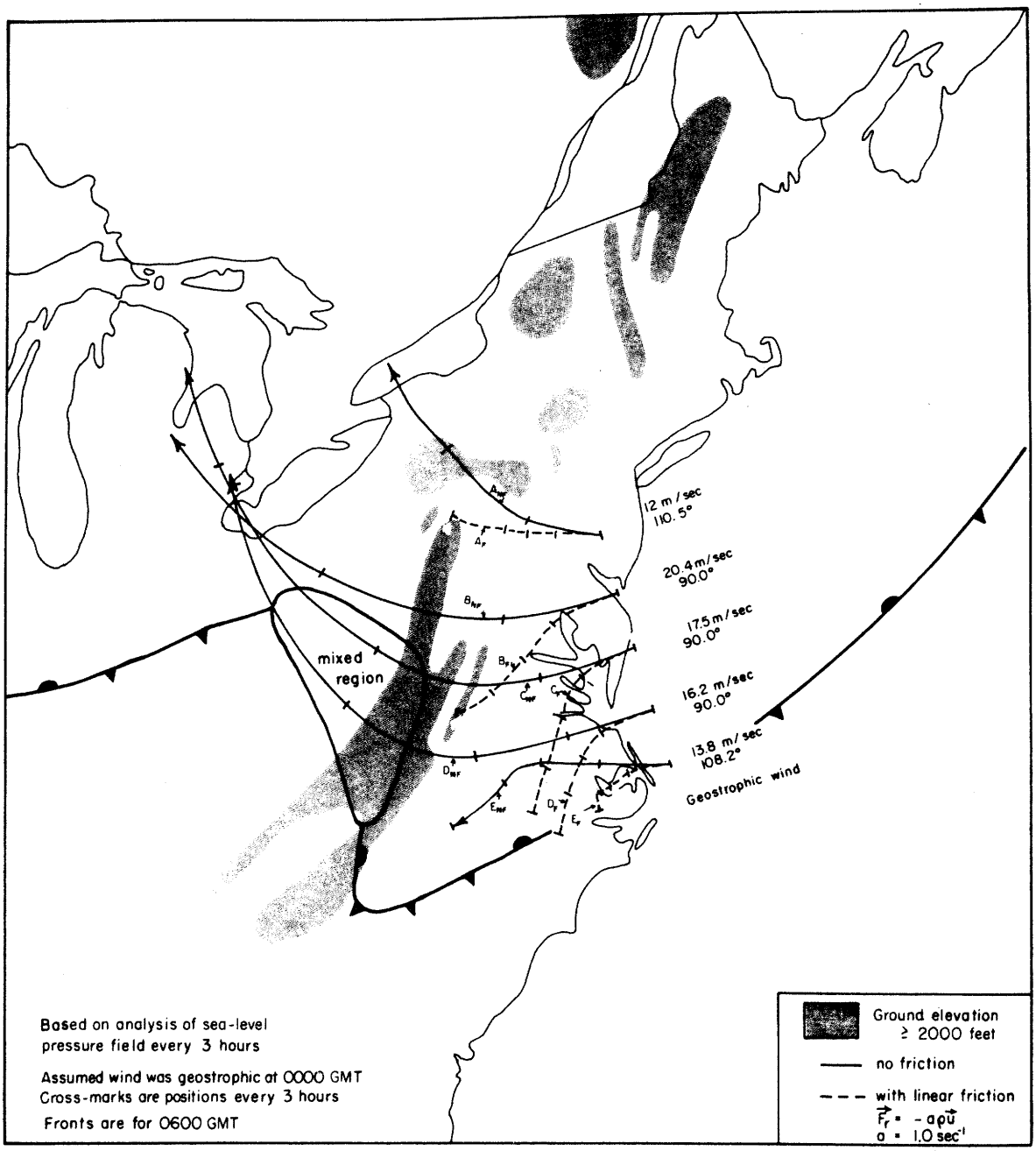

DYNAMIC TRAJECTORIES FOR PERIOD 28 APRIL 1966 0000 TO 1200 GMT

Figure 27. Case study

at the coast. The flow was assumed to be initially geostrophic. Parcel A_F travels to the left of parcel A_{NF} but still passes over the mountains. This direction of travel agrees with the observed flow in that region. A study of the calculations reveals that the reason A_F does not curve southward is the flat pressure field in eastern Pennsylvania. As $\frac{\partial p}{\partial y}$ becomes zero, the coriolis force in the y direction counteracts the tendency of A_F to turn southward. Hence, the parcel continues moving toward the west.

Parcels B_F, C_F, D_F, and E_F all curve southward and flow parallel to the mountains, producing a zone of flow parallel to the mountains. This behavior is similar to that observed in the cold air. Therefore, these trajectory calculations support the contention that the zone of parallel winds is caused by the change in the surface friction.

4.12 The inversion height variation along a cold air trajectory

Figure 28 presents the variation of sea-level pressure and inversion height along a cold air frictionless trajectory for a corner ridge. Only one trajectory is discussed here because the other trajectories have similar features.

The path of the trajectory on the earth's surface is given in the upper left. The parcel begins at 0000 GMT 28 April 1966 at the coast and crosses the mountains while a corner ridge is still present on the windward side. The surface map for 0600 GMT has been included for reference. The sea-level pressure (at 0600 GMT),

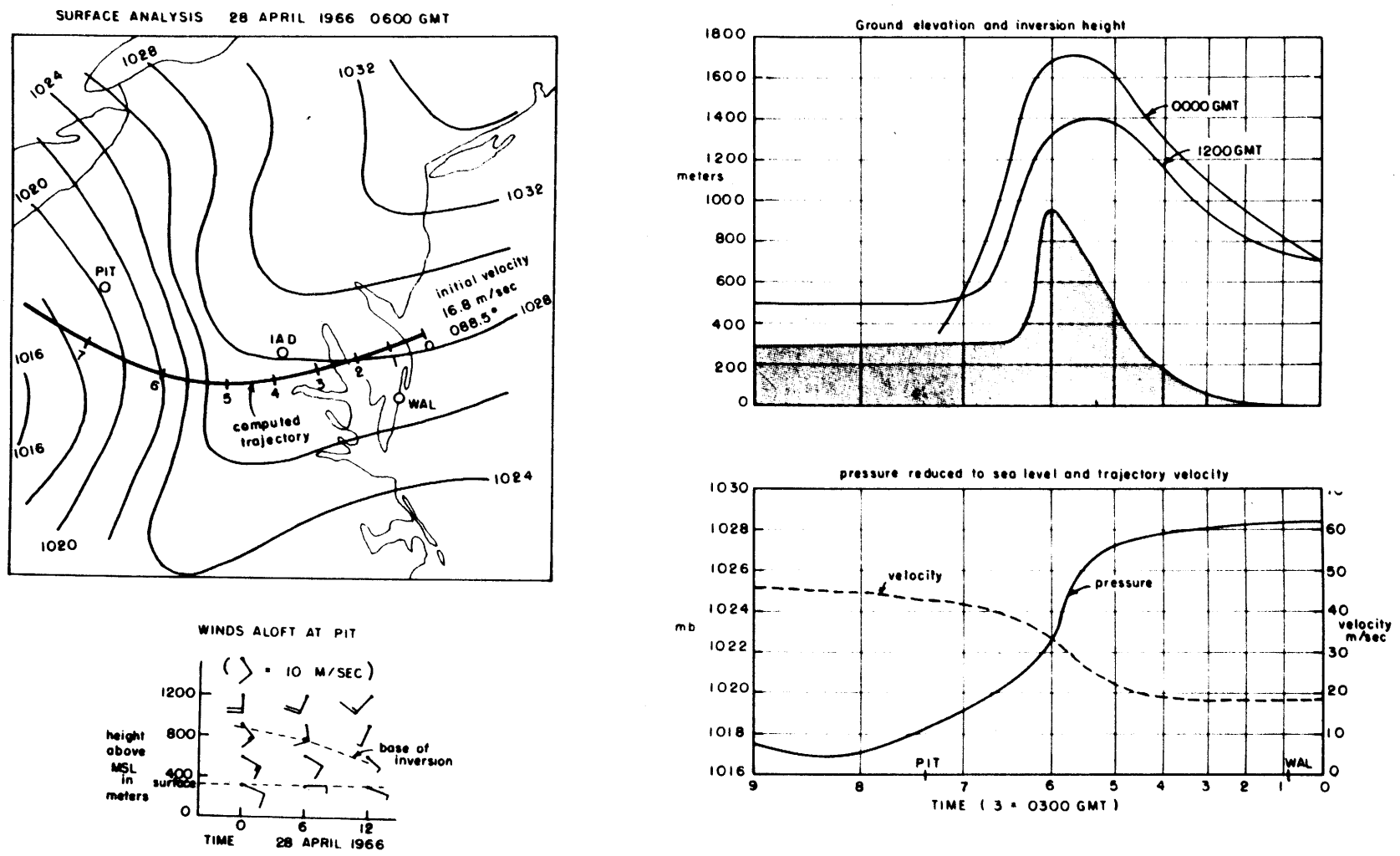

Figure 28. Case study - variation of the inversion height, terrain elevation, and sea-level pressure along a frictionless cold air trajectory

inversion height (at 0000 GMT and 1200 GMT) and terrain elevation along the trajectory are given on the right side of Figure 28. From east to west, the pressure along the trajectory never rises. It decreases slowly until about halfway up the windward slope. A rapid decrease occurs across the mountain crest, followed by a slower decrease on the lee side. The inversion height at 0000 GMT and 1200 GMT follows approximately the contours of the mountain. However, there is a marked thickening of the depth of the cold air on the windward side. This thickening is followed by a decrease in the depth which begins even before the inversion crest is reached. The inversion crest is located to the east of the mountain crest. On the lee side, the height of the inversion decreases very rapidly. In fact, at 0000 GMT the inversion even intersects the ground. A discussion of the physics of this cold airflow is given in Section 5.6.

Section 5. Physical behavior of the cold airflow

5.1 Relevance of previous theories of the pressure ridge

A re-examination of the previously proposed theories of the pressure ridge reveals that none of these theories postulates a shallow cold airflow as found in Section 4. In fact, Queney's theory explicitly excludes any inversion. Hence, none of these theories is directly applicable in this study. However, the suggested physical processes of v. Ficker and Trabert (release of latent heat) and Ekman (coriolis effects) still could be pertinent, in modified form, to the cold airflow.

In order for Ekman's theory to apply, the depth of the cold air must decrease on the windward side and increase on the lee side of the mountains. Unfortunately, in the observed cold airflow the depth first increases on the windward side and then rapidly narrows as it flows over the mountain crest onto the lee side. Hence, overall the behavior of the depth is opposite to that required by Ekman's theory. Moreover, the trajectory calculations in Section 4.9 indicate that one cannot assume geostrophic motions — another requirement of Ekman's theory. In conclusion, it appears that Ekman's theory is not applicable to the pressure ridge being studied here.

Since the pressure ridge is only an easily noticed feature of the cold airflow, the explanation of the pressure ridge should be found in the explanation of the cold airflow. This section attempts to explain the behavior of this airflow.

5.2 Steady-state assumption

Because of the long duration of the pressure ridge — an average of 30 hours for those cases in Appendix A — it is presumed that the cold airflow can be treated as if steady-state. The following discussion is limited to this steady-state airflow. Unfortunately, this limitation means that no reason for the formation of the pressure ridge can be advanced, since the formation itself is non-steady-state. Still, it is of meteorological significance that a pressure ridge can be steady-state and stationary under conditions where the large-scale flow is changing and moving.

5.3 Consequences of compressibility and the release of latent heat

In order to estimate the importance of compressibility and of condensation, their possible effects on the cold airflow in Figure 28 are considered. As a measure of this importance, the effects of these processes on the mean temperature of the surface to 1700 meter column are calculated. This mean temperature should provide a good measure since this column is high enough to include all changes in temperature associated with the cold airflow. In particular, the theoretical change in mean temperature from the coast (at 0000 GMT in Figure 28) to the location of the maximum inversion height (at 0530 GMT) is determined. In the equations below, these locations are denoted by the superscripts "1" and "2", respectively.

Let us assume, first, that the cold air mass has a dry-adiabatic lapse rate (This assumption is vital since the argument below only

holds if conditions have neutral stability. Since the cold air usually is neutrally stable, no problem should arise.) Under such a condition, there is no horizontal temperature change under 700 meters as long as parcels move adiabatically. Consequently, the lower reference level can be taken as 700 meters instead of sea level. The choice of this level also avoids the necessity of having to assign a fictitious atmosphere within the mountain.

Let us divide the mean temperature, $\bar{T}$, of the 700 to 1700 meter column into the mean temperature of the warm air, $\bar{T}_{WA}$, and of the cold air, $\bar{T}_{CA}$. The mean temperature of the whole column at any location is given by

$$\bar{T}_{WA}\left(\frac{1000-H}{1000}\right)+\bar{T}_{CA}\left(\frac{H}{1000}\right) \qquad (5.1)$$

where H equals the inversion height minus 700 meters. Hence, the difference in mean temperature between locations 1 and 2 is

$$\bar{T}^{1}-\bar{T}^{2}=\frac{1}{1000}\left[\bar{T}^{1}_{WA}(1000-H^{1})+\bar{T}^{1}_{CA}(H^{1})-\bar{T}^{2}_{WA}(850-H^{2})-\bar{T}^{2}_{CA}(H^{2})\right] \qquad (5.2)$$

If we let

$$\Delta H = H^{1}-H^{2}$$

$$\Delta\bar{T}_{WA}=\bar{T}^{1}_{WA}-\bar{T}^{2}_{WA}$$

$$\Delta\bar{T}_{CA}=\bar{T}^{1}_{CA}-\bar{T}^{2}_{CA}$$

and substitute into Equation (5.2),we get, after algebraic manipulations,

$$\bar{T}' - \bar{T}^2 = \underbrace{(\bar{T}'_{CA} - \bar{T}'_{WA})\frac{\Delta H}{1000}}_{①} + \underbrace{\Delta\bar{T}_{WA}\left(\frac{1000 - H' + \Delta H}{1000}\right)}_{②} + \underbrace{\Delta\bar{T}_{CA}\left(\frac{H' - \Delta H}{1000}\right)}_{③} \quad (5.3)$$

The three terms in Equation(5.3) are labeled ①, ② and ③ so that they can be referred to individually. ① is the contribution of the inversion height while ② and ③ are the contribution from changes in the mean temperature of the warm and cold air, respectively. Since in an incompressible neutral atmosphere $\Delta\bar{T}_{WA}$ and $\Delta\bar{T}_{CA}$ would be zero, ② and ③ can be viewed as arising from the compressibility of the atmosphere.

For the flow in Figure 28, $\Delta H = -1000$ meters and $H' = 0$ meters. Equations (5.3) then reduces to

$$\bar{T}' - \bar{T}^2 = \underbrace{(\bar{T}'_{CA} - \bar{T}'_{WA})}_{①} + \underbrace{\Delta\bar{T}_{CA}}_{③} \quad (5.4)$$

If at location 1 the temperature is Y (which is also the mean temperature), then the mean temperature of the cold air at location 2 is

$$\bar{T}^2_{CA} = \frac{2Y - .01\,(°C/m) \times 1000\,(m)}{2} = Y - 5 \quad (5.5)$$

Hence,

$$\Delta\bar{T}_{CA} = Y - Y + 5 = 5°C$$

Since the temperature difference across the inversion is approximately 10°C, from Equation (5.4),

$$\bar{T}' - \bar{T}^2 = \underset{①}{10°C} + \underset{③}{5°C} \qquad (5.6)$$

Apparently, the contribution of ① to the change in mean temperature is twice that of ③. Thus, the effects of compressibility are not as important in the cold airflow as changes in the inversion height, but clearly are not negligible.

The effects of condensation can be calculated approximately by assuming a moist-adiabatic lapse rate of .5°C/100 m and saturated conditions in the cold air. Then, Equation (5.5) becomes

$$\bar{T}^2_{CA} = \frac{2Y - .005\,(°C/m) \times 1000\,(m)}{2} = Y - 2.5 \qquad (5.7)$$

and Equation (5.6) becomes

$$\bar{T}' - \bar{T}^2 = \underset{①}{10°C} + \underset{③}{2.5°C} \,. \qquad (5.8)$$

A comparison of Equation (5.8) with Equation (5.6) shows that condensation has reduced the magnitude of ③. Thus, for saturated conditions, the effects of compressibility and condensation offset one another. Consequently, the inversion height effect, ①, is even more dominant than in unsaturated conditions. Since in the case study, the cold air was saturated, compressibility and the release of latent heat probably only modify the cold airflow, while the inversion height is of fundamental importance.

The flow in Figure 28 is associated with a corner ridge. Since vertical displacements for a wedge ridge are less than for a corner ridge, compressibility and the release of latent heat should be of

secondary importance for the wedge ridge, too.

In conclusion, the above results suggest that v. Ficker's and Trabert's proposals that the release of latent heat is the dominant physical mechanism of the pressure ridge is not valid for the Appalachian pressure ridge.

5.4 Importance of the warm air pressure gradient

The warm air pressure gradient at 0000 GMT 28 April 1966 (Figure 14) is equivalent to a geostrophic wind of around 15 m/sec over most of the east-coast region. Even though this velocity is not very high, the calculations below suggest that this warm air pressure gradient is important for the cold airflow.

If P_0 is the pressure at 700 meters and P_1 is that at 1700 meters, then the change of pressure at the lower level is given by

$$\frac{P_0' - P_0^2}{P_0} = \frac{P_1' - P_1^2}{P_1} - \frac{g^2}{R(\bar{T})^2}\left(\bar{T}_1' - \bar{T}^2\right), \qquad (5.9)$$

where z is the difference in height between these levels. If we let $\bar{T}$ = 280°K, P_1 = 830 mb, and P_0 = 950 mb in Equation (5.9), we get

$$P_0' - P_0^2 = (P_1' - P_1^2)\,1.14 - 0.41\,(\bar{T}' - \bar{T}^2). \qquad (5.10)$$

From Figure 13 we obtain $P_1' - P_1^2 = -6.0$ mb.

From Section 5.3 we have approximately $\bar{T}' - \bar{T}^2 = 10$ °C.

Hence, we find

$$p_o' - p_o^2 = -6.8\ mb + 4.1\ mb = -2.7\ mb \quad . \qquad (5.11)$$

(Figure 28 gives

$$p_o' - p_o^2 = -2.0\ mb \quad ,$$

although such a close agreement with Equation (5.11) may be fortuitous since Figure 28 gives the 0600 GMT pressure field.)

It is clear from Equation (5.11) that, as already suggested in Section 4.6, the cold air pressure difference is a necessary consequence of the warm air pressure gradient and the rise of the inversion. In conclusion, the warm air pressure gradient must be an important factor in the flow of the cold air over the Appalachian Mountains.

5.5 Effects of surface friction, coriolis force, and mixing

The above conclusions were deduced from computations that appear to be reasonably justified. The importance of surface friction, coriolis force, and mixing of the warm and cold air masses cannot be as readily estimated by quantitative arguments.

One would expect friction to be important since the cold air is not only located next to the ground, but also located over mountainous terrain, which should increase the surface friction still further.

The trajectory calculations in Section 4.9 show that the component of the coriolis force in the direction of the initial airflow is important. Moreover, since the flow is initially geostrophic, the component of the coriolis force perpendicular to this direction is obviously important. However, the existence of the mixed region

suggests that it is important, also.

5.6 Physical behavior of the cold airflow

Seven pressure ridge cases (in addition to the case study presented in Section 4) were analyzed to ascertain which features brought out in Section 4 are unique to that case and which are characteristics of pressure ridges in general. (A list of these eight cases is given in Table 3.) The schematic diagrams in Figure 29 and 30 have been prepared from the results of these eight case studies and from the physical deductions given in this section. (Noted that the Appalachian Mountains have an idealized north-south orientation in these diagrams.) Hence, these diagrams summarize to a large extent the results of this entire investigation.

In Section 5.3 through 5.5 physical factors have been considered individually. Here, an attempt is made to explain qualitatively how these processes interact.

In Section 5.4 it was shown that the warm air pressure gradient along the trajectory in Figure 28 is strong enough to offset the low-level increase in pressure associated with the rise in the inversion height. If this warm air gradient were not present, a parcel moving along the same path would experience a pressure increase of around 4 mb between the coast and the inversion crest. The trajectory calculations in Section 4.9 indicate that a pressure increase of only about 2 mb is necessary to produce blocking. Thus, without this warm air gradient, no cold air would pass over the mountains. Clearly, the cold airflow pattern depends greatly

Schematic Diagrams of Corner Ridge

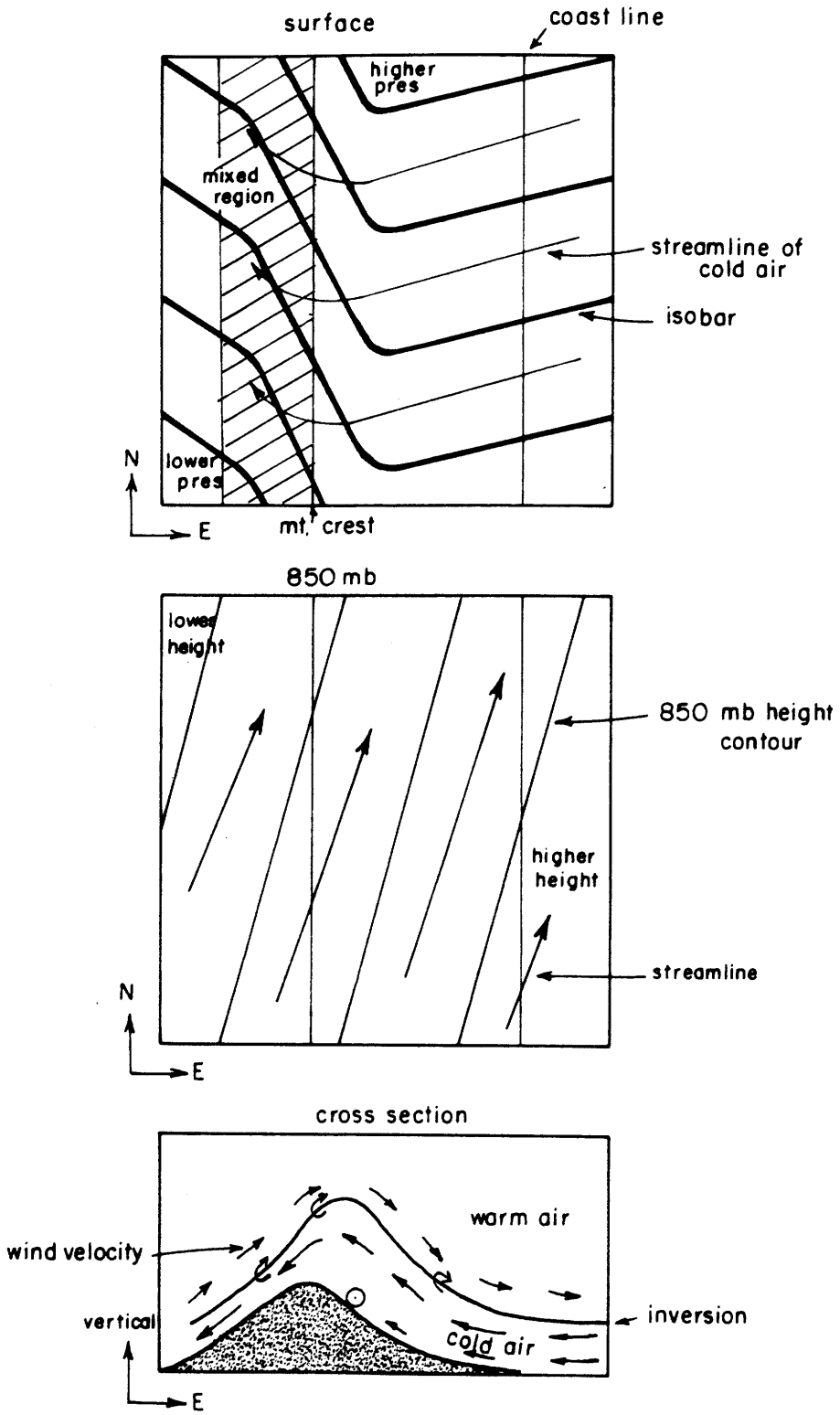

Figure 29

Schematic Diagrams of Wedge Ridge

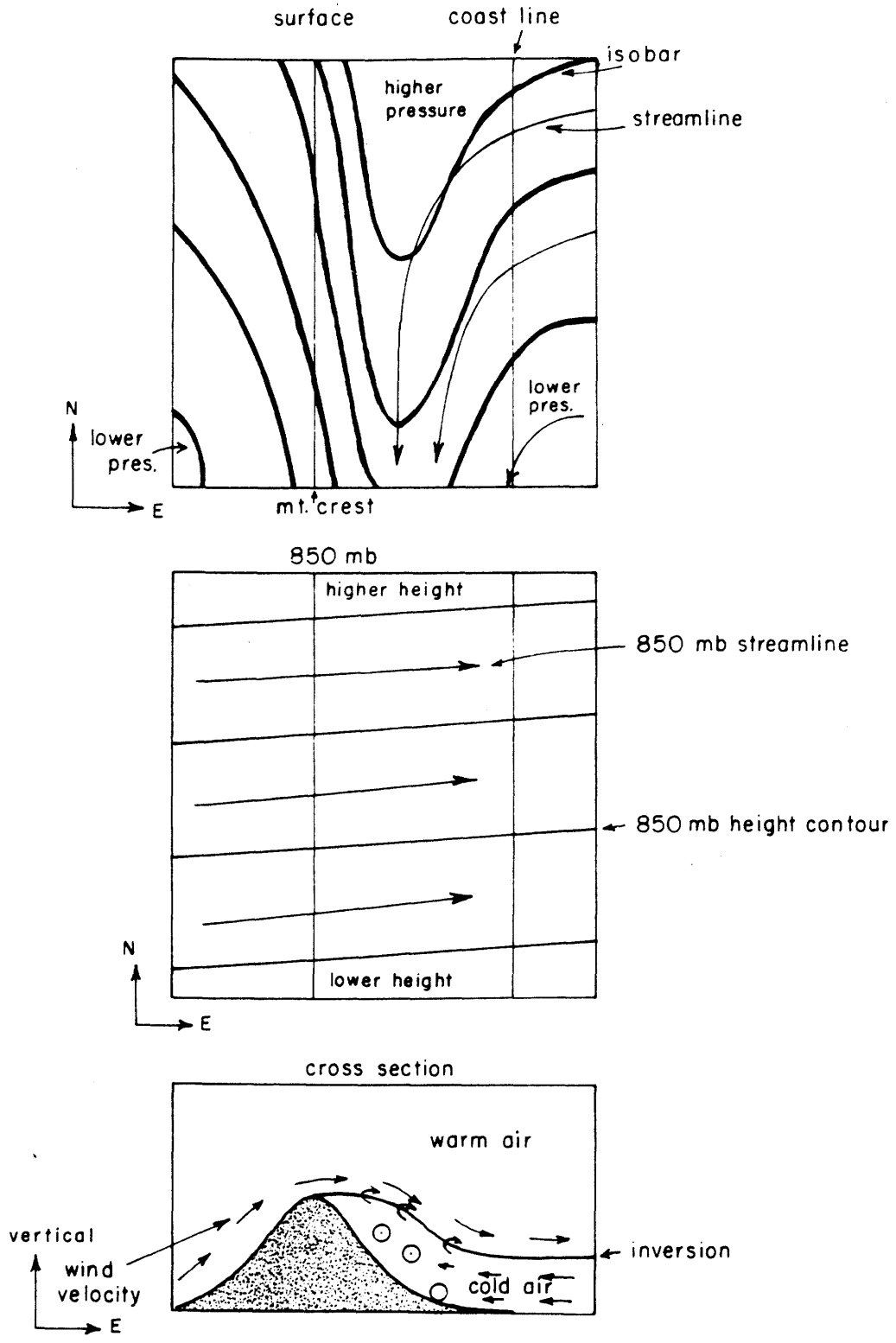

Figure 30

on the warm airflow pattern above it.

In order for the cold air to surmount the mountains, this warm air gradient must be strong enough to offset not only the pressure increase from the inversion, but also the effects of the frictional and coriolis forces. Surface friction produces a force opposite in direction to the flow and, hence, opposes the flow over the mountains. It was shown in Section 4.9 that the coriolis force hinders the westward flow of cold air in a corner ridge, once the air has passed the ridge line.

Evidently, in order for the cold air to pass over the mountains, it must flow down the warm air gradient. Moreover, since the cold air strikes the mountain range almost at a right angle, the warm airflow, which is quasi-geostrophic, should be parallel to the mountains. The eight analyzed cases were examined to confirm these conclusions. In seven of these cases the cold air did, indeed, flow down the gradient. The anomolous case (12 November 1966) had a very high inversion (around 750 mb) with a cold airflow that was difficult to interpret. Six out of the seven pertinent cases had a warm airflow which ran either along the length of the Appalachians, or at a slight angle as shown in Figure 29. One case (24 February 1966) had a flow which crossed the mountains from the east side.

When the warm air pressure gradient is sufficiently strong, a corner ridge is present and the cold air passes over the mountains. If this gradient then weakens, a wedge ridge will appear and block the flow. This weakening can be accomplished either by a reduction

in the warm air gradient and/or by a change in direction of this gradient. Of the eight cases, three had a wedge ridge develop from a corner ridge. In one of these cases (14 February 1970) the wind direction became almost perpendicular to the mountains as denoted in Figure 30. In the case study presented in Section 4, the warm airflow both weakened and veered (compare Figures 14 and 16). The remaining case (24 January 1965) had no apparent change in the warm air direction of flow. In this case the increased pressure at the surface associated with the wedge ridge formation appeared to reflect cold air coming down from the north near the surface.

In conclusion, the case studies generally confirm the importance of the warm air pressure gradient.

An interesting ramification of the above discussion is the effect of the height of the mountain crest on the cold airflow. In order for the cold air to surmount the mountains the inversion height must increase more for the higher segments of the Appalachians than for the lower. However, the warm air gradient is approximately the same for the two regions. Consequently, the increase of the inversion height that is necessary in order for the air to flow over the higher segments could be so large that a wedge ridge develops. In this case, the cold airflow will be blocked for the higher portions of the mountain range, but not for the lower. Such a behavior has already been pointed out in Section 4.7.

Consider now a parcel of the cold air streamline given in the surface diagram of Figure 29. (This streamline is the horizontal

projection of the flow given by the wind arrows just beneath the inversion in the cross section diagram.) Until this parcel reaches the "corner" of the corner ridge, the increase in the inversion height offsets the warm air gradient so that there is little pressure change along a trajectory. As the parcel approaches the inversion crest, the offsetting effect of the inversion diminishes and the pressure begins to fall more rapidly along the trajectory. Hence, the "corner" of the corner ridge is located at the place where the inversion slope starts diminishing. At the crest itself, the cold air pressure gradient along the trajectory equals the warm air gradient. To the west of the crest, the pressure change from the inversion height augments the warm air gradient, thus intensifying the cold air gradient. This augmentation accounts for the strong pressure gradient across the mountains when a ridge is present.

Since this strong cold air gradient extends above the mountain top, it is meteorologically significant. However, in the case of the wedge ridge shown in Figure 30, the increased pressure gradient across the mountains cannot be explained by changes in the inversion height. In this case, the large mean temperature difference across the mountain probably intensifies the pressure difference. However, since this difference would be beneath the mountain top, it is not meteorologically significant. In addition, the method used in reducing pressure to sea level would exaggerate the observed pressure difference since the reduction depends upon the observed

surface temperatures.

The above discussion has dealt with the hydrostatic aspects of the cold air pressure field. Let us now consider the dynamic aspects.

Once an air parcel passes the "corner", it accelerates rapidly in the forward direction. Assuming the flow is two-dimensional, this velocity increase of the parcel should be reflected in a decrease of the cold air depth. Figure 28 shows that the cold air depth does, indeed, start decreasing even before the inversion crest is reached. As also shown in Figure 28 the trajectory velocity continues to increase over the mountain crest and onto the lee side. The inversion depth, in accord with the conservation of mass flux, also decreases rapidly from the windward to the lee side. However, the predicted trajectory velocity (given in Figure 28) is of hurricane magnitude on the lee side!

Clearly, something is wrong. The most reasonable explanation for these unrealistically high predicted winds is the neglect of surface friction in the trajectory calculations.

Although it is difficult to evaluate the effects of surface friction, its effect should be greatest at the ground. The results of the theoretical calculations given in Section 4.11 show a decrease in velocity of a parcel when friction is included. In fact, for certain coefficients of linear friction the velocity perpendicular to the mountains decreases to zero, indicating that the air does not pass over the mountains at all, but flows southward parallel to the mountains. Such a zone of parallel flow was found in all eight

cases studied. In Figure 29 the component of the surface winds perpendicular to the mountains is indicated by the series of arrows closest to the ground on the windward side.

The importance of surface friction on the cold airflow depends on how far aloft significant frictional influence extends. No observational data is available to help answer this question. However, if the frictional influence did not extend to the inversion, the frictionless trajectories would be valid and hurricane winds would be observed. The fact that hurricane winds are not found suggests that significant surface-friction effects do extend to the inversion. In addition, the observed neutrally stable lapse rates in the cold air also imply considerable mixing. Evidently, surface friction is important throughout the depth of the cold air.

Another possible factor that has to be considered is the change of the pressure field with height as a consequence of the north-south temperature gradient in the cold air. Since the trajectories are most representative of the flow near the inversion, the pressure field at this level should be used in these calculations instead of the sea-level field. A comparison of Figures 7 and 15 shows that the pressure gradient at 500 meters is approximately one half that at sea level, although the direction is the same. Even if we assume that the lee-side winds are also reduced by one half, they are still considerably higher than the observed winds. Hence, one could argue that the reduced pressure gradient aloft cannot account for the observed lower velocities on the lee side. Such an argument is not

very convincing, however. Clearly, frictionless trajectories based on the pressure field aloft should be considered in future studies of cold airflow.

Now let us consider the effect of friction on the inversion height. As the friction reduces the velocity along a trajectory, the inversion height has to increase (provided the flow is two-dimensional). Thus, friction may account for the increasing inversion depth (both at 0000 GMT and 1200 GMT) in Figure 28 as a parcel moves inland from the coast.

The observed winds on the coast and on the lee side have approximately the same velocity. If friction were the only factor slowing the airflow, the cold air depth at the coast and on the lee side would be nearly the same. Since the inversion height along the trajectory decreases considerably from the coast to the lee side, there must be a loss of cold air along the trajectory. Since the surface airflow is unable to pass over the mountain, this surface layer could account for the loss of cold air. (If this loss is actually significant, then one cannot assume two-dimensional flow since $\frac{\partial v}{\partial y} \neq 0$.)

If this surface layer were the only loss of cold air flux along a trajectory, the temperatures on the windward and lee side should be approximately equal, even if the release of latent heat is taken into account. However, some of the eight cases studied had very marked mixed regions — much stronger than the mixed region brought out in Section 4.

One possible reason for the warm air in the mixed region is mixing of the warm and cold air masses. Such a mixing process would not only reduce the westward cold air mass flux but also act as a frictional drag, since the warm air above is not flowing in the same direction as the cold air.

In Figure 29 this mixing is indicated by circular wind arrows across the inversion. Since mixing probably is occurring for the corner ridge, it also should occur for the wedge ridge as well. Hence, mixing is also indicated in Figure 30.

Although the schematic diagram of the wedge ridge in Figure 30 suggests a two-dimensional airflow, actually it is impossible for the wedge ridge to be two-dimensional. When blocking occurs, there is cold air mass flux at the coast, but no flux at the mountain crest. Hence, $\frac{\partial v}{\partial y}$ cannot be zero and the airflow cannot be two-dimensional.

In summary, it appears that the warm air pressure gradient, the coriolis force, surface friction, and mixing of the air masses are all important factors in the cold airflow.

5.7 The role of the mountain range in the pressure ridge

This thesis would not be complete without a discussion of the role of the mountain range in the pressure ridge phenomenon.

The pressure ridge discussed here always appears on the windward side of mountain ranges. The author is not aware of any similar phenomenon which is independent of mountains. Therefore, it is reasonable to assume that the presence of a mountain range is a necessary requirement for the pressure ridge.

The most obvious effect of the mountain range is to produce changes in the inversion height. In fact, most of the inversion height change on the windward side of the mountains is a result of changes in the ground elevation rather than cold air depth.

A less obvious effect can be found in the case of the wedge ridge. In this case, the mountain range allows the warm air to flow up one slope, separate from the ground and flow out over the cold air at the surface on the other side. This separation allows the strong inversion initially present to persist. This strong inversion, in turn, is a fundamental characteristic of the pressure ridge. Hence, the mountain range is important in maintaining the inversion.

Section 6. Prediction of the pressure ridge by the operational six-layer P.E. model

The interactions of the physical processes of the pressure ridge are, undoubtedly, too complex for analytic solutions. Numerical models, therefore, are the only means of studying theoretically the pressure ridge. Possibly, operational models are already sophisticated enough to be able to predict the ridge. In order to find out, the author compared the predicted sea-level pressure of the operational six-layer P.E. model (see Shuman and Hovermale, 1968) with the actual sea-level pressure for a recent pressure ridge situation with subsequent Type B cyclogenesis.

Figure 31a gives the initial surface conditions prior to the ridge formation and cyclogenesis. At this time, a stationary front, extending from North Carolina to New Mexico, separates a warm high to the south from a cold high to the north.

In Figure 31b, the sea-level pressure field, 24 hours later, is given in solid lines, while the P.E. prediction is in dashed lines. The location and intensity of the high and the low are fairly well predicted by the P.E. model. However, the formation of the ridge is not forecast at all. In addition, the intensity of the trough to the west of the Appalachians is stronger than predicted. Temperatures along the east coast were predicted to rise (not shown), possibly from warmer air flowing into the region from the southeast. In actual fact, the temperatures fell. Temperatures for the northeastern United States

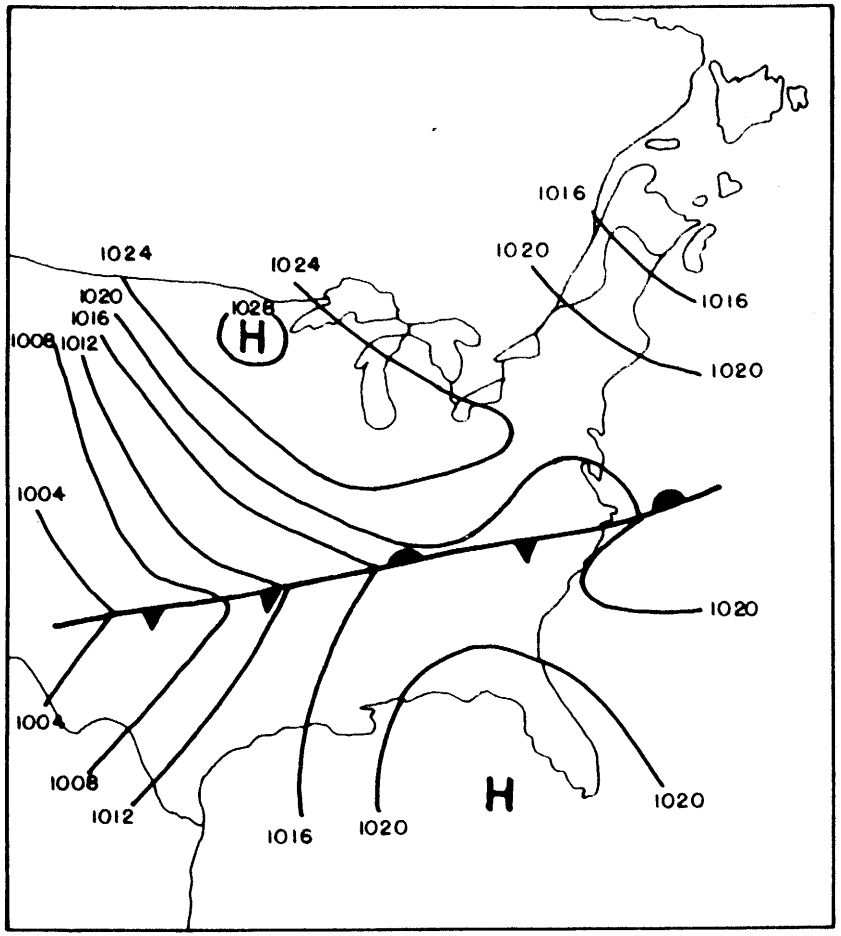

SURFACE ANALYSIS 14 FEB. 1970 0000 GMT

31a

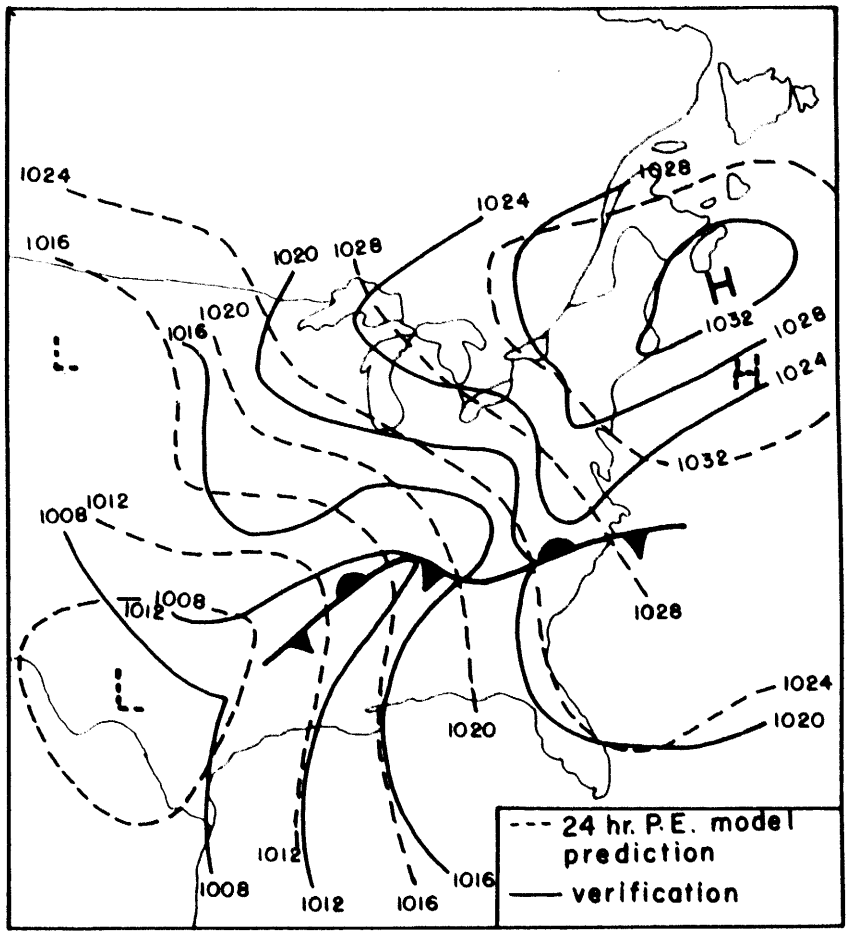

SEA LEVEL PRESSURE 15 FEB. 1970 0000 GMT

31b

Figure 31. Verification of P.E. model sea-level pressure forecast in a pressure ridge situation

averaged about 15°F lower than predicted -- a poor forecast by any standard.

The P.E. model also did not predict precipitation very well. One possible reason for this poor prediction is the failure of the P.E. model to forecast correctly the observed surface conditions. This failure would indicate poor predictions of boundary-layer vertical velocities and, hence, less accurate precipitation forecasts.

Six hours after the analysis time in Figure 31b, Type B cyclogenesis occurred east of the ridge. The P.E. model also failed to predict this cyclogenesis.

The results of this one case study suggest that the present P.E. six-layer operational model is unable to predict the pressure ridge and Type B cyclogenesis.

Let us now consider, on the basis of the results in Section 5, what revisions of the P.E. model probably would be necessary in order to predict the pressure ridge.

It can be reasonbly assumed that the accuracy of the numerical predictions will increase as the grid spacing is reduced. However, for economic and operational reasons, the grid spacing should be kept as large as possible and yet still allow the P.E. model to provide adequate forecasts. Hence, an important question is: what is the maximum grid spacing that can resolve the ridge and its essential characteristics?

The surface analyses in Section 4 indicate that a horizontal grid spacing of 100 km would resolve the ridge. The present operational

grid spacing is approximately 400 km. Recent experiments with fine mesh grids (200 km spacing) have not yet considered any cases of ridge development (personal communication from Major Howcroft, Air Weather Service).

In the vertical, a coordinate is used in the P.E. model which is a constant along the earth's surface (Shuman and Hovermale, 1968). An approximate spacing of 50 mb between levels should be able to resolve, for the stronger cases, the increase in the inversion depth as the air flows inland. However, possibly, such a spacing would not allow adequate prediction of the wedge ridge where inversion-height changes are smaller. Hence, a 25-mb spacing in the vertical would seem more appropriate.

Fortunately, extra grid points have to be added only close to the ground. Above approximately 850 mb, the present coarse grid mesh may still be adequate.

Since the lowest 50 mb is now assigned to the boundary layer, the whole boundary layer concept presently employed would have to be revised.

The only necessary modification of the basic equations in the P.E. model is a change in the frictional force term in the equation of motion. At present, the frictional force is assumed to be a function of a drag coefficient and the wind velocity squared. The frictional force is set equal to zero except in the boundary layer. Although this approach may be adequate for handling the effects of surface friction in the ridge, it eliminates entirely the possibility of

mixing. In order to include mixing, the frictional force should be set equal to

$$\frac{\partial}{\partial z}\left(K\frac{\partial \vec{V}}{\partial z}\right) ;$$

i.e. the turbulence theory approach should be used. Since the vertical grid points have to be close together in order to resolve the features of the pressure ridge, this approach seems feasible.

Section 7. Significance of this research in explaining phenomena related to the pressure ridge

7.1 The ridge and the foehn

Because of the well-established association between the ridge and the foehn, the results of this study may be relevant to an explanation of the foehn.

The type of pressure ridge investigated in this thesis was associated with a low-level inversion. To the author's knowledge, no study has been made to determine if the presence of a low-level inversion is a necessary condition for a foehn. However, Kuttner (1939) and Frey (1953) include a low-level inversion on the windward side of the Alps in their description of the foehn. Hence, there is some evidence that a pressure ridge similar to the ridge studied in this investigation is associated with the foehn. Therefore, the conclusions of this research may be pertinent to studies of the foehn.

Schweitzer (1953) and Houghton and Kasahara (1968) noted some analogous characteristics of the foehn and the flow of a one-layer fluid over a barrier. This flow can be adequately explained by solving the shallow water equations without any pressure gradient above the fluid, coriolis force, friction, or mixing. Hence, Houghton and Kasahara (1968) proceeded to investigate further ramifications of shallow water theory with these simplifications. One can infer from the results of this thesis that these four physical processes will have to be included in a model of the foehn

before an adequate explanation of the foehn can be advanced.

7.2 The ridge and the bora

Artemova (1962) describes a bora at Novorossiisk which is associated with a strong inversion aloft (monsoon bora). For this type of bora, the associated ridge should be the corner type since the cold air is clearly passing over the mountains. A verification of this hypothesis was not carried out.

7.3 The ridge and Type B cyclogenesis

Type B cyclogenesis and its accompanying weather have always been poorly forecast. Conover (1941), for instance, noted that bad weather often would be in New England before the storm center had been located. In Section 6 it was noted that Type B cyclogenesis was not predicted by the P.E. model, and its accompanying weather was poorly forecast. Hence, there seems to have been little progress over the years.

Probably an improvement could be achieved by ascertaining the physical processes involved in Type B cyclogenesis. In particular, its relationship to the pressure ridge should be determined. A brief discussion on this relationship is given below.

Analyses at three-hour intervals of the 26-28 April 1966 case showed that the wedge ridge formed before the low center appeared. In the other seven cases, the wedge ridge either preceded or developed simultaneously with the secondary low. Evidently, the wedge ridge is conducive to cyclogenesis. One possible reason for the association is given below.

Supposedly, cyclones frequently form on the lee slopes of mountain ranges because a current flowing down a slope is conducive to cyclogenesis. For a pressure ridge, the warm air may behave as if the inversion were a mountain (Oi and Sekioka, 1965). For a west wind the warm air descent would begin further to the east when a ridge is present than when it is not. Hence, with a ridge present, lee-side cyclogenesis should occur not on the eastern slope of the Appalachians, but nearer to the coast.

To test this theory a time cross section (Figure 32) of wind and potential temperature was made for WAL, the station nearest the low. Soundings every six hours were available. There was no noticeable change in the distribution of potential temperature at the time of cyclogenesis (at approximately 1200 GMT 28 April 1966). However, there was a marked windshift from south-southwest to west-northwest at 3000 feet between 1200 GMT and 1800 GMT; i.e., right at the top of the inversion. This corresponds to a shift from an upslope to a downslope wind and, hence, corroborates the above theory. Unfortunately, the other cases studied did not have such a windshift at the time of cyclogenesis. Hence, the above theory is probably not a correct explanation of Type B cyclogenesis.

Since the wedge ridge has an intrinsic cyclonic circulation, land observations in the absence of ship observations may suggest the presence of a low off the coast, when, in fact, there is no low. Hence, in ridge situations, ship reports are essential for determining the conditions just off the coast.

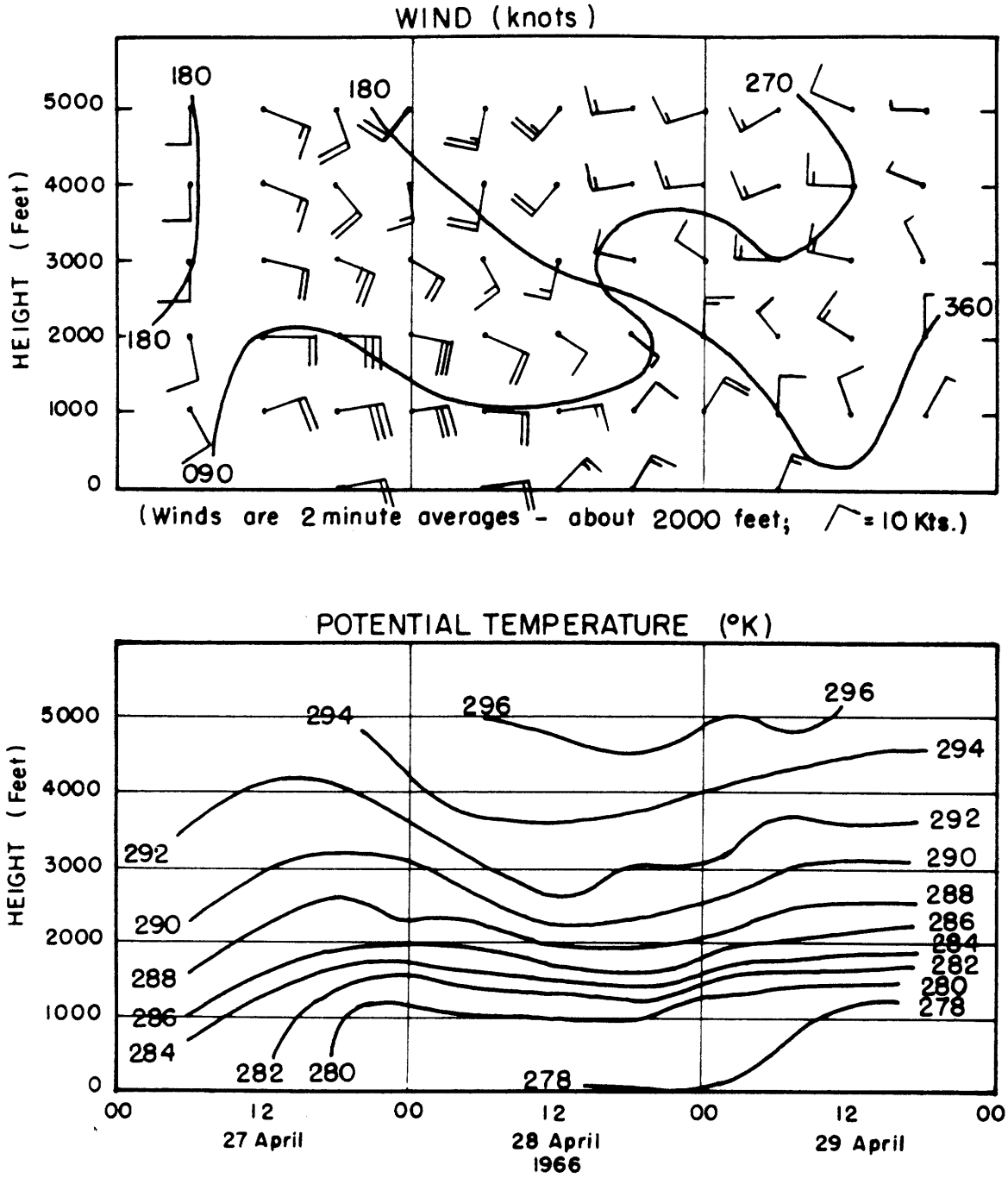

TIME CROSS - SECTION FOR WAL

Figure 32

Unfortunately, it is not possible from this research to provide an adequate explanation of Type B cyclogenesis. Clearly, more research should be devoted to this topic.

7.4 Orographic rainfall

Orography increases precipitation by (1) augmenting condensation by enhancement of the upward vertical motion and (2) releasing potential instability through this upward motion. Since the development of a pressure ridge changes the flow pattern around mountains, it alters the vertical motion field. This alteration in turn changes the distribution and intensity of the orographic precipitation. In the following, only the effects of the ridge on (1) will be discussed.

Figure 33 gives the inversion for a corner ridge as determined along the frictionless trajectory A in Figure 26. Since the cold and warm air represent two almost independent regimes, the contributions of each can be considered separately.

Let us assume that the condensed water precipitates immediately to the ground as it forms, either as drizzle or as coalescence on drops falling from above. The trajectory velocity multiplied by the terrain slope is taken as the vertical velocity of the cold air. The depth of the air comes from the difference between the inversion height and the terrain. The precipitation rate is given by the vertical motion multiplied by the depth. The upper part of Figure 33 give the contribution of the cold air to the precipitation rate— the maximum contribution is 0.25 mm/hr on the steepest part of the windward slope. The precipitation rate is negative (evaporation) at the mountain crest and on the lee slopes.

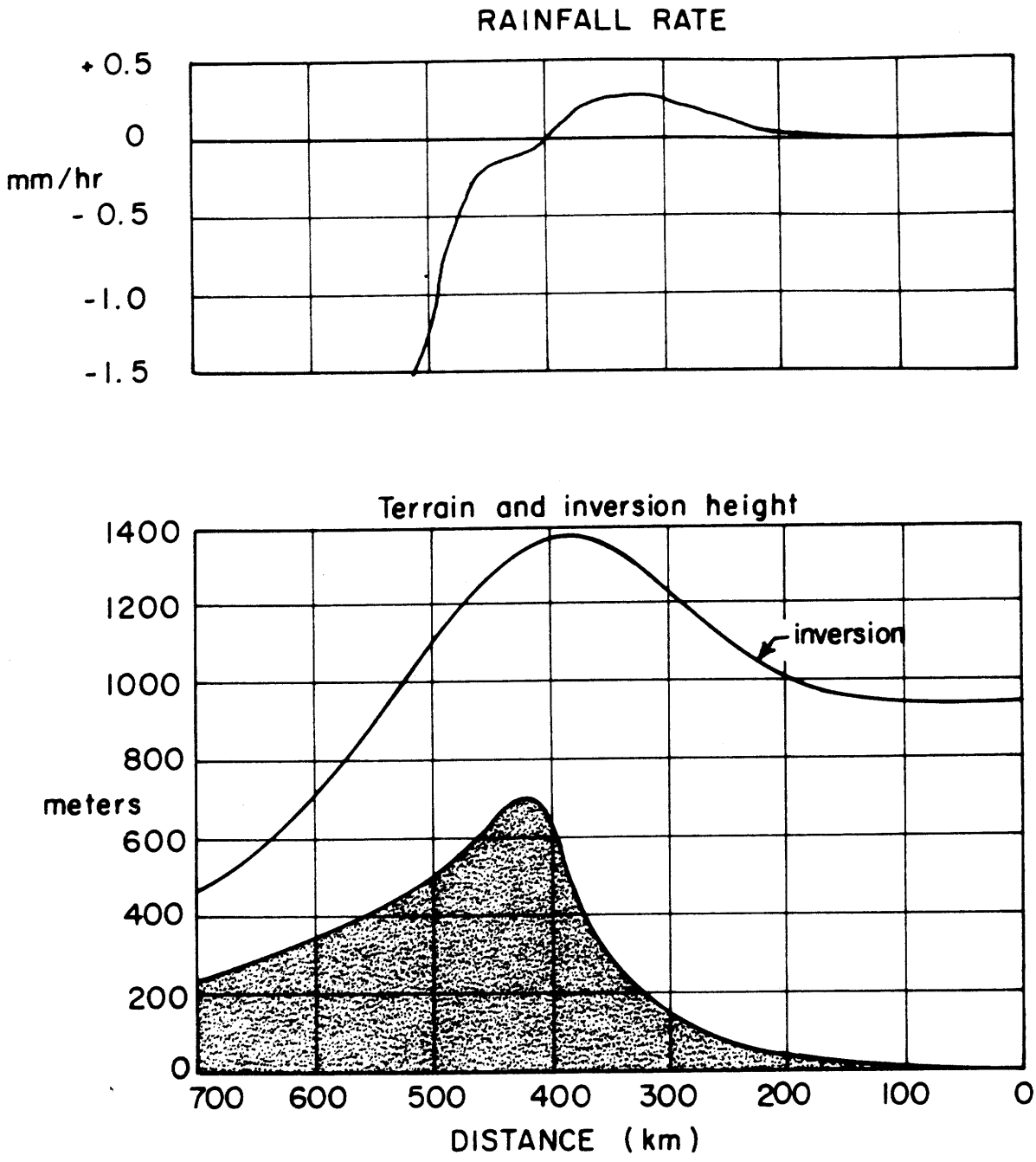

Figure 33. Contribution of the cold airflow to the rainfall rate

According to these results, this rainfall rate could be important for a long period of precipitation, while for a short period of rainfall it would be negligible. However, since trajectory velocities over-estimate the actual velocity, the precipitation rates given above are probably also over-estimated. Hence, the cold air contribution to the orographic precipitation is probably negligible at all times.

The warm air probably ascends the inversion as if the inversion were the actual mountain (although frictional effects would be different). Hence, as noted above, for the warm air, the effective shape of the mountain is different from the actual shape. Since it is unknown how far aloft orographic lifting extends, only qualitative deductions are possible.

If the warm air flows over the mountains from the east, the orographically induced warm air precipitation will enhance the cold air contribution on the eastern slopes of the mountains. Since the vertical velocity reaches a maximum before the mountain crest, the heaviest orographic rainfall should occur on the windward slopes. Over the mountain crest the vertical velocity is negative and no orographic precipitation should occur. The only confirmation in the literature of such a deduction is a study by Spinnangr and Johansen (1954). They found a distinct band of maximum precipitation well before the crest of the Norwegian Mountains in a case with a corner ridge.

If the upper-air flow comes from the west, the orographic precipitation from the warm air will fall on the western side of the

mountains. Hence, it is possible to have more orographic precipitation on the west (lee-side) than on the east (windward-side) of the mountains.

An analysis of the rainfall totals from 26-28 April 1966 was made. Data was taken from Climatological Data (United States Environmental Data Service). Any orographic effect was completely hidden by meso-scale variations in the precipitation pattern. Hence, no conclusion could be reached as to the validity of the above deductions.

With the wedge ridge the cold air is unable to flow over the mountains and must flow around. This flow reduces considerably the vertical motions and, hence, any orographic precipitation in the cold air. For warm air approaching from the west, orographic precipitation will occur on the western slope. For warm air approaching from the east, the inversion surface causes the air to start rising before it gets to the slope of the mountain. Hence, even stations not in the mountains are able to get orographically induced rainfall. This fact was first noted by Bjerknes and Solberg (1921).

Section 8. Principal conclusions and results

This thesis investigates the orographically induced pressure ridge which appears in the sea-level pressure field on the windward side of mountain ranges. It is shown that such ridges are of global extent. This study concentrates on pressure ridges forming on the eastern slopes of the Appalachian Mountains.

A statistical compilation reveals that these Appalachian pressure ridges appear about three times a month and are most pronounced in winter. The ridges develop when the prevailing flow is from the east. Many cases are very persistent — lasting at least a day — and appear to be in a steady-state.

Two types of ridges having different physical behaviors were isolated in this study. This investigation was limited to those ridges associated with a shallow cold airflow topped by a low-level inversion. These ridges are usually accompanied by low ceilings, fog, and precipitation.

A detailed synoptic study of one case and a less extensive investigation of seven other cases brought out several features of the pressure ridge. The most important result of this study was the distinction between two types of ridges with low-level inversions: the corner ridge and the wedge ridge (named after the shape of the associated isobars). It is concluded that these two ridges have fundamentally different airflows as described below.

In the corner ridge, the cold air is able to pass over the mountains according to the results obtained from a frictionless dynamic trajectory analysis. The inversion height (above sea level) along such a trajectory was found to increase from the ocean inland, reaching a peak over or to the east of the mountain crest and then rapidly decreasing on the lee side of the mountains. The cold air depth at first increases near the coast, but begins to decrease even before the inversion peak is reached. It decreases very rapidly across the top of the mountains and on the lee side. On the lee side there is a region (which has been called a mixed region in this paper) where temperatures and dew points are generally half way between those of the cold air to the east and those of the warm air to the west. In addition, there is a zone of flow parallel to the mountains on the windward slopes. It is proposed that this parallel flow is a result of surface friction. Figure 29 summarizes the flow associated with the corner ridge.

The trajectory calculations show that a cold air parcel travels down the warm air pressure gradient above the inversion. However, there is little change in the sea-level pressure along the trajectory until the inversion height reaches its peak. It is proposed that the pressure increase associated with the increase in the inversion height offsets the warm air gradient above, producing little change in the sea-level pressure as noted above. On the other side of the inversion crest, the pressure gradient associated with the changes in inversion height augments the warm air gradient. It is

proposed that this augmentation accounts for the observed strong sea-level pressure gradient across the Appalachians.

In the wedge ridge the cold air parcel coming off the ocean either does not travel down the warm air gradient or the pressure gradient associated with the inversion height rise on the windward slope is greater than the warm air gradient. The trajectory calculations suggest that the wedge ridge is usually strong enough to stop the cold air from advancing over the mountains. Hence, the air is blocked and it flows southward parallel to the mountains.

Four theories of the pressure ridge are known to the author. These theories assume, however, that no low-level inversion is present. Hence, none is applicable to this type of flow. In this study several physical factors were found to be important. The warm air gradient is of fundamental importance in determining the type of cold air flow. Evidence is also found which suggests that the coriolis force, surface friction, and mixing of the warm and cold air are also important factors.

Several aspects of orographic pressure ridges warrant further investigation. The lack of sufficient upper-air data in this study necessitated the use of an indirect method of determining the inversion height. Since the conclusions of this study are based mainly on the results of this indirect method, these results should be verified by direct observations.

Pressure ridges around other mountain ranges should be studied to determine if they have features similar to the Appalachian ridges.

It is also important to establish if these ridges in other parts of the world precede cyclogenesis similar to Type B.

Studies of pressure ridges associated with the foehn could determine if the conclusions of this investigation are also relevant to the foehn pressure ridge.

Of equal or even greater importance than these synoptic studies would be theoretical studies of the pressure ridge. Hopefully, this investigation has been carried far enough to serve as a basis for such theoretical modeling. Such theoretical models not only could show whether the conclusions of this investigation are physically realistic, but also could investigate the non-steady-state motions of the pressure ridge. In particular, an explanation of why the pressure ridge forms and what causes Type B cyclogenesis may be achieved most easily through theoretical modeling. It is hoped that this synoptic investigation will stimulate the development of such models.

TABLE 1

Number of Pressure Ridges per Month
East of the Appalachian Mountains

Month	Year 1965	1966	1967	Average
JAN	3	4	6	4
FEB	4	4	3	4
MAR	5	5	7	6
APRIL	1	4	2	2
MAY	0	3	4	2
JUNE	3	2	4	3
JULY	1	2	1	1
AUG	2	2	2	2
SEPT	2	3	1	2
OCT	1	3	5	3
NOV	2	3	3	3
DEC	1	4	4	3
Average	2	3	3.5	3

TABLE 2

Cases of Strong Ridges
Along the East Coast of the United States

Data Period: October, 1964 to April, 1968

1965

January 15 - 16
January 23 - 24
February 23 - 25
March 26
September 5
September 28
November 11 - 13
December 12 - 14

1966

January 3
February 23 - 25
February 27 - 28
March 13
March 23 - 24
April 13
April 18 - 20
April 27 - 29
June 13
September 14 - 15
September 19 - 21
December 28 - 29

1967

October 7 - 8
December 10 - 12
December 28

1968

January 11 - 13
January 27 - 28
April 22 - 24

TABLE 3

Pressure Ridge Cases Studied in Detail

1. 23 January 1965
2. 25 March 1965
3. 12 November 1965
4. 13 December 1965
5. 24 February 1966
6. 28 April 1966 (Case described in Section 4)
7. 29 December 1968
8. 14 February 1970

APPENDIX A

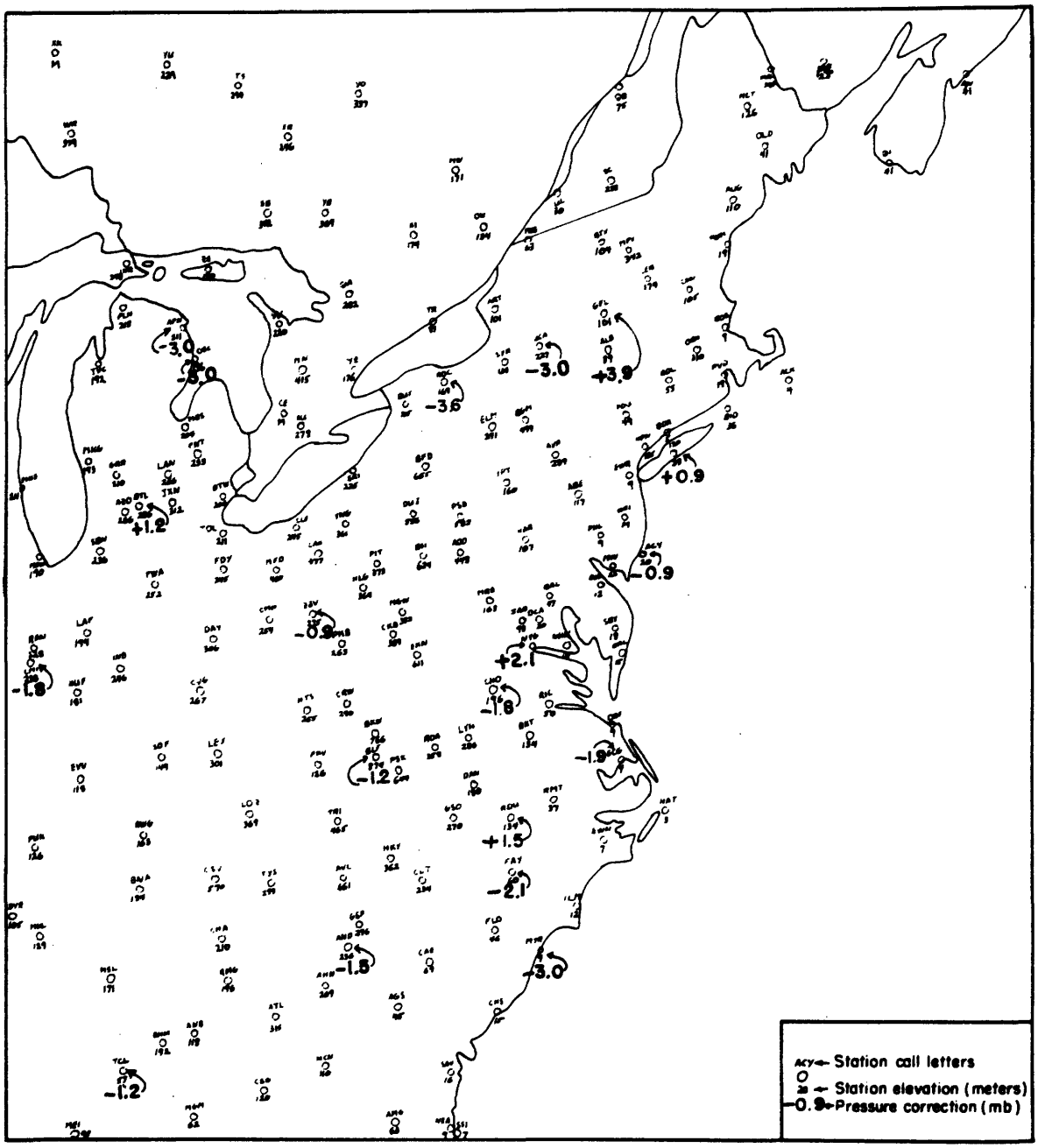

Station call letters, station elevations in meters, and pressure corrections applied in case study

APPENDIX B

Station Call Letters	Location
ACK	Nantucket, Mass.
AHN	Athens, Ga.
ALB	Albany, N.Y.
BKW	Beckley, W.Va.
BLF	Bluefield, W.Va.
BNA	Nashville, Tenn.
BUF	Buffalo, N.Y.
CHO	Charlottesville, Va.
CHS	Charleston, S.C.
CKB	Clarksburg, W.Va.
CRW	Charleston, W.Va.
DAY	Dayton, Ohio
DOV	Dover, Del.
ERI	Erie, Pa.
FNT	Flint, Mich.
GSO	Greensboro, N.C.
HAT	Hatteras, N.C.
HGR	Hagerstown, W.Va.
HTS	Huntington, W.Va.
IAD	Washington, D.C.
JFK	New York City, N.Y.
LYH	Lynchburg, Va.
MGW	Morgantown, W. Va.
MN	Mount Forest, Ont., Canada
MRB	Martinsburg, W. Va.
NYG	Quantico, Va.
PIT	Pittsburgh, Pa.
PKB	Parkersburg, W. Va.
PKV	Pikeville, Ky.
PSK	Pulaski, Va.
PWM	Portland, Me.
ROA	Roanoke, Va.
SSM	Sault Ste. Marie, Mich.
SSU	White Sulphur Springs, W. Va.
WAL	Chincoteague, Va. (Wallops Island)

APPENDIX C

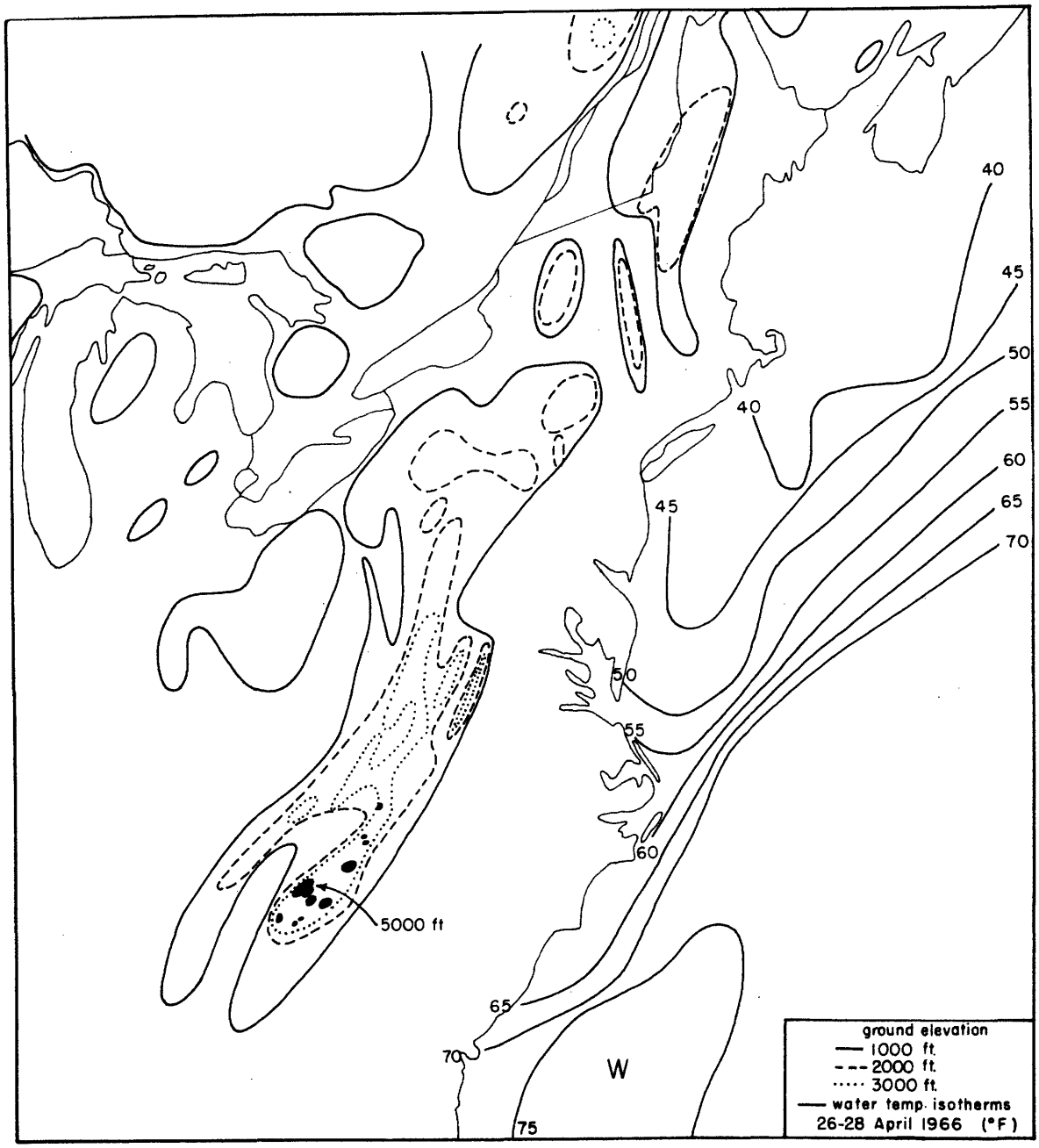

Height contours of ground elevation and
sea-water temperatures for the case study

APPENDIX D

Derivation of H_{INV}

(see Section 4.6)

$\bar{T}$, as used in Section 4.6, is a mean temperature weighted by the natural logarithm of pressure (denoted by $\bar{T}(\ln p)$ in the discussion below). It is more convenient in the derivation of H_{INV} for the mean temperature to be an average with respect to height. It is shown first that these two means differ by a negligible amount for the height interval considered in this paper.

Let z_1 and z_2 be the two levels between which the mean temperature is desired. One gets, by definition,

$$\bar{T}(\ln p) \equiv \frac{z_2 - z_1}{\int_{z_1}^{z_2} \frac{dz}{T}}$$

If we assume a constant lapse rate, γ, then at a height z

$$T = T_1 + \gamma(z - z_1)$$

and

$$\int_{z_1}^{z_2} \frac{dz}{T} = \frac{1}{\gamma} \ln\left[\frac{T_1 + \gamma(z_2 - z_1)}{T_1}\right]$$

Letting $T_2 = T_1 + \gamma(z_2 - z_1)$,

then

$$\bar{T}(\ln p) = \frac{\gamma(z_2 - z_1)}{\ln(T_2/T_1)}$$

With $\Delta T = T_2 - T_1$

$$\bar{T}(\ln p) = \frac{\Delta T}{\ln\left(1+\frac{\Delta T}{T_1}\right)}$$

Since ΔT is always much smaller than T_1, we have

$$\ln\left(1+\frac{\Delta T}{T_1}\right) \cong \frac{\Delta T}{T_1} - \frac{1}{2}\left(\frac{\Delta T}{T_1}\right)^2$$

or

$$\bar{T}(\ln p) \cong \frac{T_1}{1-\frac{1}{2}\left(\frac{\Delta T}{T_1}\right)}$$

Using the series expansion of the reciprocal we get

$$\bar{T}(\ln p) \cong T_1\left[1+\frac{1}{2}\frac{\Delta T}{T_1} + \frac{1}{2}\left(\frac{\Delta T}{T_1}\right)^2\right]$$

For the mean temperature as a function of distance

$$\bar{T}(z) = T_1 + \frac{1}{2}\Delta T$$

$$\therefore \bar{T}(\ln p) - \bar{T}(z) \cong \frac{\Delta T^2}{2T_1}$$

The larger ΔT is, the larger is the difference in the two means. In this investigation, $z_2 - z_1$ is not more than 1600 meters. Since the greatest lapse rate that would normally be observed is dry-adiabatic, ΔT would not be greater than 16°C. Hence,

$$\bar{T}(\ln p) - \bar{T}(z) \leq 0.46\ ^\circ C$$

A difference of 0.5°C is generally much less than the observed mean temperature difference between fairly close stations. For instance, the difference in mean temperature between WAL and IAD at 1200 GMT 28 April 1966 is 6.6°C.

The following is the derivation of Equation (4.4). See Figure 19 and the text for the definition of symbols. In addition, the superscripts U and L refer to the regions above and below the inversion, respectively.

$$\bar{T} = \frac{\frac{T_s + T_{INV}^L}{2}(H_{INV} - H_s) + T_{850} + T_{INV}^U (H_{850} - H_{INV})}{H_{850} - H_s} ,$$

where

$$T_{INV}^L = T_s - \gamma^L (H_{INV} - H_s)$$

$$T_{INV}^U = T_{850} + \gamma^U (H_{850} - H_{INV})$$

$$2(H_{850} - H_s)\bar{T} = [2T_s - \gamma^L (H_{INV} - H_s)](H_{INV} - H_s) + [2T_{850} + \gamma^U (H_{850} - H_{INV})](H_{850} - H_{INV})$$

Solving for H_{INV}

$$(\gamma^U - \gamma^L) H_{INV}^2 + (2T_s + 2\gamma^L H_s - 2T_{850} - 2\gamma^U H_{850}) H_{INV} - \gamma^L H_s^2 - 2T_s H_s + 2T_{850} H_{850} + \gamma^U H_{850}^2 - 2(H_{850} - H_s)\bar{T} = 0$$

Let

$$A = \frac{\gamma^u - \gamma^L}{2}$$

$$B = T_s + \gamma^L H_s - T_{850} - \gamma^u H_{850}$$

$$C = \frac{\gamma^u H_{850}^2 - \gamma^L H_s^2}{2} - T_s H_s + T_{850} H_{850} - (H_{850} - H_s)\overline{T}$$

Thus,

$$A H_{INV}^2 + B H_{INV} + C = 0$$

If $A \neq 0$,

$$H_{INV} = \frac{-B - \sqrt{B^2 - 4AC}}{2A}$$

If $A = 0$, $(\gamma^u = \gamma^L = \gamma)$

$$B = T_s - T_{850} + \gamma (H_s - H_{850})$$

$$C = \gamma \left(\frac{H_{850}^2 - H_s^2}{2} \right) - T_s H_s + T_{850} H_{850} - (H_{850} - H_s)\overline{T}$$

and

$$H_{INV} = -\frac{C}{B}$$

Let us now consider the effect of the 0.5°C error in $\bar{T}$ discussed above. If we let

$$\bar{T} = T' + \Delta\bar{T},$$

and assume, as in the text,

$$\Delta H_{INV} = \frac{-\Delta T\,(H_{850} - H_s)}{B}$$

For IAD at 1200 GMT 28 April 1966

$$B = 4.4 - 9.0 + 0.005(98 - 1563)$$
$$= -12°C$$

and thus

$$\Delta H_{INV} = \frac{-0.5\ (1465)}{12} = 61 \text{ meters}$$

Hence, an error in $\bar{T}$ of 0.5°C produces an error in ΔH_{INV} of 61 meters.

APPENDIX E

Use of Maximum-minimum Temperature Records

The United States Environmental Service publishes records of daily maximum-minimum temperature readings in Climatological Data. The density of stations taking maximum-minimum readings is about three times as great as that of the regular hourly and six-hourly synoptic network. Hence, these maximum-minimum data will resolve the temperature field of various mesometeorological phenomena which cannot be adequately resolved by the less dense observational network. The use of this data is particularly attractive if temperature contrasts are sharp, such as across a mountain range.

Nevertheless, this data source has some very clear limitations. Because observations are taken only once a day, one has to establish from the hourly data that the maxima (or minima) all occurred at approximately the same time. This requirement usually limits the use of the data to meso-scale phenomena that last at least 30 hours, since some observations are taken in the evening and others in the morning. In the United States stations report the temperature under the date the thermometer is read. For stations taking maximum temperature readings in the morning, this procedure results in the maximum temperatures being listed in Climatological Data one day later than they occur.

APPENDIX F

Equations Used in Trajectory Program

Suppose a parcel is located at X_n (latitude in degrees) and Y_n (longitude in degrees) traveling at U_n (m/sec) toward the east and V_n (m/sec) toward the north. Let R be the radius of the earth (= 6.371×10^6 meters), and ΔT be the time between time steps in minutes. Subscript n is the number of time steps taken.

Let

$$C_1 = \frac{\Delta T \times 60.0 \times 57.2958}{R} \qquad C_2 = \frac{57.2958}{R}$$

For the first approximation,

$$Y_{n+1} = Y_n + C_1 \times V_n$$

$$X_{n+1} = X_n - \left[(C_1 \times U_n) / \cos(Y_{n+1}) \right]$$

Let

$$\bar{Y}_n = \frac{Y_{n+1} + Y_n}{2} \qquad \bar{X}_n = \frac{X_{n+1} + X_n}{2}$$

$A_{px} = -\frac{1}{\rho}\frac{\partial p}{\partial x}$ and $A_{py} = -\frac{1}{\rho}\frac{\partial p}{\partial y}$ are obtained from the analyzed sea-level pressure field at point ($\bar{X}_n$, $\bar{Y}_n$).

Then,

$$A_{cx} = fv = .01458 \times SIN(\bar{Y}_n) \times V_n$$

$$A_{cy} = -fu = -.01458 \times SIN(\bar{Y}_n) \times U_n$$

$$A_{cvx} = V_n U_n \times TAN(\bar{Y}_n) \times \frac{100}{R}$$

$$A_{cvy} = -U_n^2 \times TAN(\bar{Y}_n) \times \frac{100}{R}$$

$$A_{FX} = -F \times U_n$$

$$A_{FY} = -F \times V_n$$

where F is the coefficient of linear friction.

The horizontal equation of motion states

$$A_x = A_{px} + A_{cx} + A_{cvx} + A_{Fx}$$

$$A_y = A_{py} + A_{cy} + A_{cvy} + A_{Fy}$$

so that

$$U_{n+1} = 0.6 \times A_x \times \Delta T + U_n$$

$$V_{n+1} = 0.6 \times A_y \times \Delta T + V_n$$

Let

$$\bar{U}_n = \frac{U_{n+1} + U_n}{2}$$

$$\bar{V}_n = \frac{V_{n+1} + V_n}{2}$$

For the second approximation

$$Y^s_{n+1} = Y_n + C_z \times \left(\bar{V}_n \times \Delta T \times 60.0 + A_y \times (\Delta T)^2 \times 18.0 \right)$$

$$\bar{Y}^s_n = \frac{Y_n + Y^s_{n+1}}{2}$$

$$X^s_{n+1} = X_n - C_z \times \frac{\bar{U}_n \times \Delta T \times 60.0 + A_x \times (\Delta T)^2 \times 18.0)}{\cos(\bar{Y}^s_n)}$$

$$\bar{X}^s_n = \frac{X_n + X^s_{n+1}}{2}$$

A^s_{px} and A^s_{py} are obtained for the new point $(\bar{X}^s_n, \bar{Y}^s_n)$

$$A^s_{cx} = .01458 \times SIN(\bar{Y}^s_n) \times \bar{V}_n$$

$$A^s_{cy} = -.01458 \times SIN(\bar{Y}^s_n) \times \bar{U}_n$$

and

$$A^{S}_{cvx} = \bar{V}_n \times \bar{U}_n \times TAN(\bar{\gamma}^{S}_n) \times \frac{100}{R}$$

$$A^{S}_{cvy} = -\bar{U}^{2}_n \times TAN(\bar{\gamma}^{S}_n) \times \frac{100}{R}$$

$$A^{S}_{FX} = -F \times \bar{U}_n$$

$$A^{S}_{Fy} = -F \times \bar{V}_n$$

$$A^{S}_{x} = A^{S}_{px} + A^{S}_{cx} + A^{S}_{cvx} + A^{S}_{FX}$$

$$A^{S}_{y} = A^{S}_{py} + A^{S}_{cy} + A^{S}_{cvy} + A^{S}_{Fy}$$

X^{S}_{n+1}, Y^{S}_{n+1}, U^{S}_{n+1} and V^{S}_{n+1} are then used as the initial conditions for the next time increments.

REFERENCES

Arakawa, Shōichi, 1968: Proposed mechanism of fall winds and Dashikaze. Papers in Meteorology and Geophysics, 19, 69-99.

Artemova, N.E., M. Gusev, and N.I. Riazanov, 1962: Some new methods of forecasting the bora of Novorossisk. Akademiia Nauk SSSR, Izvestiia, Ser. Geofiz., 6, 811-822; pages 519-525 in translation by American Geophysical Union.

Austin, J.M., 1941: Favorable conditions for cyclogenesis near the Atlantic coast. American Meteorological Society, Bulletin, 22, 270-272.

Baldit, Albert, 1929: Météorologie du relief terrestre: vents et nuages. Paris, Gauthier-Villars, 159-164.

Bellamy, J., 1944: The use of pressure altitude and altimeter corrections in meteorology. Journal of Meteorology, 2, 1-79.

Bjerknes, J. and H. Solberg, 1921: Meteorological Conditions for the formation of rain. Geofysiske Publikasjoner, 2(3).

_____, and _____, 1922: The life cycle of cyclones and the Polar front theory of atmospheric circulation. Geofysiske Publikasjoner, 3(1).

Bjerknes, V., J. Bjerknes, H. Solberg, and T. Bergeron, 1933: Physikalische Hydrodynamik. Berlin, Julius Springer, 488-493.

Bullrich, Kurt, 1941: Der Einfluss der Gebirge auf das Luftdruckbild. Meteorologische Zeitschrift, 58, 433-446. Referenced in Malberg, 1967.

Conover, John, 1941: Isallobars and wind directions as indicators of the direction of movement of secondary cyclones on the middle Atlantic coast in winter. American Meteorological Society, Bulletin, 22, 276-278.

Defant, F., 1951: Local winds. Compendium of Meteorology. Boston, American Meteorological Society, 655-672.

Ekman, V. Walfrid, 1932: Über die Beeinflussung der Windbahnen durch Gebirge. Beiträge zur Physik der freien Atmosphäre, 19, 272-275.

Erk, Fritz, 1886: Der Föhnsturm vom 15. and 16. Oktober 1885 und seine Wirkungen im bayerischen Gebiete. Meteorologische Zeitschrift, 3, 24-31.

Exner, F.M., 1905a: Über Druck und Temperatur bewegter Luft. Akademie der Wissenschaften, Math.-Naturw. Klasse, Sitzungberichte, 114, IIa, 1271-1296.

_____, 1905b: Das Wetter bei Keilen hohen Luftdrucks im Norden der Alpen. Jb. Zentr.-Anst. Meteor. Jahrgang 1903. Anhang. Referenced in Malberg, 1967.

v. Ficker, H., 1908: Über Keile hohen Druckes an der Alpenkette. Meteorologische Zeitschrift, 25, 230-232.

_____, 1926: Maskierte Kälteeinbrüche. Meteorologische Zeitschrift, 43, 186-188.

Frey, Karl, 1953: Die Entwicklung des Süd- und des Nordföhns. Archiv für Meteorologie, Geophysik und Bioklimatologie, Ser. A, 5, 432-477.

Garnier, B.J., 1958: The Climate of New Zealand. London, Edward Arnold Ltd.

Holmboe, Jörgen, George Forsythe and William Gustin, 1945: Dynamic Meteorology. New York, J. Wiley and Sons, Inc., 326-328.

Houghton, David and Akira Kasahara, 1968: Nonlinear shallow fluid flow over an isolated ridge. Communications on Pure and Applied Mathematics, 21, 1-23.

Küttner, Joachim, 1939: Zur Entstehung der Föhnwelle. Beiträge zur Physik der freien Atmosphäre, 25, 251-299.

Little, Delbert, 1931: Some effects of California mountain barriers on upper-air winds and sea-level isobars. Monthly Weather Review, 59, 376-380.

Malberg, Horst, 1967: Der Einfluss der Gebirge auf die Luftdruckverteilung am Erdboden. Berlin. Freie Univ. Institut für Meteorologie und Geophysik, Meteorologische Abhandlungen, 71(2), 66 p.

Miller, James, 1946: Cyclogenesis in the Atlantic Coastal Region of the United States. Journal of Meteorology, 3, 31-44.

Oi, Masamichi and Mitsuru Sekioka, 1965: Synoptic Analysis of the Perturbation of an Overrunning Current by the Intrusion of Cold Air. Monthly Weather Review, 93, 163-170.

Queney, Paul, 1948: The problem of air flow over mountains: a summary of theoretical studies. American Meteorological Society, Bulletin, 29, 16-26.

Schmidt, Wilhelm, 1910: Über die Grösse des unmittelbar dynamischen Druckstaues an Gebirge. Meteorologische Zeitschrift, 27, 406-411.

Schwitzer, H., 1953: Versuch einer Erklärung des Föhns als Luftströmung mit uberkritischer Geschwindigkeit. Archiv für Meteorologie, Geophysik und Bioklimatologie, Ser. A, 5, 350-371.

Scorer, R.S., 1952: Mountain-gap winds; a study of surface winds at Gibraltar. Royal Meteorological Society, Quarterly Journal, 78, 53-61.

Shuman, Frederick and John Havermal, 1968: An operational six-layer primitive equation model. Journal of Applied Meteorology, 7, 525-547.

Spinnangr, F. and Harald Johansen, 1954: On the distribution of precipitation in maritime tropical air over Norway. Meteorologiske Annaler, 3, 351-424.

Streiff-Becker, R., 1942: Neue Untersuchungen uber Fohn in den Schweizer Alpen. Schweizerische Naturforschende Gesellschaft, Denkschriften, 74, 244-278.

Takeuchi, M. 1951: On the influence of mountain ranges on the cold front and masked phenomena of cold air masses. Papers in Meteorology and Geophysics, 2, 30-39.

Trabert, Wilhelm, 1908a: Die langdauernde Föhnperiode im Oktober 1907 und die Luftdruckverteilung bei Fohn. Meteorologische Zeitschrift, 25, 1-9.

_____, 1908b: Über Keile hohen Druckes an der Alpenkette. Meteorologische Zeitschrift, 25, 232-233.

United States Environmental Data Service, 1965-1967: Daily Weather Maps.

_____, April 1966: Climatological Data.

_____, April 1966: Hourly Precipitation Total.

_____, April 1966: Northern Hemisphere Data Tabulations.

Watts, Ian, 1945: Forecasting New Zealand weather. New Zealand Geographer, 1, 119-138. (reprinted in Garnier, B.J. (ed.), 1950: New Zealand Weather and Climate. Christchurch, New Zealand, Witcomb and Tombs, 26-44.).

Wexler, Harry, 1951: Anticyclones. Compendium of Meteorology. Boston, American Meteorological Society, 621-629.

Wild, H., 1901: Über den Föhn und Vorschlag zur Beschränkung seines Begriffs. Schweizerische Naturforschende Gesellschaft, Denkschriften, 38.

BIOGRAPHICAL NOTE

The author attended Harvard College from 1960 to 1964, graduating cum laude in June, 1964. He has attended M.I.T. from 1964 to the present, receiving an M.S. in September, 1967. He has been a Teaching Assistant since 1966. One paper has been published: "A Study of the Squall Line of May 10, 1964" in Proceedings, Twelfth Conference on Radar Meteorology, 1966.